Stefan Brunnegger BSc

Optimization of Yielding Elements

Master's Thesis

Submitted in fulfilment of the requirements for the degree of

Diplom-Ingenieur

Master's programme Civil Engineering, Geotechnics and Hydraulics

at

Graz University of Technology

Supervisor

O.Univ.-Prof. Dipl.-Ing. Dr.mont., Wulf Schubert

Institute of Rock Mechanics and Tunnelling

Graz University of Technology

Ass.Prof. Dipl.-Ing. Dr.techn., Manfred Blümel

Institute of Rock Mechanics and Tunnelling

Graz University of Technology

Graz, January 2018

„Keep it simple and stupid.“

(W. Schubert)

AFFIDAVIT

I declare that I have authored this thesis independently, that I have not used other than the declared sources/resources, and that I have explicitly marked all material which has been quoted either literally or by content from the used sources. The text document uploaded to TUGRAZonline is identical to the present master's thesis.

Date

Signature

Acknowledgements

First, I would like to thank my supervisor, Prof. Wulf Schubert for the great support and for bringing in his excellent knowledge and practical expertise in tunnelling into my thesis.
I also like to express special thanks to Dr. Manfred Blümel for his support and for having great discussions with respect to my lab tests.

Since, I have been working in the laboratory at the institute, I would like to thank Anton Kaufmann for his help and support with my lab tests and for having some great hours in the lab.

Special thanks to my friends in Graz; the time we have had in various bar/pubs, on several excursions and the trips we have done in our rare free time would not have been that fun without of you. Furthermore, I would also like to thank my friends at home in Fischbach that have always been a part of my life.

Thank you, Dr. Günther Volkmann from DSI Underground Austria for the support and for the supply of the required material for the lab tests.

I would like to thank Roland Mayr, Manuel Entfellner, Robert Staudacher, Karoline Prall and Bernd Moritz for their support as well.

Last, but not least; I would express great appreciation to my parents Anna Maria and Armin, my brother Maximilian and my grandmother Elfriede, which have supported me in every single way during my studies.

Graz, January 2018   Stefan Brunnegger

Abstract

Tunnelling in zones with stress induced failure involving large ground volumes and large deformation need additional construction measures. Possible support elements for this boundary conditions are yielding elements with a prescribed force-shortening behaviour to prevent the shotcrete lining from cracking. This circumstance should be considered already in the design stage.

In this master's thesis, the previoursely developed system of the yielding element has been optimized. Due to the adaption of the initial stiffness and a smooth force-shortening behaviour, a better shotcrete utilization can be achieved. Steel pipes with a certain material behaviour in combination with a porous filling material and a porous concrete inlay have been used. The calculation of the shotcrete lining utilization needs a few parameters like the force-shortening behaviour of those elements, the tunnel advance, the time dependent shotcrete properties, the number of gaps in the lining and the thickness of the shotcrete lining. Furthermore, a calculation for the layout of the yielding elements with the help of an Excel-sheet has been implemented to adapt the force-shortening behaviour according to project based data.

Kurzfassung

Tunnelbau in Zonen mit spannungsbedingter tiefreichender Entfestigung bzw. Plastifizierung im Gebirge mit großen Deformationen erfordert zusätzliche Maßnahmen. Mögliche Ausbauelemente für diese Randbedingungen sind Stauchelemente mit einem vorgeschriebenen Kraft-Stauchungsverhalten damit die Spritzbetonschale nicht reißt. Dieser Umstand sollte in der Planung berücksichtigt werden.

In dieser Masterarbeit wurde das zuvor entwickelte System des Stauchelements optimiert. Durch das Anpassen der Anfangssteifigkeit und einen gleichmäßigen Anstieg der Arbeitslinie konnte eine bessere Spritzbetonauslastung erreicht werden. Stahlrohre mit einem speziellen Materialverhalten in Kombination mit einem porösen Füller und einer porösen Einlage wurden dazu verwendet. Die Berechnung der Spritzbetonauslastung erfordert einige Parameter wie das Kraft-Stauchungsverhalten des Stauchelements, die Vortriebsgeschwindigkeit, die zeitabhängigen Spritzbetoneigenschaften, die Anzahl der Schlitze in der Tunnellaibung und die Stärke der Spritzbetonschale. Außerdem wurde ein Bemessungsprogramm für die Auslegung des neu entwickelten Stauchelements mit Hilfe einer Excel-Tabelle angepasst, um das Kraft-Stauchungsverhalten dem Projekt basierenden Daten anzupassen.

Table of contents

1. Introduction

The so called "yielding element" has been a research topic at Graz University of Technology for years. Rabcewicz first introduced such a system in his dissertation "Die Hilfsgewölbebauweise" [1] in 1950, where he had the idea to integrate timber elements in the shotcrete lining to deal with the large amount of deformations, but this knowledge fell into oblivion for a long time so that no further research has been done.

At several tunnel construction sites in Austria a concept with open gaps was in use for a long time, until a collapse at the "Galgenberg Tunnel".

This event enforced Schubert et al [2] in 1996 to do some further development. They introduced a system where single pipes are loaded in axial direction. A big disadvantage of this system was the high oscillation of the force-shortening curve.

Moritz [3] adapted the system in 1999, to obtain an increase in its bearing capacity and to reduce the oscillation of the force-shortening curve (System LSC).

This system LSC has been refined by Sitzwohl [4] in 2011, by Verient [5] in 2014 and by Brunnegger [6] in 2016 with a porous filling material and different inlays to obtain a smooth force-shortening behaviour and to decrease the initial stiffness.

With this knowledge, the rearrangement of the system LSC during this master's thesis can be finalized to launch a new product on the market (System LSC-N). These development steps are visualized in Figure 1.
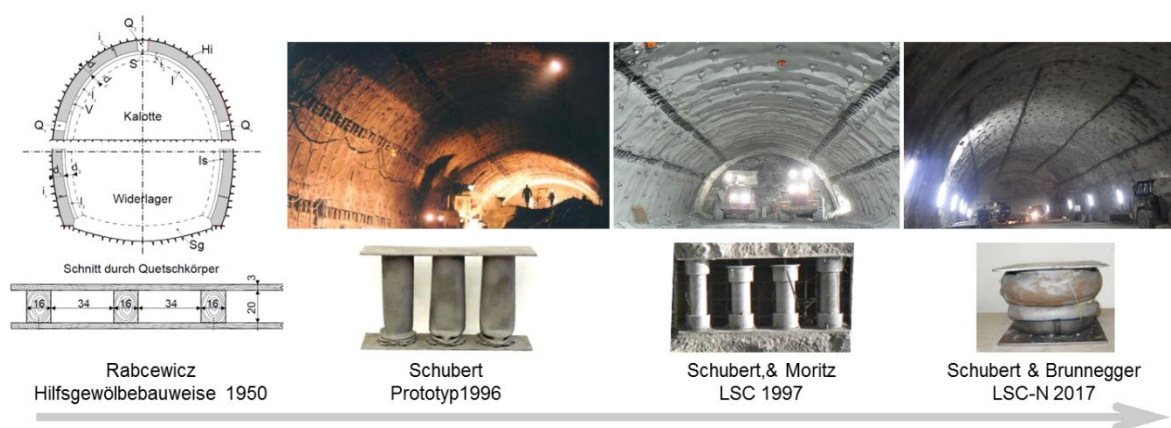
Figure 1: from left: wooden elements [1], LSC Prototype [2], LSC [3], LSC-N [7]
picture from Moritz [8]

2 State of the Art

Yielding elements are niche products and there is already a wide range on the market. They can be separated in different types according to Radončić [9]:

- Steel elements
- Porous concrete elements
- Hybrid elements

2.1 System – Welle

The system "Welle" is produced and distributed by SZ Schacht- und Streckenausbau GmbH. Depending on the wave geometry (wave height, wave number and wavelength of the profile waves) and the dimensioning of the element (sheet thickness, sheet length and choice of material and/or steel quality), the force-shortening behaviour of the yielding element can be adapted. Due to the design of the element, even during rock deformation the load absorption can be adapted according the appearing rock conditions, for example by inserting further sheet metal pieces [10].

Figure 2: Welle – SZ Schacht- und Streckenausbau
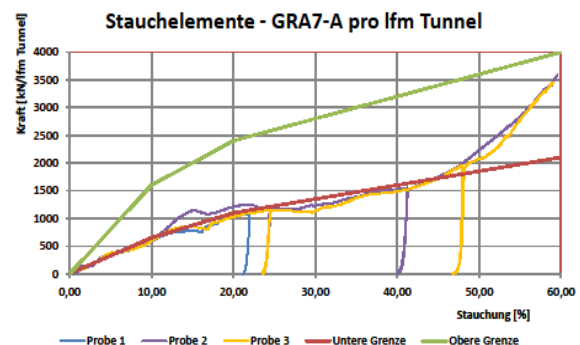
Figure 3: Force-Shortening behaviour - Welle

Advantages

- During the deformation of the rock mass this system is adaptable → insert of additional plates lead to a higher resistance
- Different force-shortening behaviours due to variable dimensions (length, thickness) and steel quality applicable

Disadvantages

- Relative high weight due to the high amount of steel → difficult installation
- Relative high production effort → high amount of weld seams

2.2 **System – hiDCon**

The system hiDCon (highly deformable concrete) has been developed and is being distributed by Solexperts AG. It consists of a high strength concrete matrix with porous additives (See Figure 4). Furthermore, this system can be modified with styrofoam sheets to reduce the initial high stiffness. [9]

Figure 4: hiDCon – Solexperts [9]
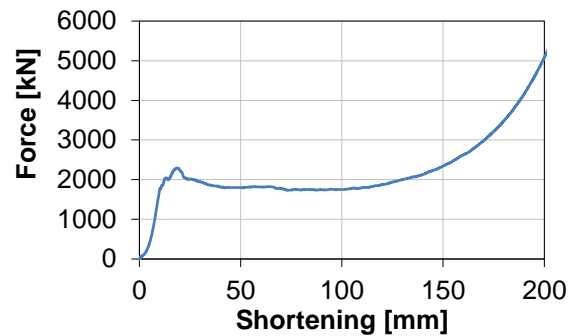
Figure 5: Force-Shortening behaviour – hiDCon courtesy of Prof.Giovanni Barla

Advantages

- Relative low weight → cement based porous material
- First peak can be modified by an insertion of styrofoam sheets

Disadvantages

- No significant increase of the resistance after reaching the first peak
- No adaption of the resistance during the deformation of the rock mass possible

2.3 **System – WABE**

The system WABE has been developed and is being distributed by Bochumer Eisenhütte Heintzmann GmbH & Co.KG. This element consists of a group of steel tubes, which are loaded perpendicular to their axis. By insertion of additional steel tubes, the bearing capacity can be increased during the deformation of the rock mass (Figure 6) [9].

Figure 6: WABE – Bochumer Eisenhütte [11]
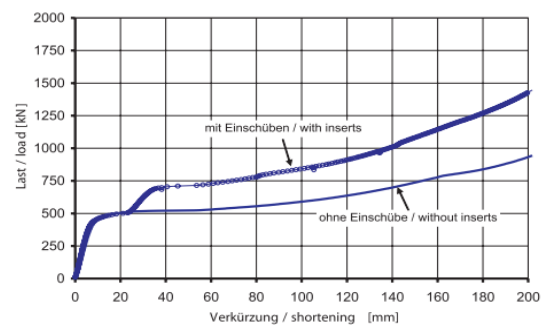
Figure 7: Force-Shortening behaviour - WABE [11]

Advantages

- During the deformation of the rock mass this system is adaptable → insertion of additional pipes lead to a higher resistance
- Different force-shortening behaviours due to variable dimensions (diameter, wall thickness) and steel quality applicable

Disadvantages

- First peak is dependent on steel properties and therefore it cannot be easily eliminated
- Relative high weight due to the high amount of steel → difficult installation

2.4 **System – LSC**

The system LSC has been developed by Moritz [3] and is being distributed by DSI Underground Austria GmbH. This element consists of a group of steel tubes, which are loaded axially (Figure 8). The force-shortening curve can be adapted by increase/lower the number of pipes per element and by changing the pipe dimensions (length, wall thickness and diameter) [11].

Figure 8: LSC – DSI Underground [9]   Figure 9: Force-Shortening behaviour – LSC [11]
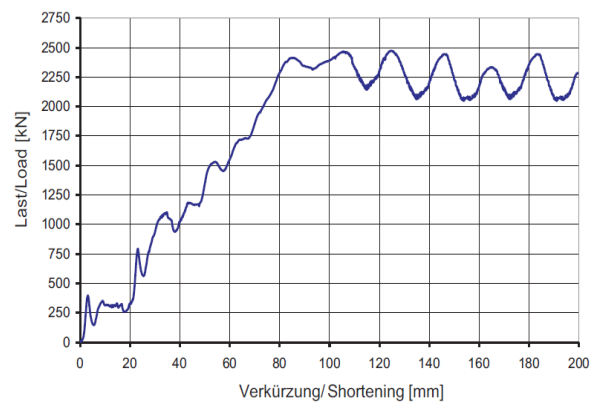
Advantages

- First peak can be relocated by installing shorter pipes (Figure 8)
- Different force-shortening behaviours due to variable dimensions (diameter, wall thickness) and steel quality applicable

Disadvantages

- Asymmetric buckling can lead to higher oscillation of the force-shortening behaviour

3 Yielding Element LSC-N

The yielding element called Lining Stress Controller (LSC) is produced and distributed by DSI Underground (as mentioned in chapter 2.4). Due to the loading in axial orientation it shows a relative high initial stiffness in combination with an oscillating force-shortening behaviour.

In different previous master's theses by Sitzwohl [4] in 2011, by Verient [5] in 2014 and bachelor projects by Brunnegger [6] in 2016 the LSC has been refined to achieve a higher shotcrete utilization, to reduce weight, to decrease the initial stiffness, to gain a smooth force-shortening behaviour and the modifications should also lead to reduced production costs.

In this master's thesis the system of the LSC has been optimized. The new elements are called LSC-N, which are distributed already by DSI Underground Austria GmbH.

3.1 Composition

The elements consist of steel pipes with a certain material behaviour and a porous filling material (hybrid element), a porous concrete inlay and two end plates (See Figure 10).

The porous concrete inlay reduces the initial stiffness and in combination with steel pipes filled with a porous filling material, the system allows a smooth force-shortening behaviour. According to this "simple system" the production costs and the weight can kept low.
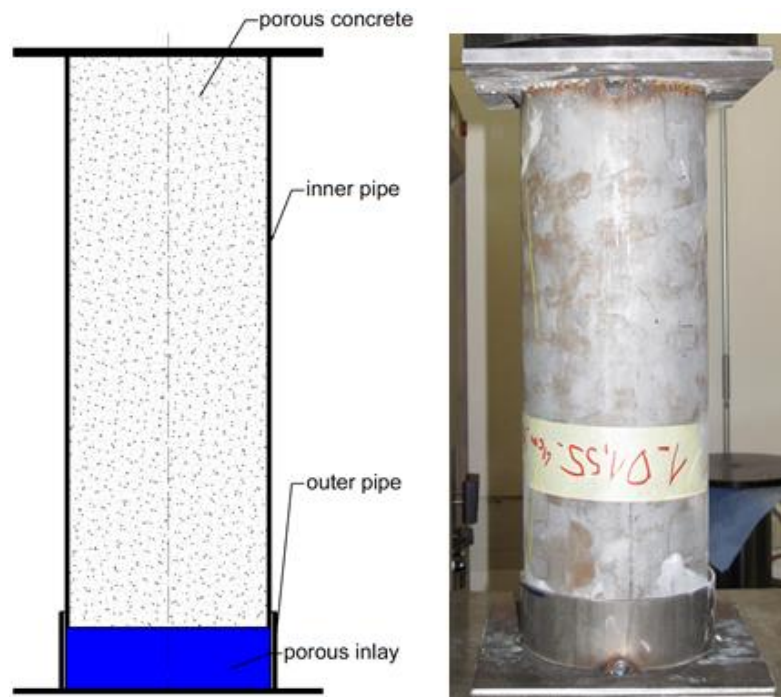
Figure 10: Scheme of LSC-N (left), LSC-N before compression (right)

3.2 **Mixture of the Porous Filling Material**

To obtain different porous cement based filling materials with different densities and material parameters, different mixtures have been used (see Table 2). The used materials are shown in Table 1.

Table 1: Used materials

Botament Botacem M51	CEM II/B-M (S-L) 32.5 N	Sand 0-2mm	Liapor 1-4mm

Based on knowledge from previous lab tests [6] the mass percentages of the materials with respect to the final density of the filling material can be determined (see Figure 11).
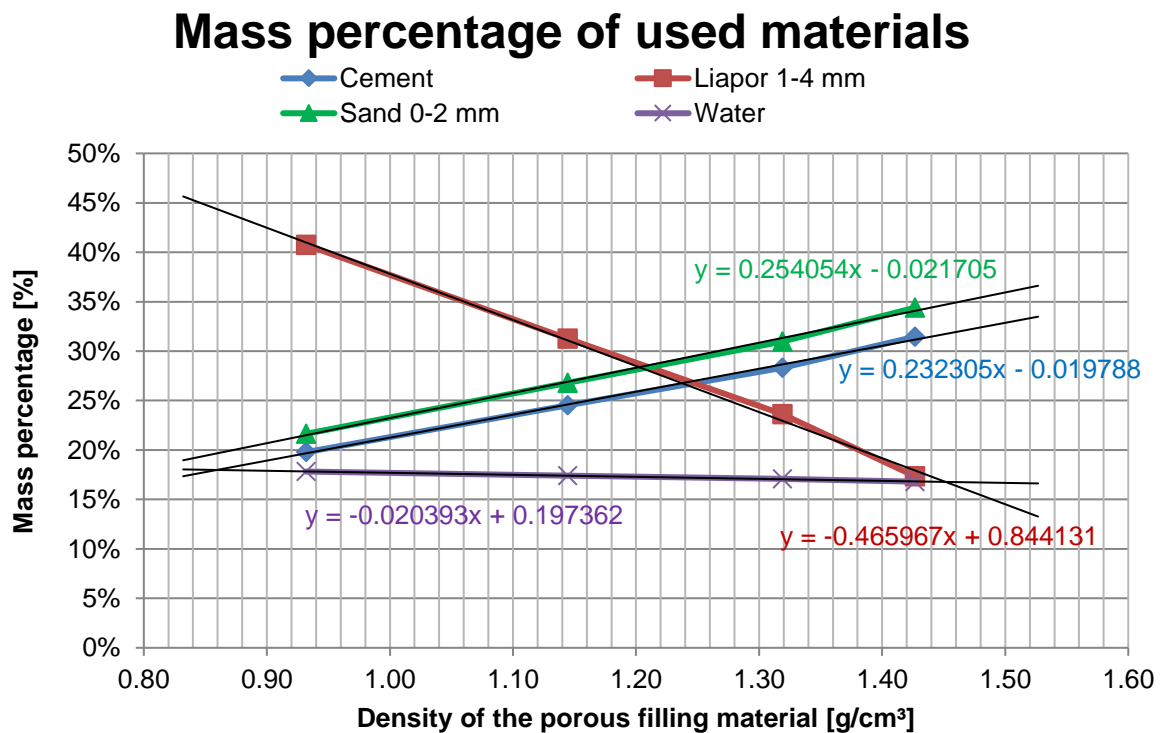
Figure 11: Density influence of the mass percentage of the used materials

Due to the higher water absorption behaviour of Liapor the water/cement ratio is defined in Eq. 1. This refers to the basics of the master's thesis of Sitzwohl [4], but instead of the volume-proportion, the mass-proportion is used.

$$W/_C = 0,4 + 0,2432 * \frac{m - proportion_{Liapor1-4mm}}{m - proportion_{Cement}}$$ Eq. 1

Table 2: Mass percentage of used materials

Mixture	Botament Botacem M51	CEM II/B-M (S-L) 32.5 N	Liapor 1-4mm	Sand 0-2mm	Water	W/C-ratio
D1,5	-	32.87%	14.52%	35.94%	16.68%	0.51
D1,55	-	34.03%	12.19%	37.21%	16.58%	0.49
D1,6	-	35.19%	9.86%	38.48%	16.47%	0.47
D1,37	-	29.85%	20.58%	32.63%	16.94%	0.57
Botament1,37	59.05%	-	26.90%	-	14.06%	0.51
Botament1,55	62.91%	-	17.35%	-	11.98%	0.47

3.3 **Porous Concrete Inlay**

A porous concrete inlay is used to reduce the initial stiffness. Thickness variations lead to different force-shortening behaviours at the initial state (see Figure 12). The material used is produced and distributed by Xella International S.A. with the product name YTONG. It has a density of 0.6 g/cm³, a compressive strength of 5 MPa and an E-Modulus of 2500 MPa.
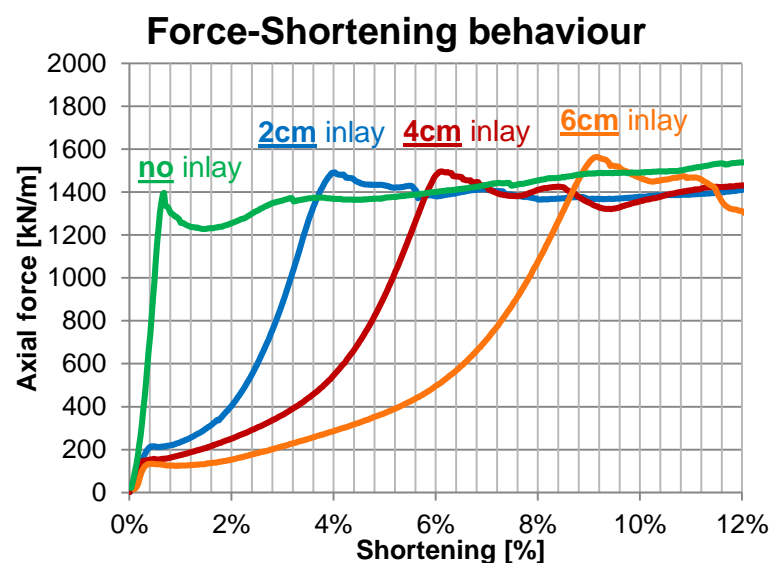
Figure 12: 4cm porous inlay (left), Influence of the porous inlay (right)

3.4 **Compensation Layer**

Due to the shrinkage of the porous filling material during the hydration process, a compensation layer of gypsum needs to be installed to provide full contact (see Figure 13).

Figure 13: Filling material shrinkage (left) [6], Compensation layer (right) [6]

Otherwise the inner pipe penetrates into the porous concrete inlay (see Figure 14) and cannot properly be activated in the initial state (see Figure 15).
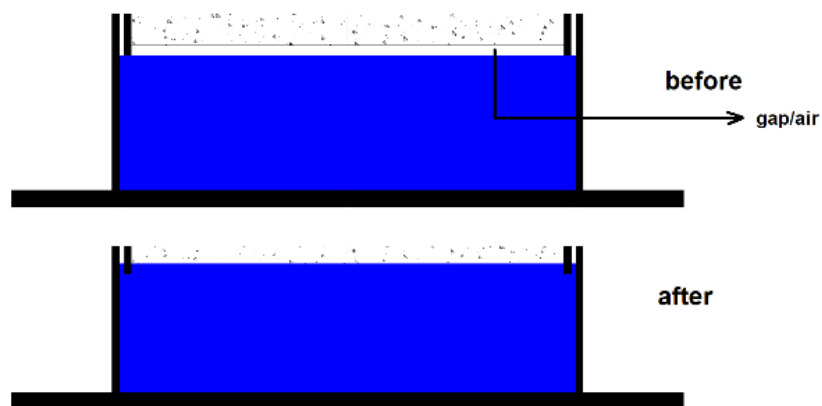
Figure 14: Penetrate into the porous concrete inlay [6]
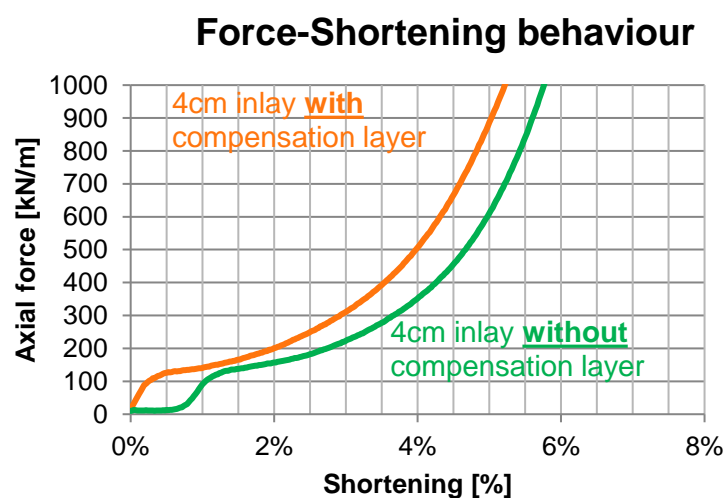
Figure 15: Influence of the compensation layer [6]

3.5 **Manufacturing**

The manufacturing steps are shown and described from Figure 16 to Figure 23.

Figure 16: Cut inner and outer pipe to length

Figure 17: Weld pipe with end plate

Figure 18: Weigh materials

Figure 19: Mix materials

Figure 20: Fill the inner pipe with the porous filling material and compact it in layers

Figure 21: Add the compensation layer (gypsum) [6]

Figure 22: Shape the porous inlay

Figure 23: Insert inlay and install lid

4 Installation of the Yielding Element

The following pictures (Figure 24 - Figure 32) have been kindly provided by Prall (Amberg Engineering), showing the installation steps of the yielding elements on the construction site Semmering Base Tunnel 1.1.

Steel bars are used for fixing the elements between the lattice girders in position before shotcreting (see red square in Figure 24).
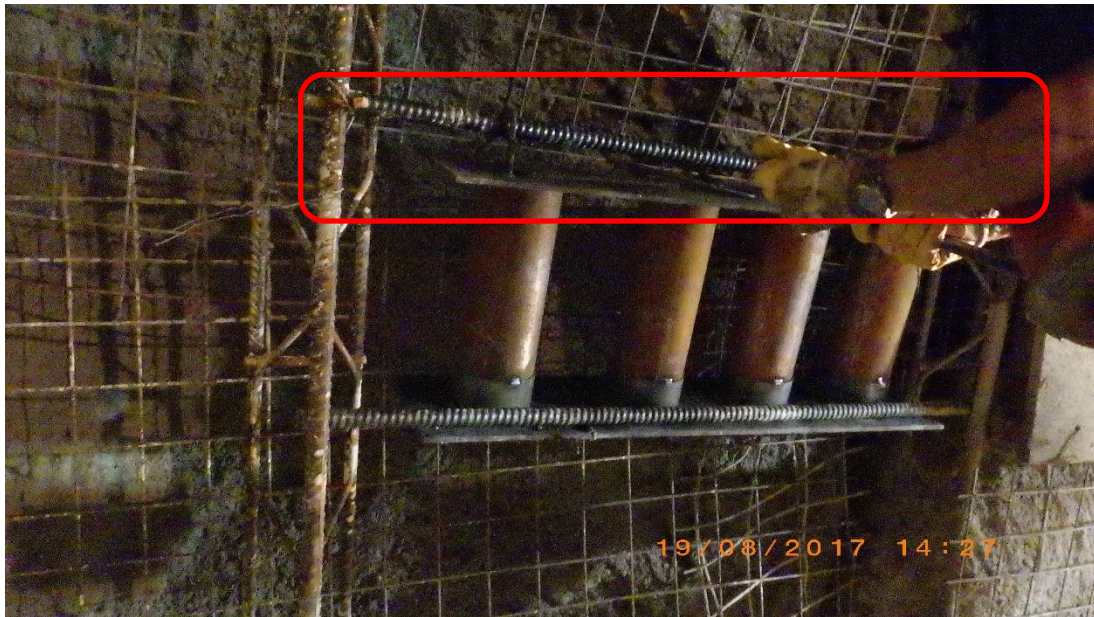
Figure 24: Mounting the steel bar (red) with positioned yielding element

picture from Moritz

The yielding element can then be fixed with hooks, welded to the upper end plate (see Figure 25 and Figure 26) on the previously installed steel bar.

Figure 25: Installation hooks

Figure 26: Mounting the yielding element

Afterwards it is positioned and the reinforcement on the end plates are connected with the first layer of wire mesh (see Figure 27 and Figure 28).

Figure 27: Positioning

Figure 28: Connection with the first layer of wire mesh

The yielding elements are protected with a formwork panel, to prevent shotcreting of the open space between the steel tubes (see Figure 29). Then the first layer of shotcrete (actual round) and the second layer of shotcrete (last round) can be applied in one procedure (see Figure 30).
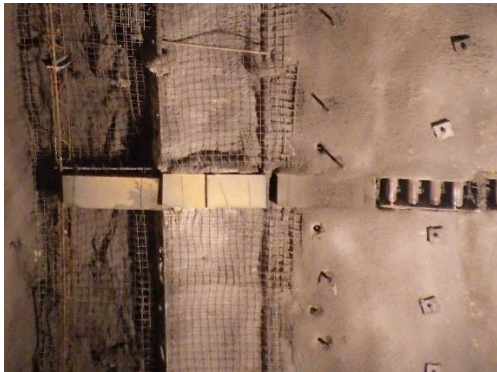
Figure 29: Protection against shotcrete

Figure 30: Applying the shotcrete

After shotcreting the first layer, the second layer of wire mesh needs to be connected with the reinforcement of the yielding element (see Figure 31). The framework panel can be removed as soon as shotcreting in the vicinity of the yielding element is finished.

Figure 31: Connection with the second layer of wire mesh

Figure 32: Göstritz Cavern October 2017

Figure 32 is showing the installed yielding elements at the Semmering Base Tunnel.

5 Controlling Initial Stiffness

A general problem of most yielding elements is a relatively high stiffness in the initial loading stage. Different inlays have been tested to control the initial stiffness. The lab tests with different inlay height show after reaching the first peak quite a similar behaviour (see Figure 33), which can be mathematically described. If the force-shortening curve is divided into three parts it is possible to describe it mathematically. These three parts are shown in Figure 34.

Part I describes the first increase until the matrix of the porous inlay is destroyed, **Part II** shows the influence of the inlay height and **Part III** describes the force-shortening behaviour until the yielding element fails.
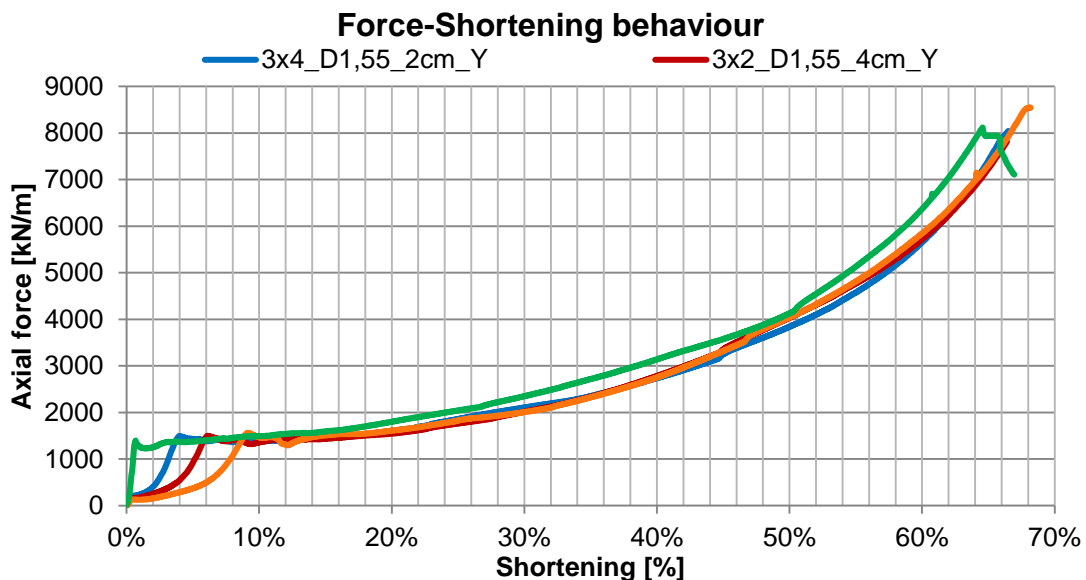
Figure 33: Similar behaviour of the force-shortening behaviour
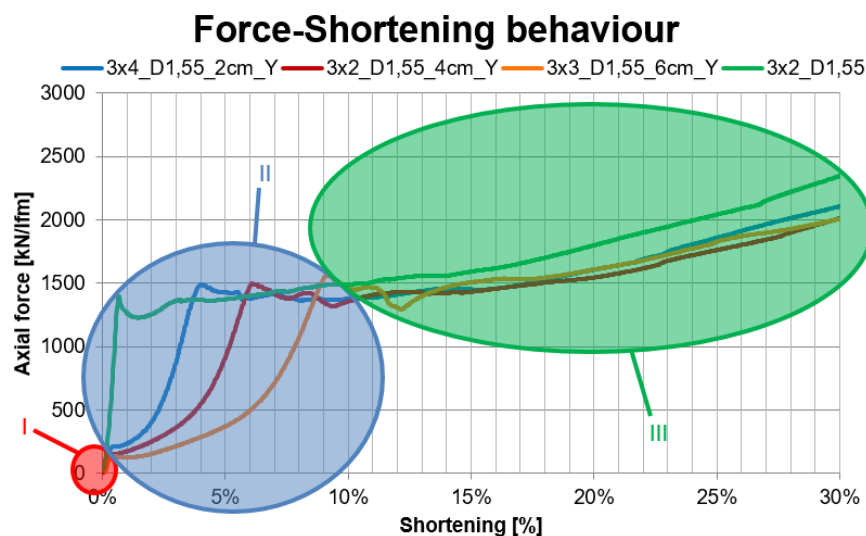
Figure 34: Separation into three parts

5.1 **Part I – Inlay Influence**

By analysing Part I with the assumption that the pipe with the porous filling material is not activated at all, a linear behaviour of the porous concrete inlay can be noticed (see Eq. 2). The boundary criterion has been set to 0.3% shortening.

$$F(\varepsilon) = 11000 * n_{YE} * \varepsilon \qquad\qquad \varepsilon \leq 0.003 \qquad\qquad \text{Eq. 2}$$

        F(ε)...............force depending on shortening [kN]
        ε....................shortening [-]
        n_{YE} ....number of the Yielding Elements [-]

5.2 **Part II – Inlay Height Influence**

By analysing Part II with the assumption that the pipe with the porous filling material is not activated at all, an exponential behaviour of the porous concrete inlay can be noticed (see Eq. 3).

$$F(\varepsilon) = 80 * e^{A*\varepsilon} \qquad\qquad 0.003 < \varepsilon \leq \varepsilon_{Peak} \qquad\qquad \text{Eq. 3}$$

        F(ε)...............force depending on shortening [kN]
        ε....................shortening [-]
        A....................inlay factor [-]

5.2.1 Inlay Factor

The exponent A is called the inlay factor and it is dependent on the inlay height, which can be seen in Eq. 4 and Figure 35.

Table 3: Inlay Factor

A	H_{Inlay}
[-]	[cm]
85	2
52	4
38	6
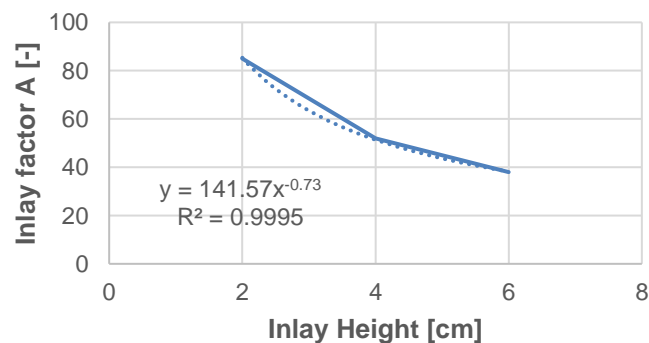
Figure 35: Inlay Factor

$$A \cong 141.6 * H_{Inlay,calc}^{-0.73} \qquad \text{Eq. 4}$$

A.....................inlay factor [-]

H_{Inlay}...............calculated inlay height [cm]

5.2.2 Inlay Compaction Behaviour

For Part II a statistical analysis of the values from the first peak needs to be done to determine a boundary criterion (see Table 4). Therefore, the lab tests from Brunnegger [6] with similar first peak values can be considered as well.

Table 4: First Peak Data

	First Peak		Height	First Peak - mean value		Height - mean value	Lab Test
	Shortening	Force		Shortening	Force		
	[%]	[kN]	[mm]	[%]	[kN]	[mm]	[-]
2 cm inlay	4.00%	1500	410	4.00%	1600.00	403.33	4_D1,55_2cm_Y
	4.00%	1600	400				M2_3_Y_5,0
	4.00%	1700	400				M4_2_Y_5,0
3 cm inlay	5.20%	1600	410	5.00%	1750.00	410.00	M2_4_Y_5,0
	4.80%	1900	410				M3_2_Y_5,0
4 cm inlay	6.00%	1750	420	6.17%	1585.71	417.14	4_D1,6_Y_5,0
	5.50%	1300	420				1_D1,55_Y_5,0
	6.00%	1500	410				1_D1,55_4cm_Y
	6.00%	1450	410				2_D1,55_4cm_Y
	6.60%	1600	420				M2_6_Y_5,0
	7.00%	1700	420				M4_3_Y_5,0
	6.10%	1800	420				M3_3_Y_5,0
6 cm inlay	9.00%	1500	410	9.00%	1500.00	410.00	3_D1,55_6cm_Y
7 cm inlay	10.00%	1400	410	9.75%	1200.00	410.00	D_1,55_7cm_Y_
	11.00%	1200	410				Botament_7cm_Y_
	9.00%	1100	410				Botoment1,37_7cm_Y
	9.00%	1100	410				D1,37_7cm_Y

Table 5: Mean Values - First Peak

Inlay Height	First Peak	Inlay Efficiency
	Shortening	
[mm]	[mm]	[%]
20	16.13	80.67%
30	20.50	68.33%
40	25.74	64.36%
60	36.90	61.50%
70	39.98	57.11%
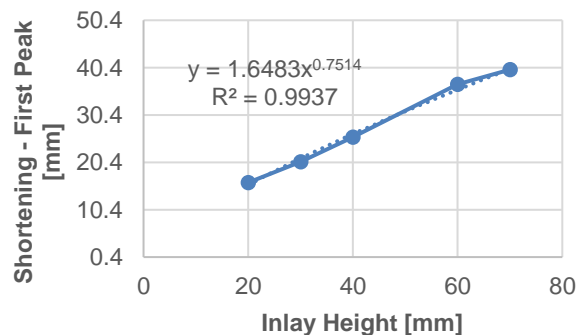
Figure 36: Inlay compaction behaviour

For the further calculation, the mean values are used. With this information, the inlay compaction behaviour can be described (Eq. 5).

$$\varepsilon_{Peak} \cong 1.65 * \frac{H_{Inlay,calc}^{0.75}}{H_{ref}}$$ Eq. 5

A....................inlay factor [-]
$H_{Inlay,calc}$ ....calculated inlay height [cm]
H_{ref}.................reference height of the Yielding Element [mm]

5.2.1 Curve Fitting

The exponents of Eq. 4 and Eq. 5 are quite similar, therefore it has been set to a constant called η_{Inlay}. If those functions are implemented for Part II, it doesn't show a good fitting if it's compared with the force-shortening behaviour of the lab tests. Therefore, they need to be adjusted to deliver a suitable result (see Eq. 6 and Eq. 7). So η_{Inlay} has been set to 0.77.

$$\varepsilon_{Peak} = 1.55 * \frac{H_{Inlay,calc}^{\eta_{Inlay}}}{H_{ref}} \quad \rightarrow \quad H_{Inlay,calc} = e^{\frac{\ln\left(\varepsilon_{Peak}*H_{ref}*\frac{1}{1.55}\right)}{\eta_{Inlay}}}$$ Eq. 6

$$A = 135 * H_{Inlay,calc}^{-\eta_{Inlay}}$$ Eq. 7

ε_{Peak} ....shortening at the First Peak [-]
A....................inlay factor [-]
$H_{Inlay,calc}$ ....calculated inlay height [cm]
H_{ref}.................reference height of the Yielding Element [mm] **H_{ref} = 410 mm**
η_{Inlay} ....inlay efficiency factor [-] **η_{Inlay}=0.77**

A reference correction factor β, dependent on the height of the yielding element (see Eq. 8) is introduced for the shortening e_{Peak}=36 mm, to finally calculate a proper height for the inlay.

$$\beta = \frac{H_{Inlay,target}}{H_{Inlay,calc}}$$ Eq. 8

β....................inlay height correction factor [-]
$H_{Inlay,calc}$ ....calculated inlay height [mm]
$H_{Inlay,target}$ ....target inlay height [mm]

Table 6: Height influence

H_{YE}	e_{Peak}	$H_{Inlay,calc}$	$H_{Inlay,target}$	β
[mm]	[mm]	[mm]	[mm]	[-]
200.00	36.00	150.96	61.36	0.41
300.00	36.00	89.16	61.36	0.69
400.00	36.00	61.36	61.36	1.00
500.00	36.00	45.93	61.36	1.34
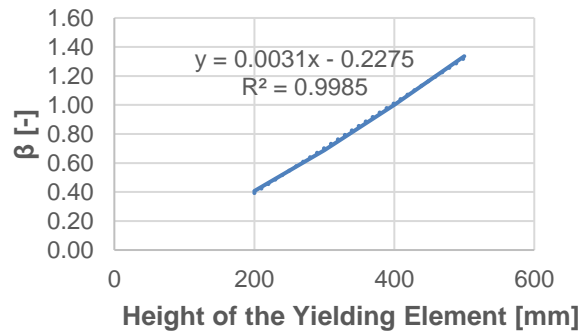
Figure 37: Height influence

With this information the target inlay height can be described with Eq. 9 and Eq. 10.

$$H_{Inlay,target} = H_{Inlay,calc} * \beta(H_{YE})$$ Eq. 9

with:

$$\beta(H_{YE}) = 0.0031 * H_{YE} - 0.2275$$ Eq. 10

β(H$_{YE}$) ....inlay height correction factor [-]
H$_{Inlay,calc}$ ....calculated inlay height [mm]
H$_{Inlay,target}$ ....target inlay height [mm]
H$_{YE}$.................height of the Yielding Element [mm]

With this information, the force-shortening behaviour for Part II can be described with Eq. 11.

$$F(\varepsilon) = 26.5 * n_{YE} * e^{A*\varepsilon} \qquad\qquad 0.003 < \varepsilon \le \varepsilon_{Peak}$$ Eq. 11

F(ε)................force depending on shortening [kN]
ε.....................shortening [-]
ε$_{Peak}$ ....shortening at the First Peak [-]
A....................inlay factor [-]
n$_{YE}$ ....number of the Yielding Elements [-]

5.3 **Part III – Steel and Filling Influence**

In this part of the force-shortening behaviour plastic deformation of the yielding element is occurring. Therefore, no meaningful analytical approach can be achieved. The best fitting of the force-shortening behaviour is shown by Eq. 12.

$$F(\varepsilon) = n_{YE} * \left[200 * e^{\left(\varepsilon^{1.4}*4.3\right)} + 250\right] \qquad \varepsilon_{Peak} < \varepsilon \le \text{failure}$$ Eq. 12

F(ε)................force depending on shortening [kN]
ε.....................shortening [-]
ε$_{Peak}$ ....shortening at the First Peak [-]
n$_{YE}$ ....number of the Yielding Elements [-]

5.4 **Comparison with Lab Tests**

The mathematical description is based on varying the inlay height. All other parameters used for the calculation are kept constant.

D$_{YE}$=133 mm...........................diameter of the inner pipe [mm]
σ$_{Inlay}$=5 MPa............................compressive Strength of the inlay [MPa]
E$_{Inlay}$=2500 MPa......................E-Modulus of the inlay [MPa]
s=2.5 mm...............................wall thickness of the inner pipe [mm]
D1,55.....................................porous filling material [-]
S235+N ....steel type of the inner pipe [-]

The calculated force-shortening curve (red line) shows a good agreement with the lab test results (blue line) (see Figure 38, Figure 39 and Figure 40).

Force-Shortening behaviour
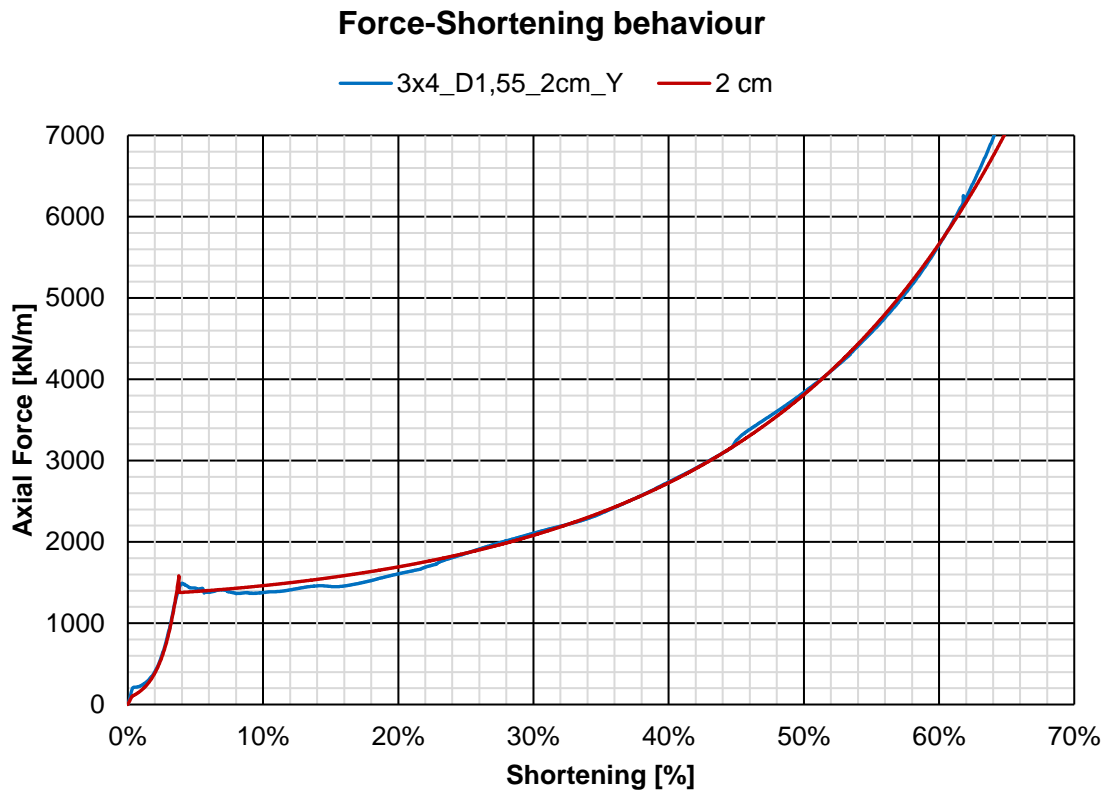
Figure 38: Comparison with 2 cm inlay height

Force-Shortening behaviour
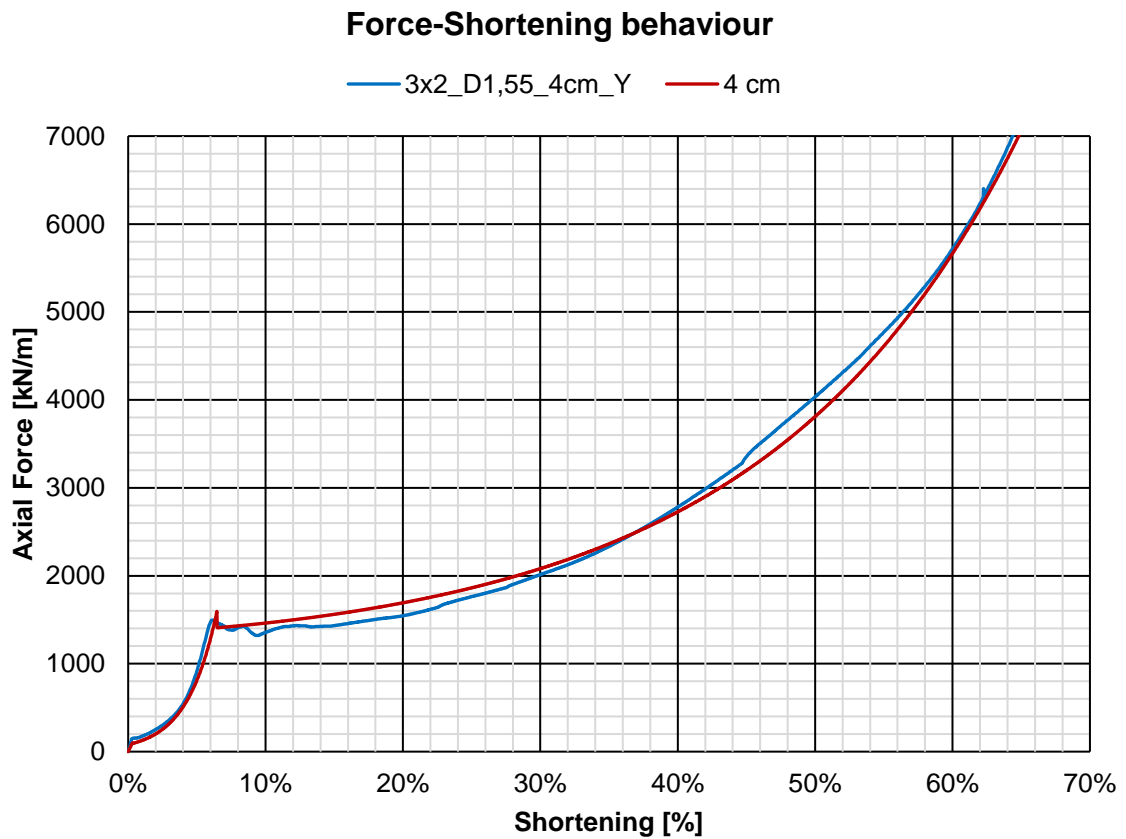
Figure 39: Comparison with 4 cm inlay height

Force-Shortening behaviour
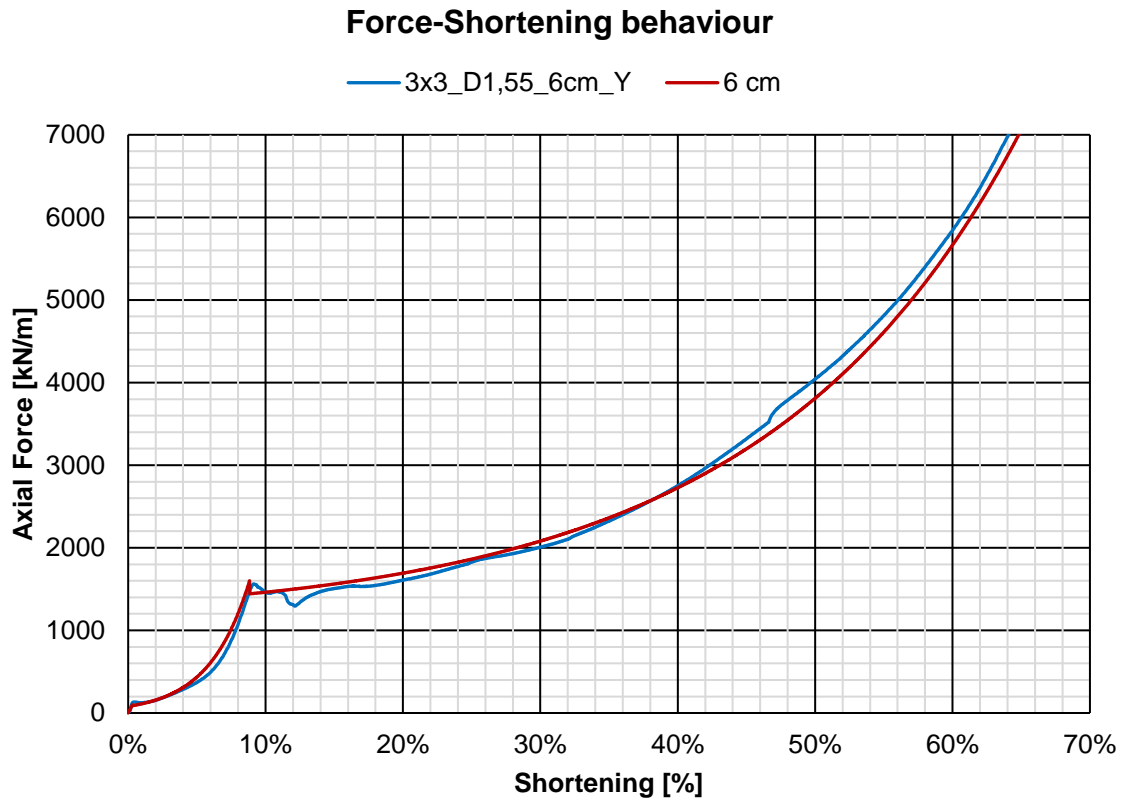
Figure 40: Comparison with 6 cm inlay height

6 Shotcrete Lining Utilization

In weak zones, the shotcrete lining cannot resist large displacements, which leads to cracks in the lining and the requirement of expensive repair works. Yielding elements are installed in the lining to avoid the shotcrete from failing, but those elements must fulfil certain requirements. The force-shortening behaviour must be capable with the project based parameters to obtain a shotcrete utilization of µ<100%.

6.1 Time-dependent Compressive Strength

The major share of the deformations occurs directly behind the face, which means the "young" shotcrete must cope with those deformations. The time-dependent behaviour of standard concrete is defined in Eurocode 2 [12]. Entfellner [13] adapted the parameters s and α1 to describe the behaviour of shotcrete. Nevertheless, this adaption is not valid for the very early stage within the first hours (see Figure 43).

$$f_{cm}(t) = \beta_{cc}(t) * f_{cm}$$ Eq. 13

with:

$$\beta_{cc}(t) = e^{\left\{ s* \left[1 - \left(\frac{28}{t} \right)^{\alpha 1} \right] \right\}}$$ Eq. 14

$f_{cm}(t)$ ....mean shotcrete compressive strength at t days [MPa] [12]
f_{cm} ....mean cylinder compressive strength at 28 days [MPa]
$\beta_{cc}(t)$ ....coefficient, depending on the shotcrete age [-] [13]
s ....cement hardening coefficient [-] [13]
t ....age of the shotcrete [d]
α1 ....exponent of the shotcrete strength [-] [13]
         (0.5 for standard concrete, adapt for shotcrete)

f_{cm} = 45 MPa
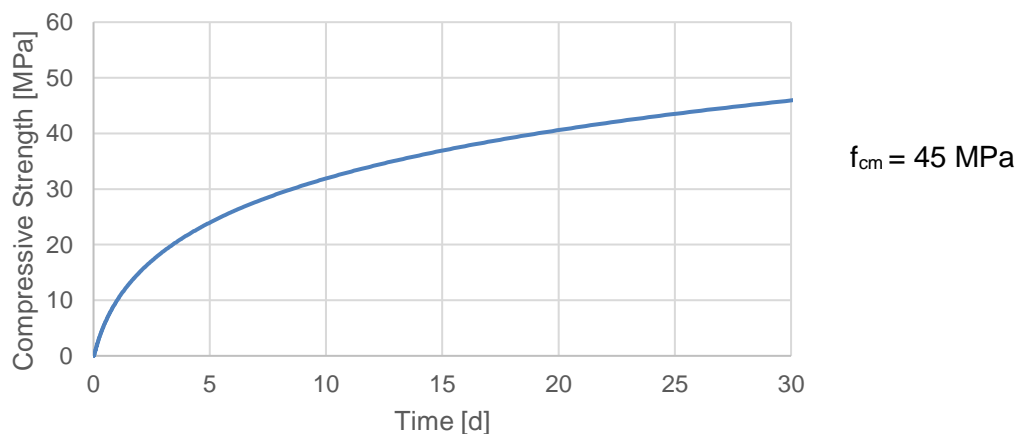
Figure 41: Time-dependant Compressive Strength acc. to [12]

6.1.1 Early Strength Development

The early strength development for the first 24 hours is defined in three classes according to the Austrian Society for Construction Technology: Guideline Sprayed Concrete [14].

- **Class J1** sprayed concrete is appropriate for application in thin layers on a dry surface. No structural requirements are to be expected in this type of sprayed concrete during the first hours after application.
- **Class J2** sprayed concrete is used in applications where thicker layers have to be achieved within short time. This type of sprayed concrete can be applied over head and is suitable even in difficult circumstances, e.g. in case of slight water inflow and immediate subsequent work steps like drilling and blasting.
- **Class J3** sprayed concrete is used in case of highly fragile rock or strong water inflow. Due it's rapid setting, more rebound occurs during the application and therefore, class J3 sprayed concrete is only used in special cases.
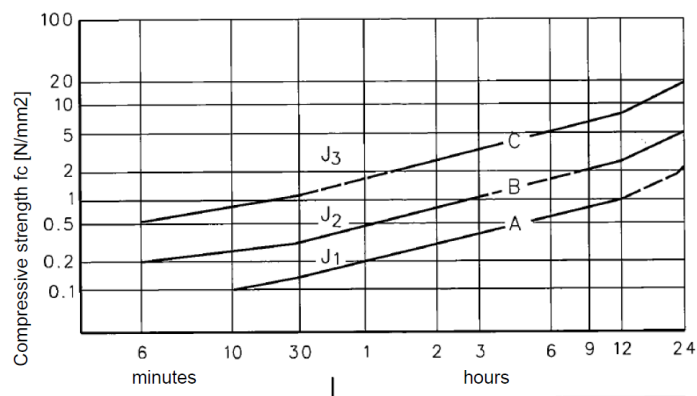
Figure 42: Early Strength Development acc. to [14]

The limit curves A, B, and C define the classes J1, J2 and J3. The usual classes applied in tunnelling are J2 and J3. The calculated strength development using Eurocode 2 [12] (Eq. 13) and Entfellner [13] (Eq. 14) cannot describe the proper compressive strength development in the very early stage (see Figure 43, $f_{cm}(t)$).
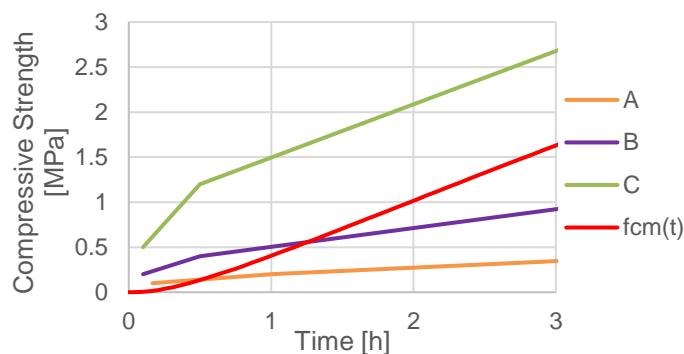
Figure 43: Early Strength Development acc. to Eq. 13 & Eq. 14

Test results on very young shotcrete samples, provided by BASF SE, have been used to describe the very early strength development $f_{cm}(t \leq 3\,h)$ with Eq. 15 & Eq. 16. This approximation of the very early strength development is valid for one certain mixture of the shotcrete. The fitting parameters used in Eq. 15 & Eq. 16 will probably differ if the shotcrete components are varied.

$$f_{cm}(t) = \frac{f_{cm}}{45} * [0.12 * \ln(t) + 1.15] \qquad\qquad t \leq 0.4\,h \qquad\qquad \text{Eq. 15}$$

$$f_{cm}(t) = \frac{f_{cm}}{45} * [0.59 * e^{10*t}] \qquad\qquad 0.4\,h < t \leq 3\,h \qquad\qquad \text{Eq. 16}$$

$f_{cm}(t)$ ....mean shotcrete compressive strength at t days [MPa]
f_{cm} ....mean cylinder compressive strength at 28 days [MPa]
t ....age of the shotcrete [d]
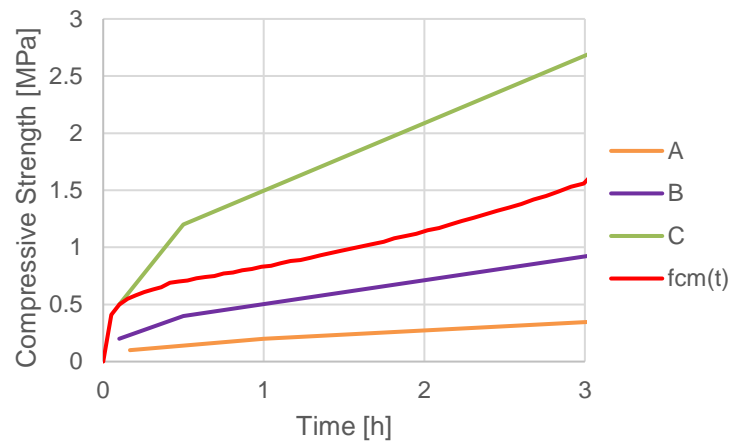
Figure 44: Adapted Early Strength Development acc. to Eq. 15 & Eq. 16

6.2 Time-dependent Stiffness

The time-dependant stiffness development is defined as the Elastic-Modulus in Eq. 17 from Entfellner [13].

$$E_{cm}(t) = \left(\frac{f_{cm}(t)}{f_{cm}}\right)^{\alpha 2} * E_{cm} \qquad\qquad \text{Eq. 17}$$

$E_{cm}(t)$ ....mean shotcrete E-modulus at t days [MPa] [13]
E_{cm}.................mean shotcrete E-modulus at 28 days [MPa]
$f_{cm}(t)$..............mean shotcrete compressive strength at t days [MPa]
f_{cm} ....mean cylinder compressive strength at 28 days [MPa]
α2 ....exponent of the shotcrete E-modulus [-] [13]
                    (0.3 for standard concrete; adapt for shotcrete)
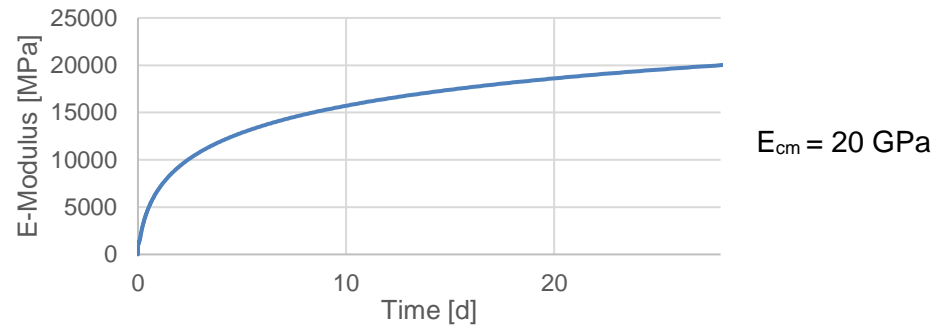
Figure 45: Time-dependant E-Modulus acc. to [13]

6.3 **Rheological Behaviour of Shotcrete**

In addition to the time dependent behaviour of the shotcrete, the rheological behaviour on the basics of the flow-rate-method (P. Schubert [15] and W. Aldrian [16]) should be considered as well. The stresses with a predefined strain behaviour [15] are calculated with Eq. 18.

$$\sigma_2 = \frac{\varepsilon_2 - \varepsilon_1 + \frac{\sigma_1}{E_{cm}(t)} + \varepsilon_{d,2} * \left[1 - e^{\left(\frac{-\Delta C(t)}{Q}\right)}\right] - \Delta\varepsilon_{sh} - \Delta\varepsilon_t}{\frac{1}{E_{cm}(t)} + \Delta C(t) + C_{d,\infty} * \left[1 - e^{\left(\frac{-\Delta C(t)}{Q}\right)}\right]}$$

Eq. 18

σ_i ....total stress in the lining at the end of timespan Δt_i [MPa]
ε_i ....total strain in the lining at the end of timespan Δt_i [-]
$E_{cm}(t)$ ....age-dependent E-modulus of shotcrete [MPa]
$\Delta C(t)$..............age-dependent change of viscous strain
$\varepsilon_{d,i}$ ....visco-elastic strain at the end of timespan Δt_i [-]
$\Delta\varepsilon_{sh}$................change of shrinkage strain [-]
$\Delta\varepsilon_t$.................change of temperature strain [-]
$C_{d,\infty}$ ....limit value of reversible creep deformation
Q ....creep-constant

All parameters in Eq. 18 are calculated with Eq. 19 to Eq. 23 and the used flow-rate-method parameters are provided from a current project (Semmering Base Tunnel, ÖBB), shown in Table 7.

Table 7: Used Flow-Rate-Method Parameters

Flow-Rate-Method Parameters		
A =	0.0000024	[-]
B =	10	[-]
Q =	0.0000221	[-]
Cd,oo =	0.000214	[-]
εsh,oo =	0.000974	[-]

Stresses are back calculated using ultimate strains at shotcrete lining failure (provided from Semmering Base Tunnel) with Eq. 18. These stresses are used for the flow-rate-method calculation (Eq. 19 - Eq. 23).

$$\varepsilon_2 = \varepsilon_1 + \frac{\sigma_2 - \sigma_1}{E_{(t)}} + \sigma_2 * \Delta C(t) + \Delta \varepsilon_{sh} + \Delta \varepsilon_t \qquad \text{Eq. 19}$$

ε_i ....total strain in the lining at time t_i [-]
σ_i ....total stress in the lining at time t_i [MPa]
$E(t)$ ....age-dependent E-modulus of shotcrete [MPa]
$\Delta C(t)$..............age-dependent change of viscous strain
$\Delta \varepsilon_{sh}$................change of shrinkage strain [-]
$\Delta \varepsilon_t$.................change in temperature strain [-] [16]

$$C(t) = A * (t_h - t_1)^{0,25} \qquad \text{Eq. 20}$$

$C(t)$ ....time-dependent trend of irreversible viscous strain [16]
A....................flow-parameter [-]
t_h....................age of the shotcrete [h]
t_1....................age of the shotcrete at the beginning of the loading [h]
            (load starts with excavation of next round)

$$\varepsilon_{sh} = \varepsilon_{sh\infty} * \frac{t}{B + t} \qquad \text{Eq. 21}$$

ε_{sh} ....shrinkage strain [-] [15]
$\varepsilon_{sh\infty}$................limit value of shrinkage strain [-]
B....................shrinkage-constant
t ....age of shotcrete in days [d]
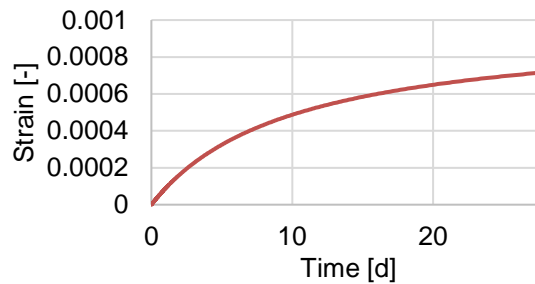
Figure 46: Shrinkage Strain

$$\varepsilon_t = (- \cos(t^{0.25} * 113) + 1) * 30 * 10^{-6} \qquad \text{Eq. 22}$$

ε_t....................temperature strain [-] [16]
t....................age of shotcrete in hours [h]
- temperature strain ε_t just appears in the first four days after applying the shotcrete
- $-\cos(t^{0.25} * 113)$ must be inserted in [rad]
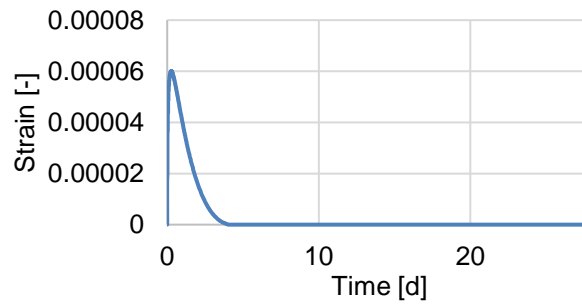
Figure 47: Temperature Strain

$$\varepsilon_{d,2} = \left(\sigma_1 * C_{d\infty} - \varepsilon_{d,1}\right) * \left[1 - e^{\frac{-\Delta C(t)}{Q}}\right] + \varepsilon_{d,1}$$ Eq. 23

$\varepsilon_{d,i}$ .... visco-elastic strain at the end of timespan Δt_i [-] [15]
σ_i .... total stress in the lining at end of timespan Δt_i [MPa]
$C_{d\infty}$ .... limit value of reversible creep deformation
$\Delta C(t)$ .... age-dependent change of viscous strain
Q .... creep-constant
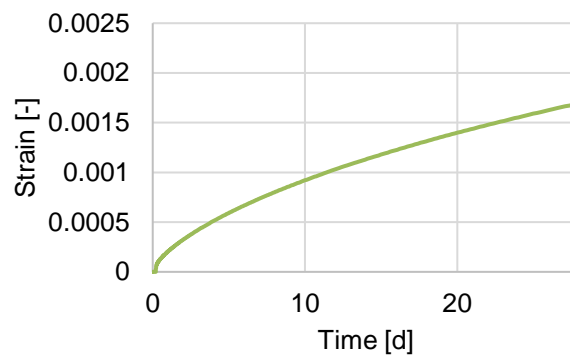
Figure 48: Visco-Elastic Strain

For the determination of the function parameters a quotaion from Entfellner [13] is used:

"The last long-term tests on shotcrete in Austria have been performed at the beginning of the 1990's, about 25 years ago. Ever since the constituents, mix composition and production of the shotcrete significantly changed. Hence, an adjustment of the flow-rate parameters (A, B, Q, $C_{d\infty}$, $\varepsilon_{sh\infty}$) is necessary. For the thesis, this was done for a shotcrete SpC 25/30 J2, based on a detailed displacement monitoring and visual observation of the support at a specific monitoring section at the Semmering Base Tunnel. Since the moment when first cracks in the lining occurred ($\triangleq$ μ = 100 % utilization) and strains at that time are known, these parameters could be roughly back-calculated. For an accurate determination, further laboratory tests are necessary." [13]

6.4 **Deformation of the Rock Mass**

To predict the radial deformation of the surrounding rock mass according the project based data, the Convergence-Law of Sulem et al. [17] need to be applied (see Eq. 24). The equation consists out of a time-dependent and a time-independent part [17].

$$C(x,t) = C_{\infty,x} * \left[1 - \left(\frac{X}{x+X}\right)^2\right] * \left\{1 + m * \left[1 - \left(\frac{T}{T+t}\right)^{0,3}\right]\right\}$$

Eq. 24

C(x,t) ....face- & time-dependent radial displacement [mm]
$C_{x\infty}$ ....ultimate time-independent radial displacement [mm]
                      ($\neq$ final displacement!)
X ....curve-fitting parameter [m]
                      (describes the influence length of time-independent
                      displacements)
m ....ratio of ultimate time-dependent displacements and
                      time-independent displacements [-]
T ....curve-fitting parameter [d]
                      (describes how fast time-dependent displacements develop)
x ....distance between monitoring section and current excavation
                      face [m] (function of advance rate)
t ....elapsed time since excavation of the round where the
                      monitoring section is located [d]
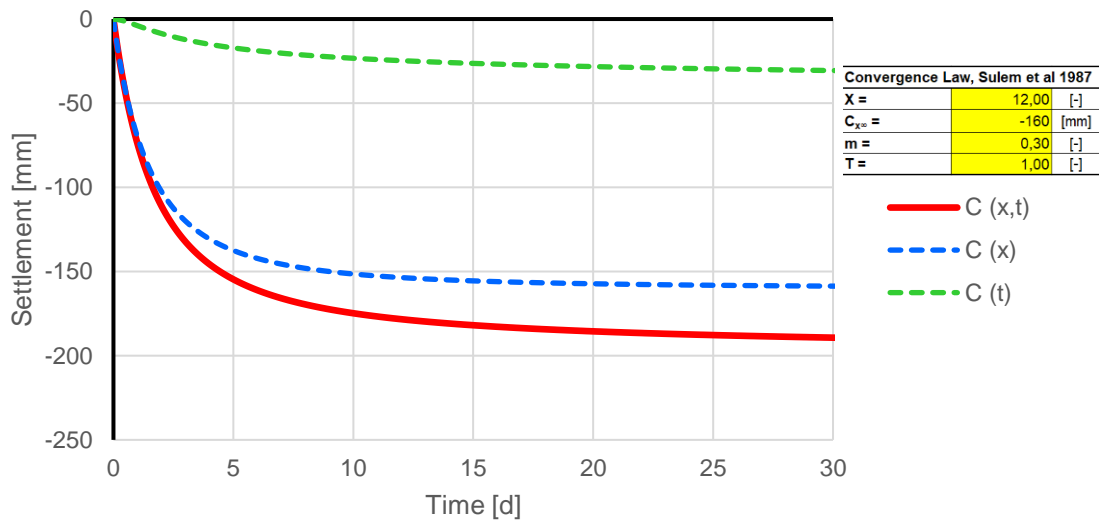
Figure 49:Convergence Law

For the further calculation of the shotcrete utilization, it is necessary to calculate the tangential deformation of the rock mass, which has been done with Eq. 25.

$$u_{tan}(t) = C(x,t) * 2 * \pi$$

Eq. 25

u_{tan}(t)..............face- & time-dependent tangential displacement [mm]
C(x,t) ....face- & time-dependent radial displacement [mm]

6.5 **Shortening per Gap**

For the calculation of the shortening per gap, a simple approach of a full-face excavation with a circular tunnel shape has been considered. Therefore, the circumference of the shotcrete is calculated with Eq. 26.

$$l_{SpC} = D * \pi - h_{Gap} * n_{Gap}$$

Eq. 26

> D....................tunnel diameter [m]
> l_{SpC} ....circumference of the shotcrete lining [m]
> h_{Gap} ....height of the gap [m]
> n_{Gap} ....number of gaps [-]
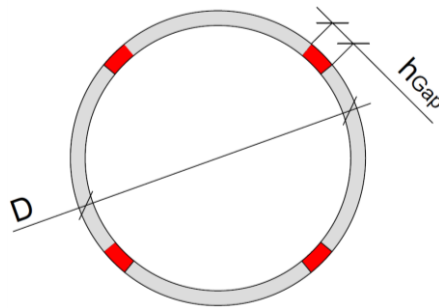
Figure 50: Circumference of the shotcrete lining

The radial strain of the shotcrete according to it's rheological behaviour can be calculated with Eq. 27.

$$e_{SpC}(t) = \varepsilon(t) * l_{SpC}$$

Eq. 27

> $e_{SpC}(t)$ ....time dependent radial deformation of the shotcrete [m]
> $\varepsilon(t)$ ....time dependent radial strain of the shotcrete [-]
> l_{SpC} ....circumference of the shotcrete lining [m]

To compute the shortening of the gap, Eq. 28 must be applied.

$$u_{Gap}(t) = \frac{u_{tan}(t) - e_{SpC}(t)}{n_{Gap}}$$

Eq. 28

> $u_{Gap}(t)$.............time dependent shortening of the gap [m]
> $u_{tan}(t)$..............face- & time-dependent tangential displacement [m]
> $e_{SpC}(t)$ ....time dependent radial strain of the shotcrete [m]
> n_{Gap} ....number of gaps [-]

6.6 **Utilization**

By applying a yielding element with its special force-shortening behaviour, the force depending on its according shortening of the gap can be calculated with Eq. 29.

$$F_{YE}(t) = f(u_{Gap})$$
<div align="right">Eq. 29</div>

$F_{YE}(t)$..............time dependent force of the yielding element [MN]
$u_{Gap}(t)$............time dependent shortening of the gap [m]

The tolerable force is calculated with Eq. 30.

$$F_{tol}(t) = \frac{\sigma(t) * (d_{SpC} * b_{Gap})}{\gamma_c}$$
<div align="right">Eq. 30</div>

$F_{tol}(t)$ ....time dependent tolerable force [MN]
$\sigma(t)$................time dependent shotcrete strength acc.to Eq. 13 - Eq. 16 [MPa]
d_{SpC}................thickness of the shotcrete lining [m]
b_{Gap}................wideness of the gap [m]
γ_c...................factor of safety for shotcrete [-]

Finally, the shotcrete utilization is calculated with Eq. 31 and is visualized in Figure 51 for one certain case.

$$\mu(t) = \frac{F_{YE}(t)}{F_{tol}(t)}$$
<div align="right">Eq. 31</div>

$\mu(t)$.................time dependent shotcrete utilization [-]
$F_{YE}(t)$..............time dependent force of the yielding element [MN]
$F_{tol}(t)$ ....time dependent tolerable force [MN]
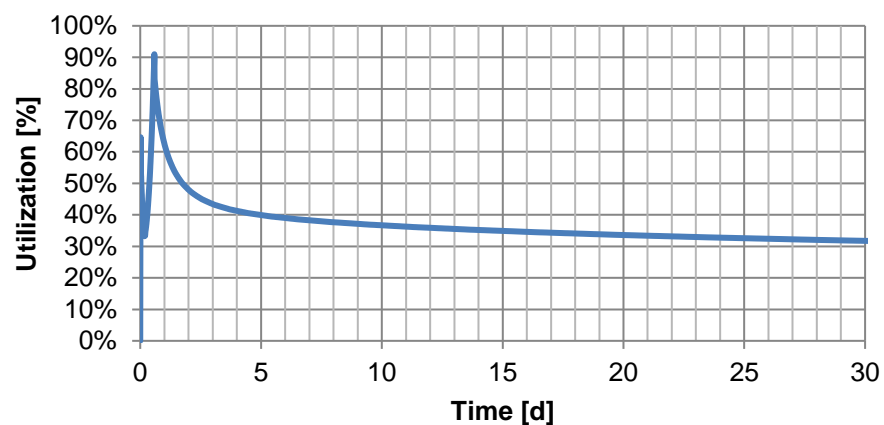
Figure 51: Shotcrete Utilization

6.7 **Case Study – SBT 1.1 - Gloggnitz**

With the project based data it is possible to calculate the shotcrete lining utilization. For this example, the data from the Semmering Base Tunnel (SBT) of the construction lot SBT 1.1 Gloggnitz was used. These data sets (see Table 8), which have been kindly provided by the Austrian Federal Railways (ÖBB), should describe the deformation behaviour for a certain rock mass.

Table 8: Input Parameter

Tunnel Advance			
r	5	[m]	Tunnel Radius
a	4	[m/d]	Advance Rate
l_{rl}	1.2	[m]	Round Length
b_{LG}	0.2	[m]	Latice Girder Width
b_{Gap}	1	[m]	Gap Width
t_{rl}	5	[h]	Time per Round
t_{SpB}	3	[h]	Time between applying SpC and next Excavation
x_{end}	300	[m]	Max Face Distance for calculation progress

Shotcrete - SpC			
d	25	[cm]	SpC Thickness
β_{28}	40	[MPa]	SpC Strength - 28 days
s	1.15	[-]	Cement Hardening Coefficient
α_1 (f_{cm}) =	0.240	[-]	Exponent of SpC Strength
E_{28} =	20000.00	[MPa]	E-Modulus - 28 days
α_2 (E_{cm}) =	0.70	[-]	Exponent of SpC E-Modulus
γC =	1	[-]	Factor of Safety - SpC

Gap			
n_{Gap}	2	[-]	Number of Gaps
h_{Gap}	40	[cm]	Gap Height
l_{SpC}	30.62	[m]	Shotcrete Circumference

LSC-N Design			
ε_{Peak} =	9%	[%]	Target First Peak Shortening [%]
H_{YE}=	400	[mm]	Yielding Element Height [mm]
H_{inlay}=	62.13	[mm]	Target Inlay Height [mm]
n_{YE} =	3	[-]	Number of Pipes/Element [-]

Convergence Law, Sulem et al 1987			
X =	15.00	[-]	curve fitting parameter describing the shape of C1(x)
$C_{x\infty}$ =	-75	[mm]	max time independent settlement
m =	0.20	[-]	Constant ~Ct/Cx [0.2-0.8]
T =	1.20	[-]	curve fitting parameter describing the shape of C2(t)

Flow-Rate-Method Parameters			
A	0.0000024	[…]	Creep Constant
B	10	[d]	Shrinkage Constant
Q	0.0000221	[1/MPa]	Reversible Creep Constant
$C_{d,oo}$	0.000214	[1/MPa]	Boundary Value of the Creep Constant
$\varepsilon sh,_{oo}$	0.000974	[-]	Final Shrinkage

6.7.1   Results

The input parameters lead to the following radial displacements according Sulem et al [17] (see Figure 52).
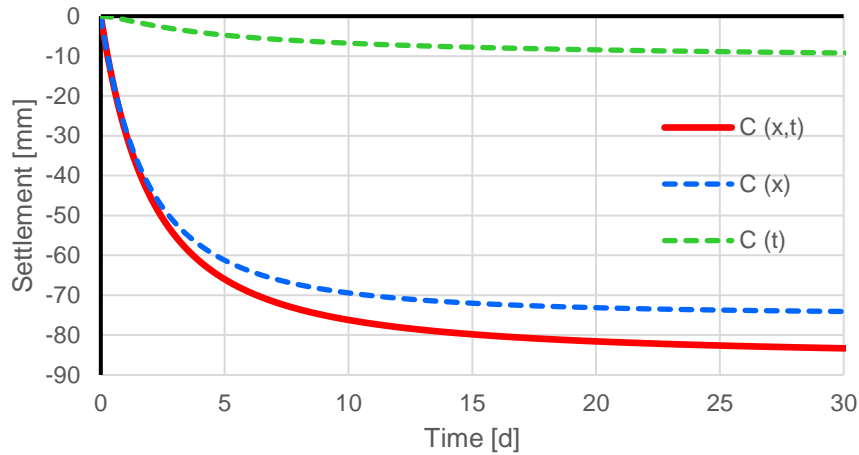
Figure 52: Radial Displacement acc. [17]

The result shows, that the used yielding elements fulfil the requirement that the shotcrete lining will not fail under this circumstances (see Figure 53 and Figure 54).
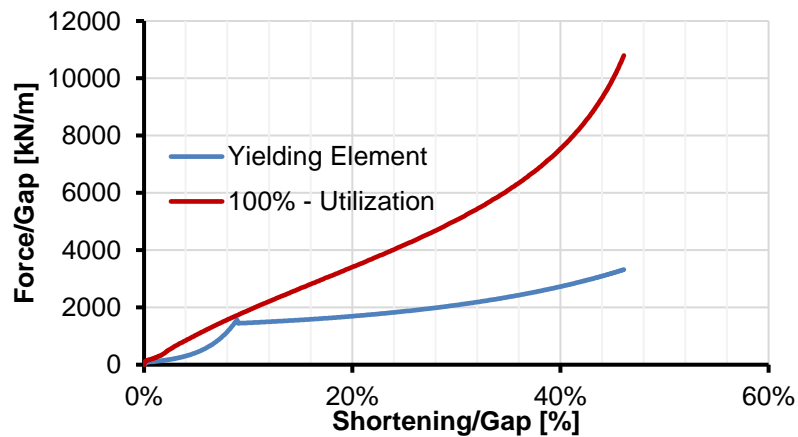
Figure 53: Force-Shortening behaviour of the yielding element (blue) and tolerable Force-Shortening behaviour of the shotcrete lining (red)
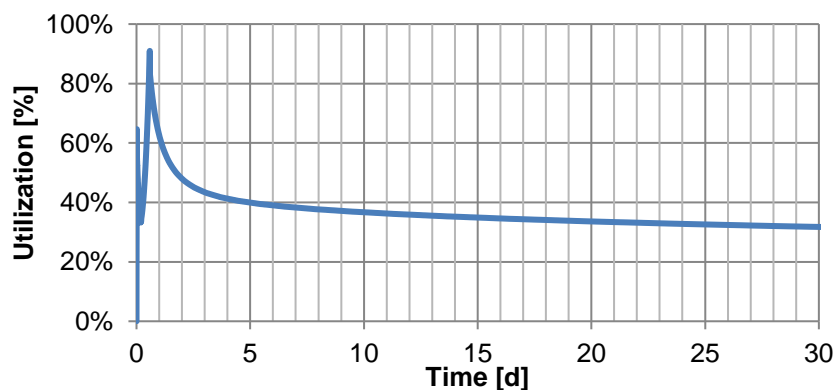
Figure 54: Shotcrete Lining Utilization

7 Conclusion

The aim of this thesis was to find a suitable yielding element which fulfils the requirements of a tender for a current construction lot. A newly developed yielding element (LSC-N) consists of steel pipes with a certain material behaviour which are filled with a porous material to provide a smooth force-shortening behaviour. An adjusted inlay provides an appropriate stiffness in the initial state. In contrast to the former LSC, possible asymmetrical buckling does not affect the overall force-shortening performance. The LSC-N yielding elements require a relatively small amount of steel. This leads to a decrease in weight, which simplifies the installation process on the construction site. The force-shortening behaviour of this new yielding element can be adapted for the required boundary conditions. Installed LSC-N elements at the Semmering Base Tunnel showed that these improvements meet the requirements, and the elements are easily installed.

Furthermore, a mathematical description of the force-shortening behaviour of the yielding element was developed to design the layout of the yielding elements, according to the project requirements. All together 26 design relevant input parameters are used in the calculation for dimensioning the ductile support.

Possible variables, like the pipe diameter, the wall thickness and the type of steel are not taken into account yet. More test series would be required to show the influence of such parameters.

8 References

[1] L. v. Rabcewicz, "Die Hilfsgewölbebauweise," Graz University of Technology, Graz/Austria, 1950.

[2] W. Schubert, J. Golser and P. Schwab, "Weiterentwicklung des Ausbaues für stark druckhaftes Gebirge," Felsbau 14, Nr.1, p. 36-42., 1996.

[3] B. Moritz, "Ductile Support System for Tunnels in Squeezing Rock," PhD Thesis, Institute of Rock Mechanics and Tunnelling, Graz University of Technology, Graz/Austria, 1999.

[4] M. Sitzwohl, "Optimierung der Lining Stress Controller durch zementgebundene poröse Füllung," Master's Thesis, Institute of Rock Mechanics and Tunnelling, Graz University of Technology, Graz/Austria, 2011.

[5] M. Verient, "Investigation on telescope yielding elements with porous filling," Master's Thesis, Institute of Rock Mechanics and Tunnelling, Graz University of Technology, Graz/Austria, 2014.

[6] S. Brunnegger, "Optimierung der Lining Stress Controller (LSC)," Bachelor's Project, Institute of Rock Mechanics and Tunnelling, Graz University of Technology, Graz/Austria, 2016.

[7] W. Schubert, M. Blümel, R. Staudacher and S. Brunnegger, "Support aspects of tunnels in fault zones," Geomechanics and Tunnelling, vol. 10, no. 4, Graz/Austria, 2017.

[8] B. Moritz, "Trotz widrigster Bedingungen und gröbster Sichteinschränkung den Durchschlag geschafft," Wulfsche Presse, 25 Jahre FMT-Institut (interne Veröffentlichung des Instituts), Graz/Austria, 2017.

[9] N. Radončić, "Tunnel design and prediction of system behaviour in weak ground," PhD Thesis, Institute of Rock Mechanics and Tunnelling, Graz University of Technology, Graz/Austria, 2011.

[10] SZ Schacht- und Streckenausbau GmbH, "Nachgiebigkeitselement". Germany Patent DE 20 2014 000 435 U1, 1 4 2015.

[11] N. Radončić, W. Schubert and B. Moritz, "Ductile support design," Geomechanics and Tunnelling 2, No. 5, p. 561-577, Graz/Austria, 2009.

[12] "ÖNORM EN 1992-1-1: Bemessung und Konstruktion von Stahlbeton-und Spannbetontragwerken. Teil 1-1: Allgemeine Bemessungsregeln und Regeln für den Hochbau," 2015.

[13] M. Entfellner, "Prediction of Displacements and Shotcrete Lining Utilization," Master's Thesis, Institute of Rock Mechanics and Tunnelling, Graz University of Technology, Graz/Austria, 2017.

[14] Austrian Society for Construction Technology, "Guideline Sprayed Concrete: Edition 2009," Austrian Society for Construction Technology, Vienna/Austria, 2009.

[15] P. Schubert, "Beitrag zum rheologischen Verhalten von Spritzbeton," Felsbau, vol. 6, no. 3, Page 150-153, 1988.

[16] W. Aldrian, "Beitrag zum Materialverhalten von früh belastetem Spritzbeton," PhD Thesis, Montanuniversität Leoben, Leoben/Austria, 1991.

[17] J. Sulem, A. Panet and A. Guenot, "Closure Analysis in Deep Tunnels," Int. J. Rock Mech. Min. Sci. & Geomech., vol. 24, no. 3, pp. 145-154, 1987.

Appendix

Laboratory Tests

The laboratory tests were carried out in the laboratory at the Institute of Rock Mechanics and Tunnelling at Graz University of Technology.

To simulate the deformation in the shotcrete gap, the test procedure of a uniaxial compressive test was executed with a displacement rate of 2mm/min. In Figure 55 a typical test set-up is shown.

Figure 55: Test set-up [5]

According to the tender documents of the Semmering Base Tunnel two different force-shortening boundaries called type I (red lines) and type II (blue lines) are defined.
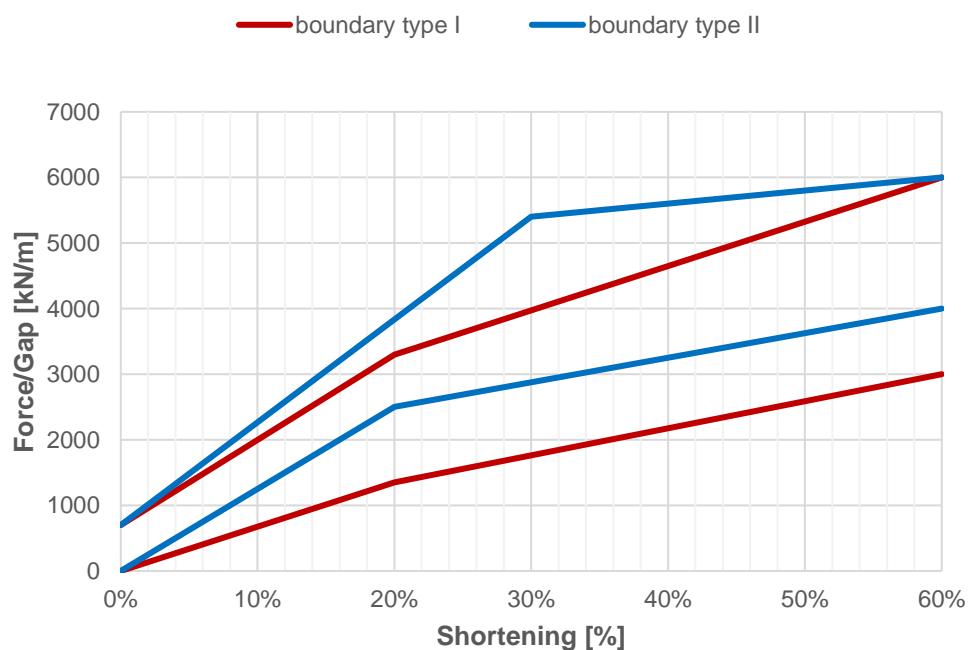
Figure 56: Tender of a current project

Table 9: Summary of the lab tests

Lab test name	Filling material	Inner pipe, steel quality, dimension	Outer pipe, steel quality, dimension	Height [mm]	Inlay
Test1,9m_1,6	D1,6	34CrMo4 133x2x370	DD 11 140x2x50	380	-
Test2,0m_1,5	D1,5	34CrMo4 133x2x370	DD 11 140x2x50	380	-
2_D1,5	D1,5	E235+SR 133x2x370	DD 11 140x2x50	380	-
4_D1,55	D1,55	E235+SR 133x2x370	DD 11 140x2x50	380	-
6_D1,6	D1,6	34CrMo4 133x2x370	DD 11 140x2x50	380	-
3_D1,6	D1,6	S235+N 133x2.5x370	DD 11 140x2x50	380	-
2_D1,55	D1,55	S235+N 133x2.5x370	DD 11 140x2x50	380	-
5_D1,55_Y_5,0	D1,55	E235+SR 133x2x370	DD 11 140x2x50	420	4 cm porous inlay 5 MPa
4_D1,6_Y_5,0	D1,6	S235+N 133x2.5x370	DD 11 140x2x50	420	4 cm porous inlay 5 MPa
1_D1,55_Y_5,0	D1,55	S235+N 133x2.5x370	DD 11 140x2x50	420	4 cm porous inlay 5 MPa
1_D1,55_4cm_Y	D1,55	S235+N 133x2.5x360	DD 11 140x2x50	410	4 cm porous inlay 5 MPa
2_D1,55_4cm_Y	D1,55	S235+N 133x2.5x360	DD 11 140x2x50	410	4 cm porous inlay 5 MPa
4_D1,55_2cm_Y	D1,55	S235+N 133x2.5x380	DD 11 140x2x50	410	2 cm porous inlay 5 MPa
3_D1,55_6cm_Y	D1,55	S235+N 133x2.5x340	DD 11 140x2x70	410	6 cm porous inlay 5 MPa
D_1,55_7cm_Y_ Bohrung	D1,55	S235+N 133x2.5x330	DD 11 140x2x80	410	7 cm porous inlay 5 MPa 32 mm borehole
Botament_7cm_Y_ Bohrung57	Botament 1,55	S235+N 133x2.5x330	DD 11 140x2x80	410	7 cm porous inlay 5 MPa 57 mm borehole
Botoment1,37_7cm_Y	Botament 1,37	S235+N 133x2.5x330	DD 11 140x2x80	410	7 cm porous inlay 5 MPa
D1,37_7cm_Y	D1,37	S235+N 133x2.5x330	DD 11 140x2x80	410	7 cm porous inlay 5 MPa
Liapor4_8_WZ0,75	-	34CrMo4 133x2.5x370	DD 11 140x2x50	380	-

Lab Test "Test1,9m_1,6"

The filling material has been estimated with a density of 1.6 kg/dm³. The boundaries refer to the tender documents of the Semmering Base Tunnel (see Figure 56).

Table 10: Specifications "Test1,9m_1,6"

Filling material	Mass percentage		Inner pipe, steel quality, dimension	Outer pipe, steel quality, dimension	Inlay
D1,6	35.19%	CEM II/B-M (S-L) 32.5 N	34CrMo4 133x2x370	DD 11 140x2x50	-
	9.86%	Liapor 1-4 mm			
	38.48%	Sand 0-2 mm			
	0.47	W/C-ratio			

Figure 57: before/after "Test1,9m_1,6"   Figure 58: Scheme "Test1,9m_1,6"
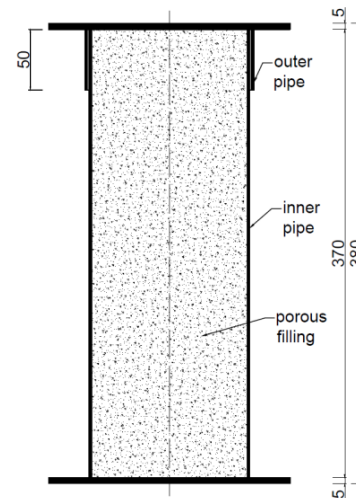
Type I: The force-shortening curve shows at the beginning a steep increase and intersects the upper boundary at a shortening of ~0.4% and an axial force of ~800 kN. The first peak appears at ~2% shortening and an axial force of ~2000 kN. At a shortening of ~10% and an axial force of ~2000 kN the force-shortening curve lies within the specified range. From this point the force-shortening curve shows a quasi-constant behaviour until an axial force of ~3200 kN and a shortening of ~39% is reached.

Type II: The force-shortening curve shows at the beginning a steep increase and intersects the upper boundary at a shortening of ~0.4% and an axial force of ~800 kN. The first peak appears at ~2% shortening and an axial force of ~2000 kN. At a shortening of ~9% and an axial force of ~2000 kN the force-shortening curve lies within the specified range until it intersects the lower boundary at an axial force of ~2200 kN and a shortening of ~17%. From this point the force-shortening curve shows a quasi-constant behaviour until an axial force of ~3200 kN and a shortening of ~39% is reached.

Force-Shortening behaviour
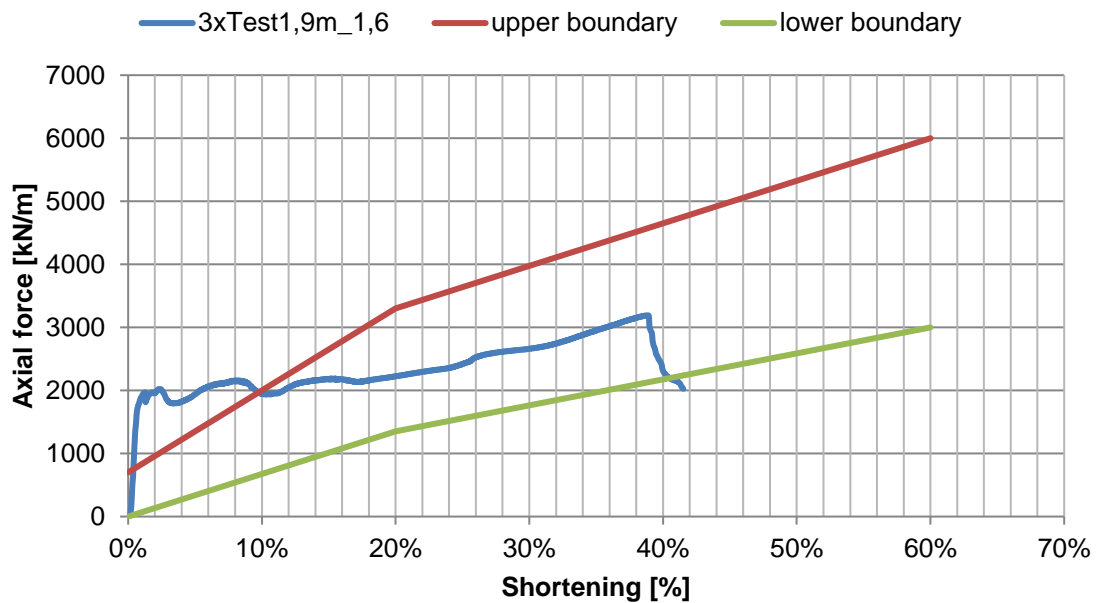
Figure 59: Force-Shortening behaviour "Test1,9_1,6" Type I

Force-Shortening behaviour
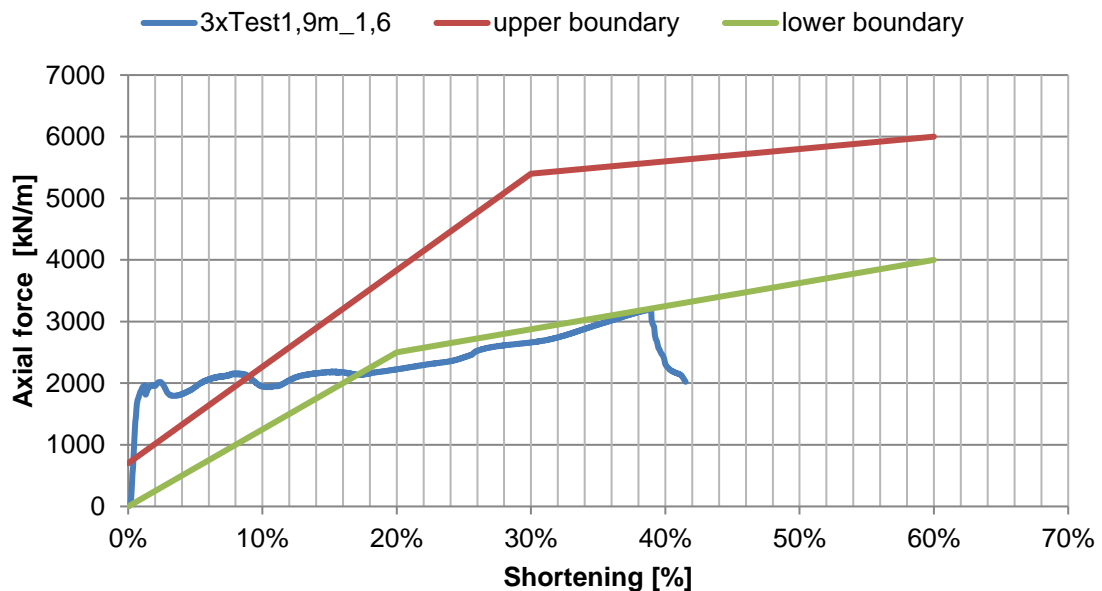
Figure 60: Force-Shortening behaviour "Test1,9_1,6" Type II

The steep increase at the beginning relates to the direct contact of the inner pipe with its filling material and the endplate. The decrease of the force-shortening curve at ~39% shortening relates to the increase of the inner pressure which leads to bursting of the inner pipe.

Lab Test "Test2,0m_1,5"

The filling material has been estimated with a density of 1.5 kg/dm³. The boundaries refer to the tender documents of the Semmering Base Tunnel (see Figure 56).

Table 11: Specifications "Test2,0m_1,5"

Filling material	Mass percentage		Inner pipe, steel quality, dimension	Outer pipe, steel quality, dimension	Inlay
D1,5	32.87%	CEM II/B-M (S-L) 32,5 N	34CrMo4 133x2x370	DD 11 140x2x50	-
	14.52%	Liapor 1-4 mm			
	35.94%	Sand 0-2 mm			
	0.51	W/C-ratio			

Figure 61: before/after "Test2,0m_1,5"   Figure 62: Scheme "Test2,0m_1,5"
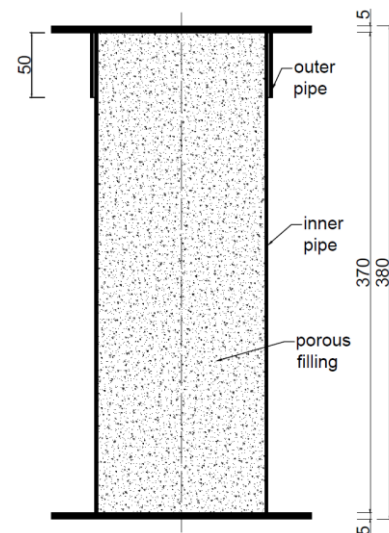
Type I: The force-shortening curve shows at the beginning a steep increase and intersects the upper boundary at a shortening of ~0.4% and an axial force of ~800 kN. The first peak appears at ~1.8% shortening and an axial force of ~2000 kN. Then the force-shortening curve shows an oscillating behaviour along the upper boundary. At a shortening of ~10% the force-shortening curve lies between the upper and lower boundary until ~32% shortening with an axial force of ~ 3200 kN is reached:

Type II: The force-shortening curve shows at the beginning a steep increase and intersects the upper boundary at a shortening of ~0.4% and an axial force of ~800 kN. The first peak appears at 1.8% shortening and an axial force of ~2000 kN. Then the force-shortening curve shows an oscillating behaviour along the upper boundary. At a shortening of ~18% the force-shortening curve lies between the upper and lower boundary until ~32% shortening with an axial force of ~ 3200 kN is reached:

Force-Shortening behaviour
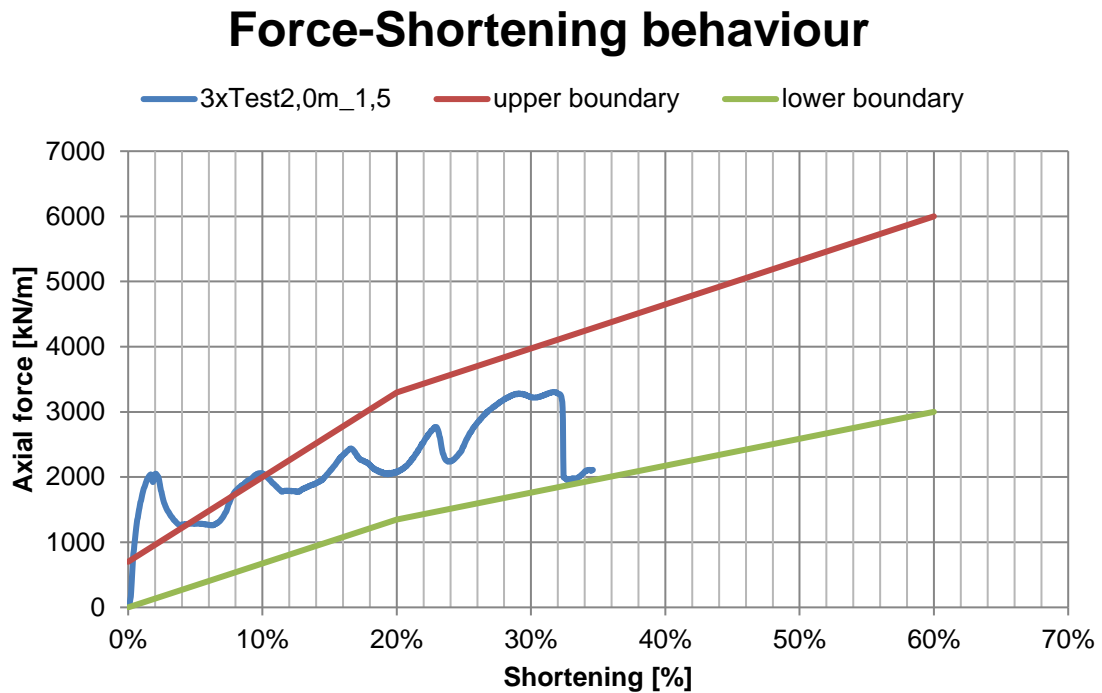
Figure 63: Force-Shortening behaviour "Test2,0_1,5" Type I

Force-Shortening behaviour
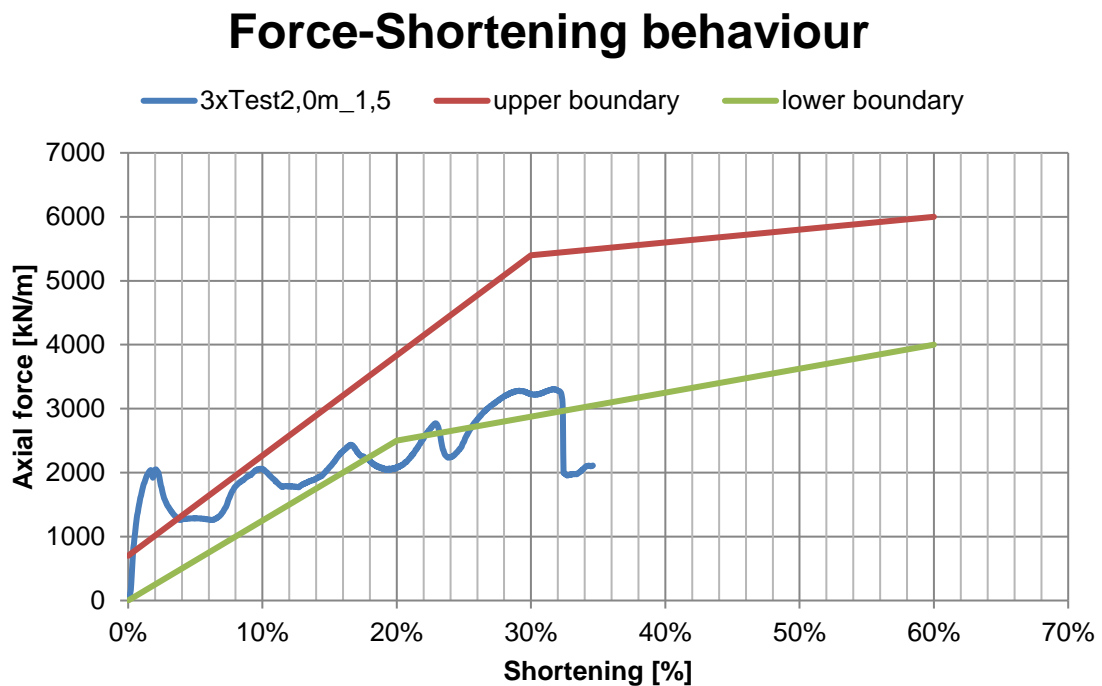
Figure 64: Force-Shortening behaviour "Test2,0_1,5" Type II

The steep increase at the beginning relates to the direct contact of the inner pipe with its filling material and the endplate. The decrease of the force-shortening curve at ~32% shortening relates to the increase of the inner pressure which leads to bursting of the inner pipe.

Lab Test "2_D1,5"

The filling material has been estimated with a density of 1.5 kg/dm³. The boundaries refer to the tender documents of the Semmering Base Tunnel (see Figure 56).

Table 12: Specifications "2_D1,5"

Filling material	Mass percentage		Inner pipe, steel quality, dimension	Outer pipe, steel quality, dimension	Inlay
D1,5	32.87%	CEM II/B-M (S-L) 32,5 N	E235+SR 133x2x370	DD 11 140x2x50	-
	14.52%	Liapor 1-4 mm			
	35.94%	Sand 0-2 mm			
	0.51	W/C-ratio			

Figure 65: before/after "2_D1,5"   Figure 66: Scheme "2_D1,5"
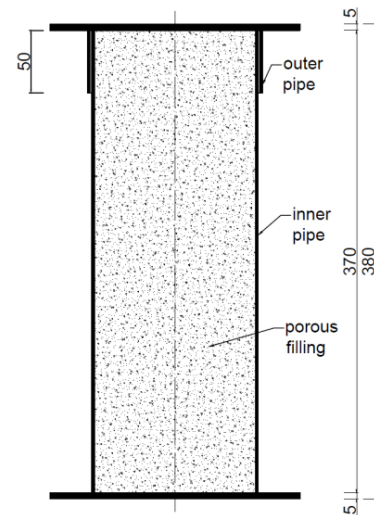
Type I: The force-shortening curve shows at the beginning a steep increase and intersects the upper boundary at a shortening of ~0.4% and an axial force of ~800 kN. The first peak appears at ~1.5% shortening and an axial force of ~1350 kN. After that the force-shortening curve shows an oscillating behaviour until ~26% shortening, where it intersects the lower boundary at a shortening of ~20%. From this point the force-shortening curve shows a quasi-constant behaviour until an axial force of ~4500 kN and a shortening of ~52% is reached.

Type II: The force-shortening curve shows at the beginning a steep increase and intersects the upper boundary at a shortening of ~0.4% and an axial force of ~800 kN. The first peak appears at ~1.5% shortening and an axial force of ~1350 kN. After that the force-shortening curve shows an oscillating behaviour until ~26% shortening, where it intersects the lower boundary at a shortening of ~8.5%. From this point the force-shortening curve shows a quasi-constant behaviour and it intersects the lower boundary again, until an axial

force of ~3200 kN and a shortening of ~39% is reached.

Force-Shortening behaviour
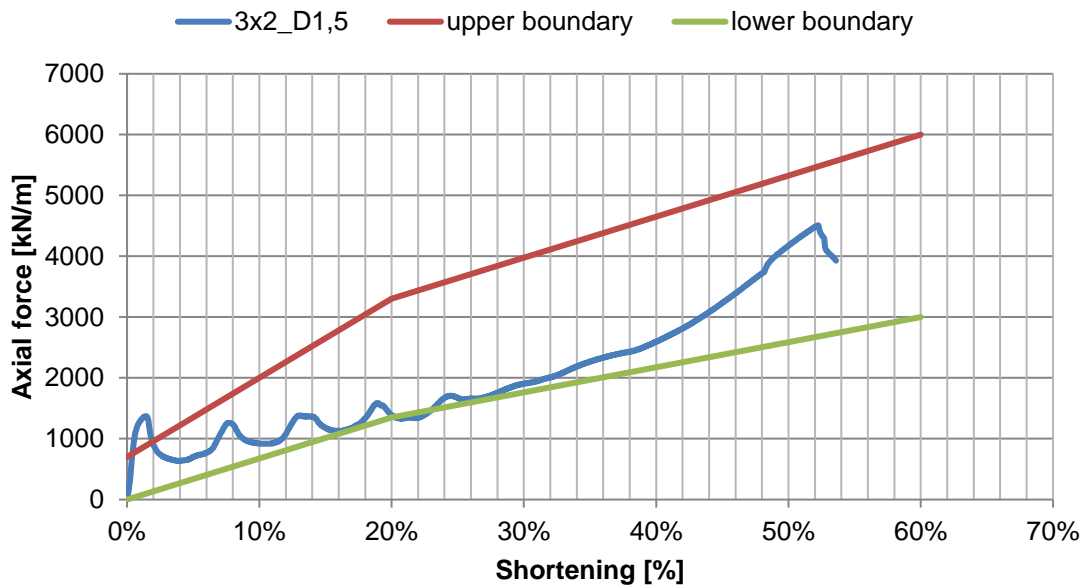
Figure 67: Force-Shortening behaviour "2_D1,5" Type I

Force-Shortening behaviour
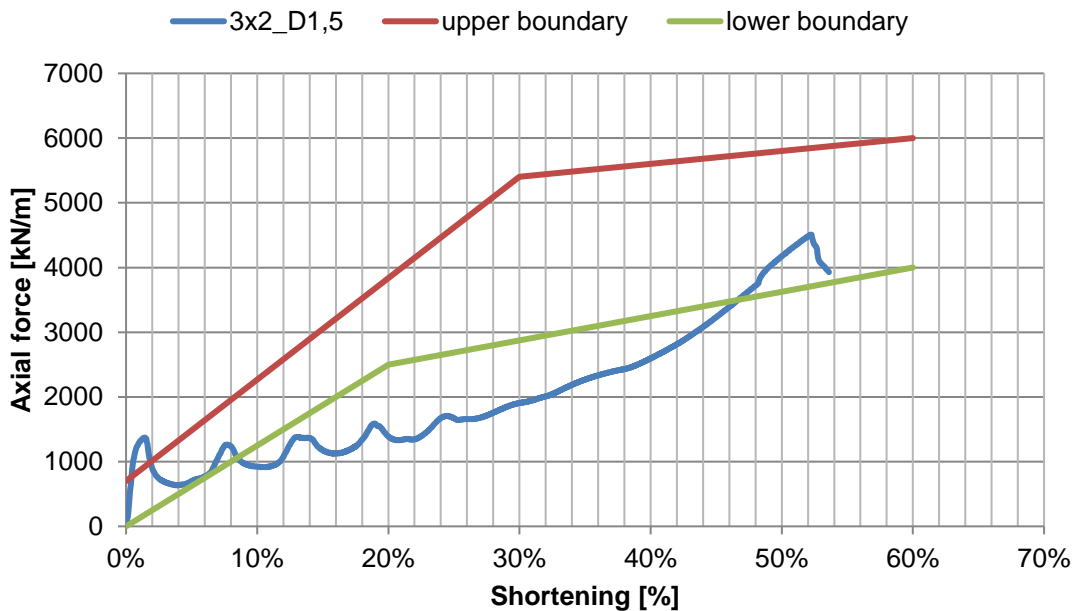
Figure 68: Force-Shortening behaviour 2_D1,5 Type II

The steep increase at the beginning relates to the direct contact of the inner pipe with its filling material and the endplate. The decrease of the force-shortening curve at ~52% shortening relates to the increase of the inner pressure which leads to bursting of the inner pipe.

Lab Test "4_D1,55"

The filling material has been estimated with a density of 1.55 kg/dm³. The boundaries refer to the tender documents of the Semmering Base Tunnel (see Figure 56).

Table 13: Specifications "4_D1,55"

Filling material	Mass percentage		Inner pipe, steel quality, dimension	Outer pipe, steel quality, dimension	Inlay
D1,55	34.03%	CEM II/B-M (S-L) 32,5 N	E235+SR 133x2x370	DD 11 140x2x50	-
	12.19%	Liapor 1-4 mm			
	37.21%	Sand 0-2 mm			
	0.49	W/C-ratio			

Figure 69: before/after "4_D1,55"
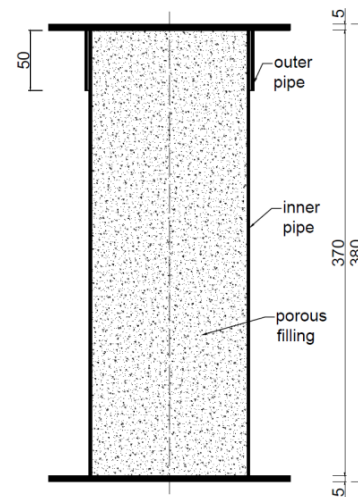
Figure 70: Scheme "4_D1,55"

Type I: The force-shortening curve shows at the beginning a steep increase and intersects the upper boundary at a shortening of ~0.8% and an axial force of ~800 kN. The first peak appears at ~2% shortening and an axial force of ~1300 kN. After that the force-shortening curve shows an oscillating behaviour until ~22% shortening, where it goes along and intersects the lower boundary at a shortening of ~16%. From this point the force-shortening curve shows a quasi-constant behaviour until an axial force of ~3750 kN and a shortening of ~48% is reached.

Type II: The force-shortening curve shows at the beginning a steep increase and intersects the upper boundary at a shortening of ~0.8% and an axial force of ~800 kN. The first peak appears at ~2% shortening and an axial force of ~1300 kN. After that the force-shortening curve shows an oscillating behaviour until ~22% shortening, where it intersects the lower boundary at a shortening of ~8.5%. From this point the force-shortening curve shows a quasi-constant behaviour and it intersects the lower boundary again, until an axial

force of ~3750 kN and a shortening of ~48% is reached.

Force-Shortening behaviour

Figure 71: Force-Shortening behaviour „4_D1,55" Type I

Force-Shortening behaviour
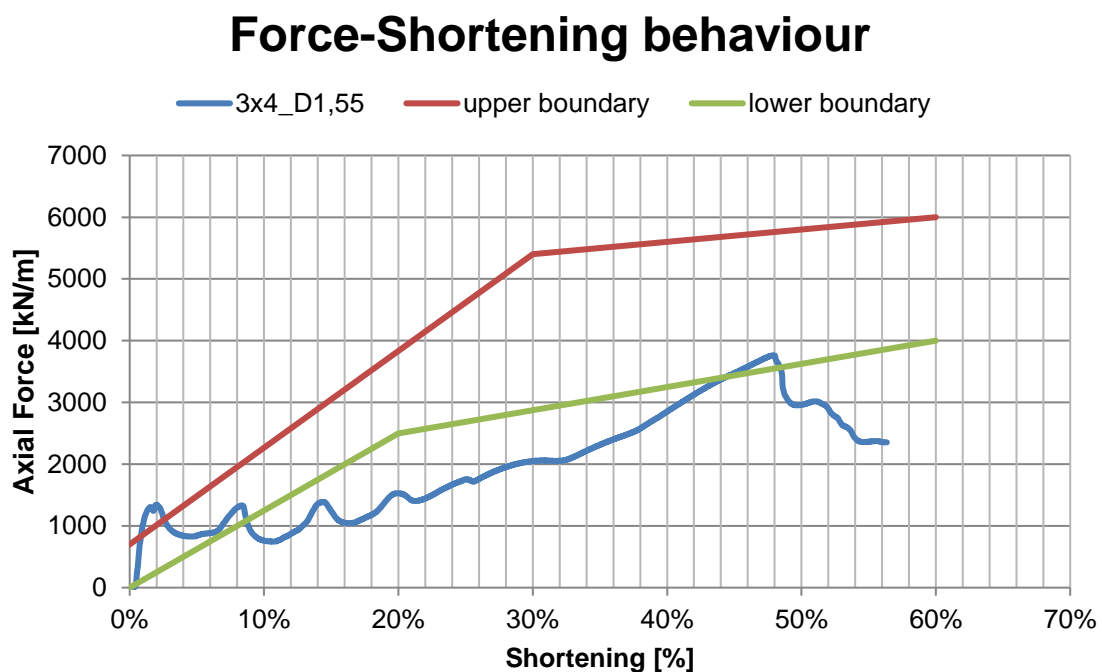
Figure 72: Force-Shortening behaviour "4_D1,55" Type II

The steep increase at the beginning relates to the direct contact of the inner pipe with its filling material and the endplate. The decrease of the force-shortening curve at ~48% shortening relates to the increase of the inner pressure which leads to bursting of the inner pipe.

Lab Test "6_D1,6"

The filling material has been estimated with a density of 1.6 kg/dm³. The boundaries refer to the tender documents of the Semmering Base Tunnel (see Figure 56).

Table 14: Specifications "6_D1,6"

Filling material	Mass percentage		Inner pipe, steel quality, dimension	Outer pipe, steel quality, dimension	Inlay
D1,6	35.19%	CEM II/B-M (S-L) 32,5 N	34CrMo4 133x2x370	DD 11 140x2x50	-
	9.86%	Liapor 1-4 mm			
	38.48%	Sand 0-2 mm			
	0.47	W/C-ratio			

Figure 73: before/after "6_D1,6"   Figure 74: Scheme "6_D1,6"
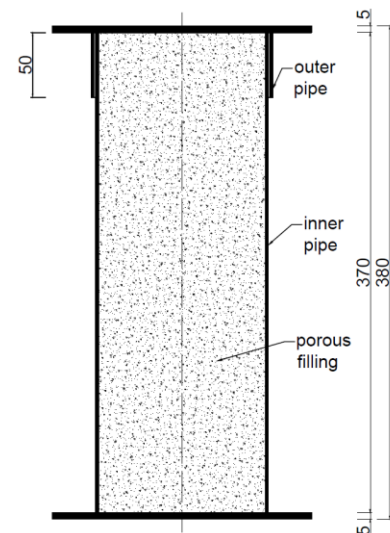
Type I: The force-shortening curve shows at the beginning a steep increase and intersects the upper boundary at a shortening of ~0.4% and an axial force of ~800 kN. The first peak appears at ~1% shortening and an axial force of ~2100 kN. At a shortening of ~10% and an axial force of ~2000 kN the force-shortening curve lies within the specified range. From this point the force-shortening curve shows a quasi-constant behaviour until an axial force of ~3000 kN and a shortening of ~34% is reached.

Type II: The force-shortening curve shows at the beginning a steep increase and intersects the upper boundary at a shortening of ~0.4% and an axial force of ~800 kN. The first peak appears at ~1% shortening and an axial force of ~2100 kN. At a shortening of ~10% and an axial force of ~2000 kN the force-shortening curve lies within the specified range and it shows a quasi-constant behaviour. It intersects the lower boundary at ~18% shortening and could be loaded until an axial force of ~3000 kN at a shortening of ~34% is

reached.

Force-Shortening behaviour
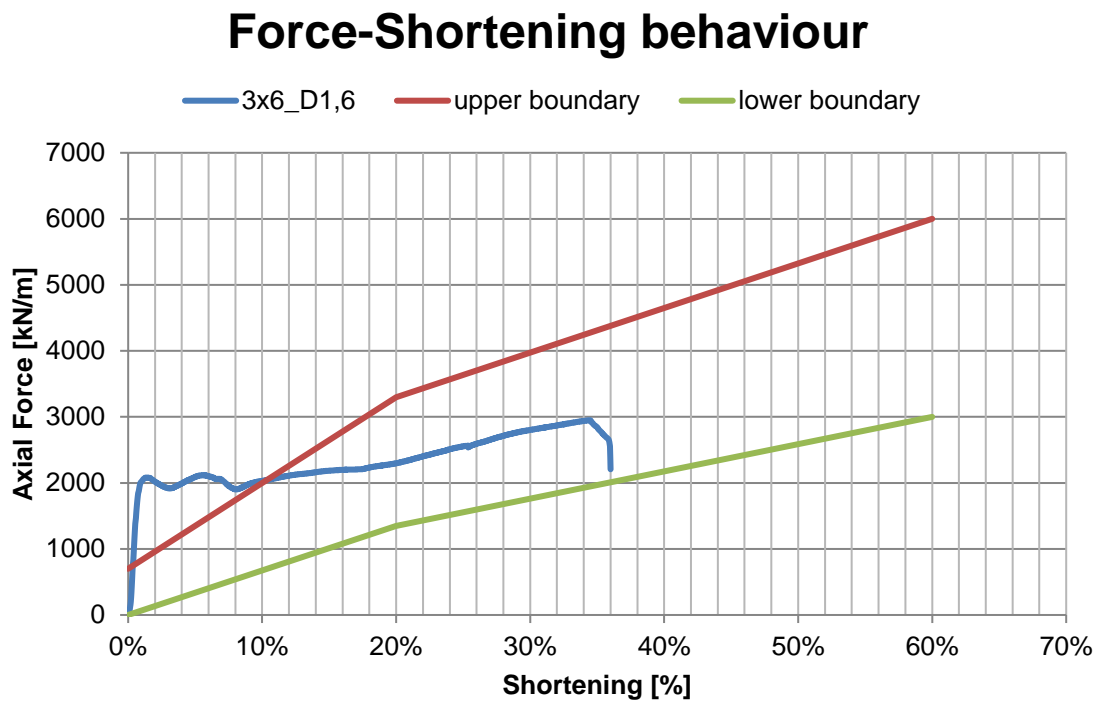
Figure 75: Force-Shortening behaviour "6_D1,6" Type I

Force-Shortening behaviour
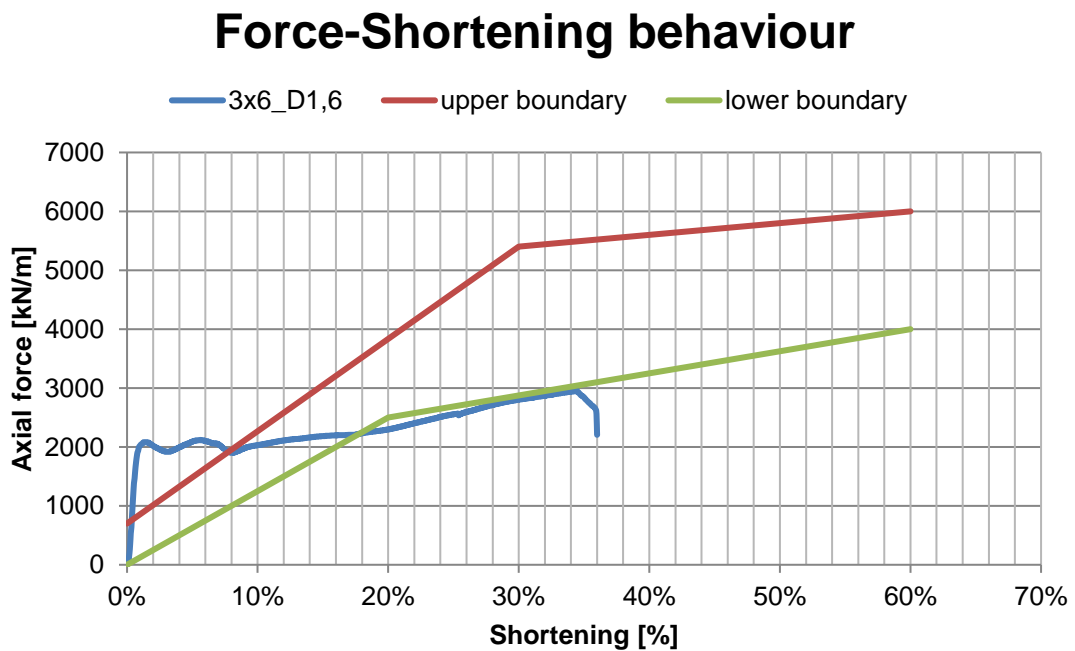
Figure 76: Force-Shortening behaviour "4_D1,6" Type II

The steep increase at the beginning relates to the direct contact of the inner pipe with its filling material and the endplate. The decrease of the force-shortening curve at ~34% shortening relates to the increase of the inner pressure which leads to bursting of the inner pipe.

Lab Test "3_D1,6"

The filling material has been estimated with a density of 1.6 kg/dm³. According to previous lab tests it turned out that the steel cracks before the desired shortening, so a new steel type has been used for this lab test. The boundaries refer to the tender documents of the Semmering Base Tunnel (see Figure 56).

Table 15: Specifications "3_D1,6"

Filling material	Mass percentage		Inner pipe, steel quality, dimension	Outer pipe, steel quality, dimension	Inlay
D1,6	35.19%	CEM II/B-M (S-L) 32,5 N	S235+N 133x2.5x370	DD 11 140x2x50	-
	9.86%	Liapor 1-4 mm			
	38.48%	Sand 0-2 mm			
	0.47	W/C-ratio			

Figure 77: before/after "3_D1,6"   Figure 78: Scheme "3_D1,6"
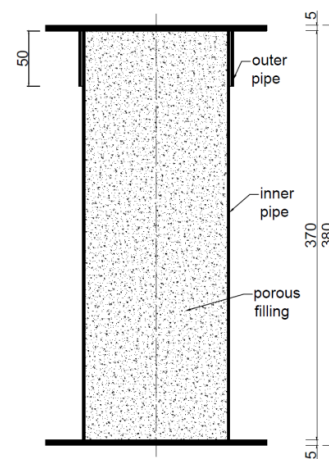
Type I: The force-shortening curve shows at the beginning a steep increase and intersects the upper boundary at a shortening of ~0.3% and an axial force of ~800 kN. The first peak appears at ~0.8% shortening and an axial force of ~1700 kN. At a shortening of ~5.5% and an axial force of ~1500 kN it lies within the specified range and it shows a quasi-constant behaviour until it intersects the upper boundary at a shortening of ~58% and an axial force of ~5900 kN again. It can be loaded until a shortening of ~64% and an axial force of ~8100 kN is reached.

Type II: The force-shortening curve shows at the beginning a steep increase and intersects the upper boundary at a shortening of ~0.3% and an axial force of ~800 kN. The first peak appears at ~0.8% shortening and an axial force of ~1700 kN. At a shortening of ~5% and an axial force of ~1500 kN the force-shortening curve lies within the specified range and it shows a quasi-constant behaviour. It intersects the lower boundary at ~13.5%

shortening and an axial force of ~1700 kN. The force-shortening curve reaches the specified range again at a shortening of ~40% and an axial force of ~3200 kN. It intersects the upper boundary again at a shortening of ~58% and an axial force of ~5900 kN and could be loaded until an axial force of ~8100 kN at a shortening of ~34% is reached.

Force-Shortening behaviour
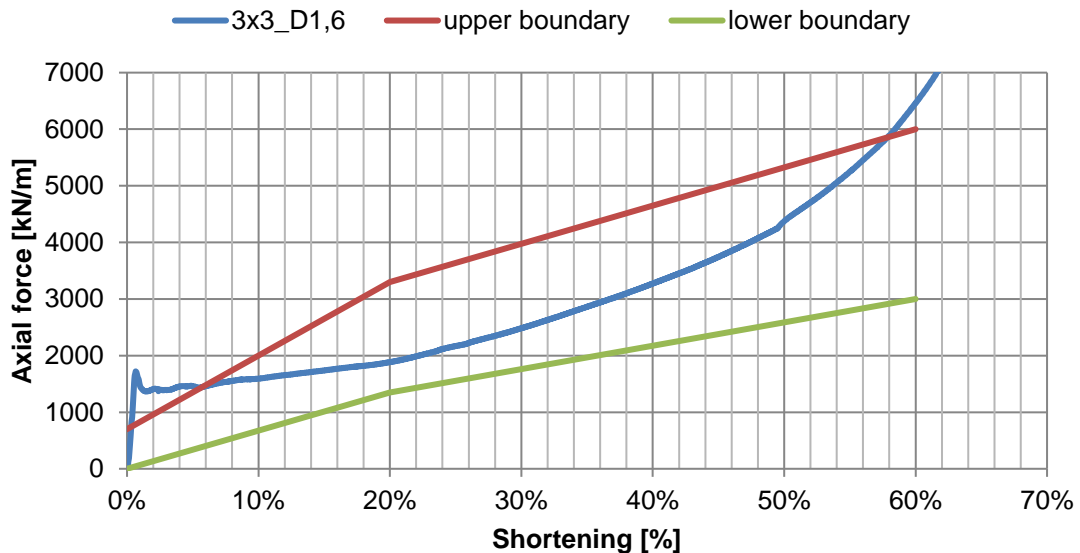
Figure 79: Force-Shortening behaviour "3_D1,6" Type I

Force-Shortening behaviour
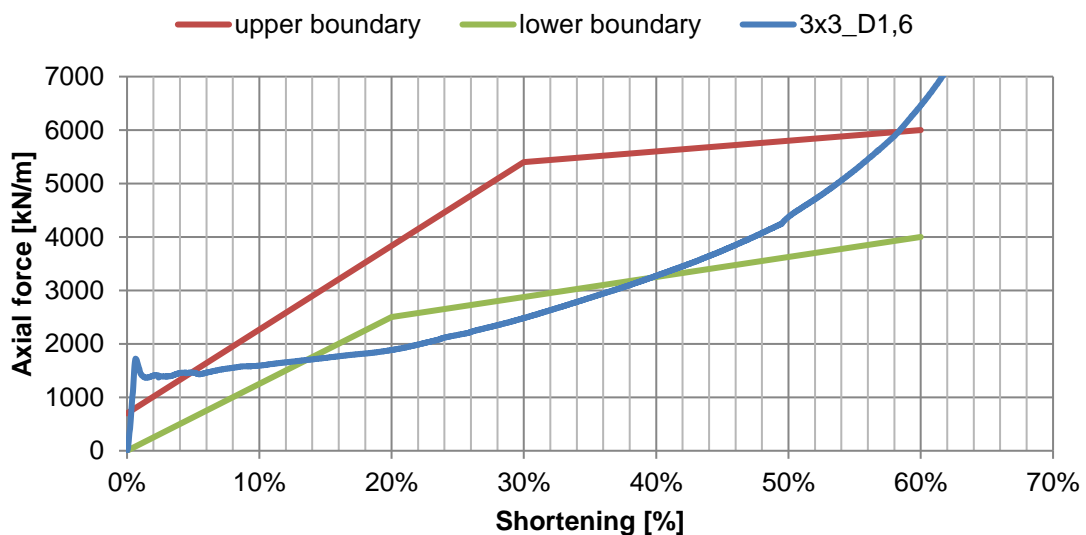
Figure 80: Force-Shortening behaviour "3_D1,6" Type II

The steep increase at the beginning relates to the direct contact of the inner pipe with its filling material and the endplate. According to the high load and the high amount of shortening, the used steel shows a very good behaviour.

Lab Test "2_D1,55"

The filling material has been estimated with a density of 1.55 kg/dm³. To verify the behaviour of the steel another lab test need to be done. The boundaries refer to the tender documents of the Semmering Base Tunnel (see Figure 56).

Table 16: Specifications "2_D1,55"

Filling material	Mass percentage		Inner pipe, steel quality, dimension	Outer pipe, steel quality, dimension	Inlay
D1,55	34.03%	CEM II/B-M (S-L) 32,5 N	S235+N 133x2.5x370	DD 11 140x2x50	-
	12.19%	Liapor 1-4 mm			
	37.21%	Sand 0-2 mm			
	0.49	W/C-ratio			

Figure 81: before/after "2_D1,55"
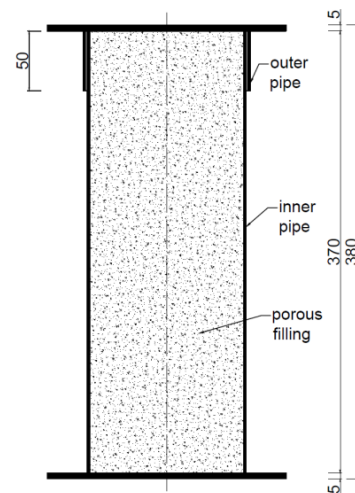
Figure 82: Scheme "2_D1,55"

Type I: The force-shortening curve shows at the beginning a steep increase and intersects the upper boundary at a shortening of ~0.4% and an axial force of ~800 kN. The first peak appears at ~0.7% shortening and an axial force of ~1400 kN. At a shortening of ~4.5% and an axial force of ~1400 kN it lies within the specified range and it shows a quasi-constant behaviour until it intersects the upper boundary at a shortening of ~58% and an axial force of ~5900 kN again. It can be loaded until a shortening of ~64% and an axial force of ~8100 kN is reached.

Type II: The force-shortening curve shows at the beginning a steep increase and intersects the upper boundary at a shortening of ~0.4% and an axial force of ~800 kN. The first peak appears at ~0.7% shortening and an axial force of ~1400 kN. At a shortening of ~4.5% and an axial force of ~1400 kN the force-shortening curve lies within the specified range and it shows a quasi-constant behaviour. It intersects the lower boundary at ~12.5%

shortening and an axial force of ~1550 kN. The force-shortening curve reaches the specified range again at a shortening of ~42% and an axial force of ~3300 kN. It intersects the upper boundary again at a shortening of ~58.5% and an axial force of ~5950 kN and could be loaded until an axial force of ~8100 kN at a shortening of ~64% is reached.

Force-Shortening behaviour
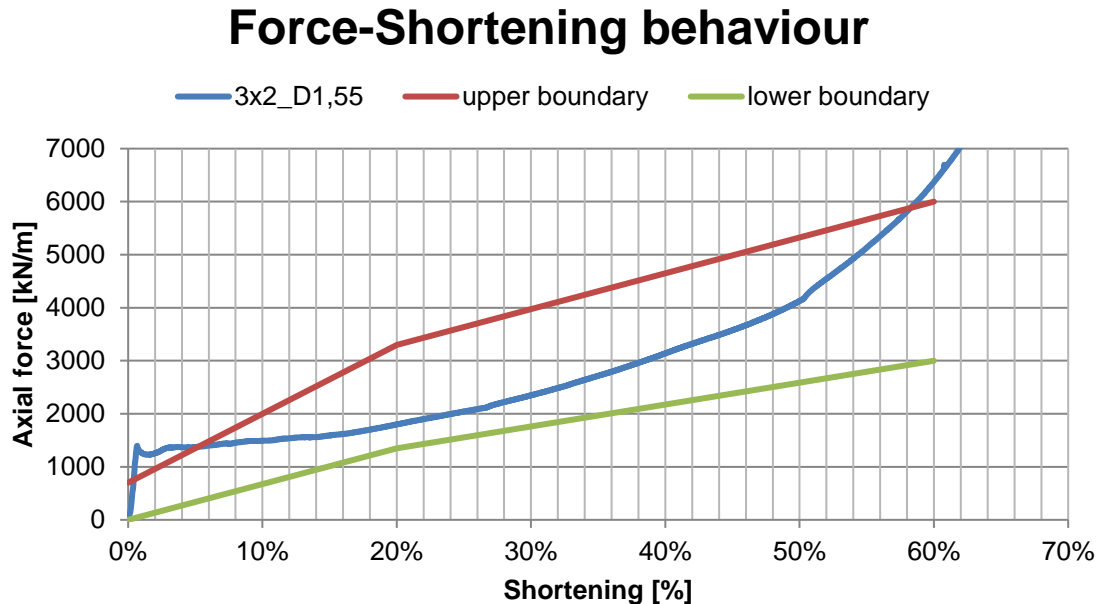
Figure 83: Force-Shortening behaviour "2_D1,55" Type I

Force-Shortening behaviour
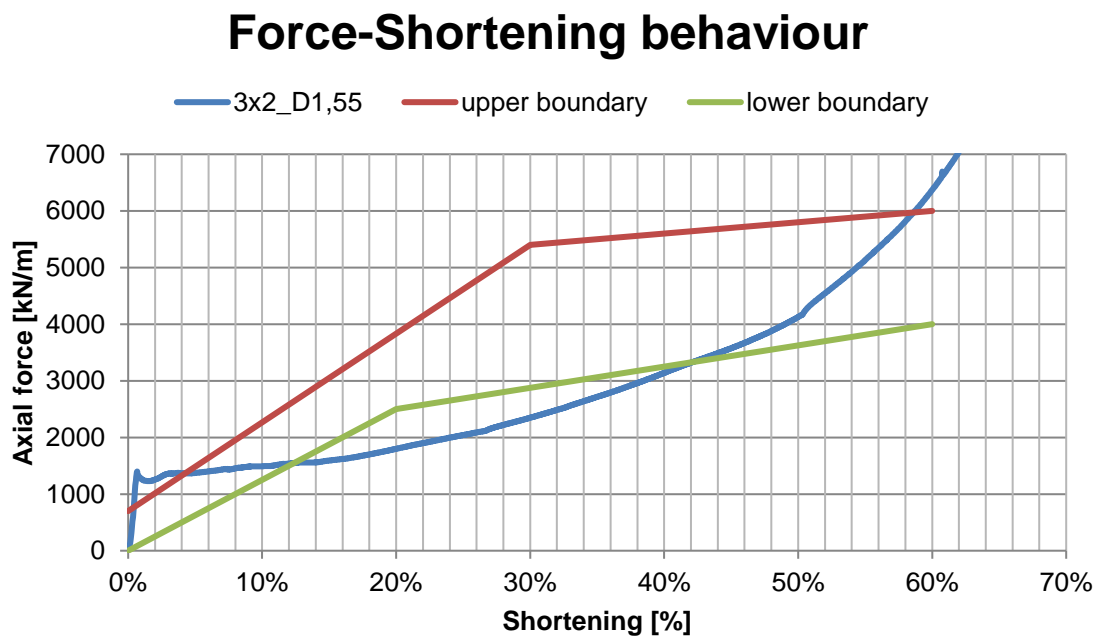
Figure 84: Force-Shortening behaviour "2_D1,55" Type II

The steep increase at the beginning relates to the direct contact of the inner pipe with its filling material and the endplate. According to the high load and the high amount of shortening, the used steel shows a very good behaviour and it verifies Lab Test "3_D1,6".

Lab Test "5_D1,55_Y_5,0"

The filling material has been estimated with a density of 1.55 kg/dm³. To avoid a high initial stiffness, a 4 cm porous inlay with a compressive strength of 5 MPa is used. A compensation layer of gypsum needs to be installed to provide full contact. The boundaries refer to the tender documents of the Semmering Base Tunnel (see Figure 56).

Table 17: Specifications "5_D1,55_Y_5,0"

Filling material	Mass percentage		Inner pipe, steel quality, dimension	Outer pipe, steel quality, dimension	Inlay
D1,55	34.03%	CEM II/B-M (S-L) 32,5 N	E235+SR 133x2.5x370	DD 11 140x2x50	4 cm porous inlay 5 MPa
	12.19%	Liapor 1-4 mm			
	37.21%	Sand 0-2 mm			
	0.49	W/C-ratio			

Figure 85: before/after "5_D1,55_Y_5,0"   Figure 86: Scheme "5_D1,55_Y_5,0"
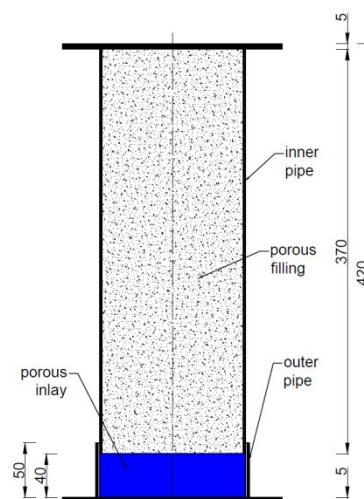
Type I: The force-shortening curve shows at the beginning a smooth increase and it stays in the specified range. The first peak appears at ~10.5% shortening and an axial force of ~1800 kN. Then it shows an oscillating behaviour until a shortening of ~18%. From this point, it shows a quasi-constant behaviour until an axial force of ~2900 kN and a shortening of ~39% is reached.

Type II: The force-shortening curve shows at the beginning a smooth increase but it intersects the lower boundary from ~1 - ~4% shortening. The first peak appears at ~10.5% shortening and an axial force of ~1800 kN. Then it shows an oscillating behaviour until a shortening of ~18% where it intersects the lower boundary at ~11.5% shortening and an axial force of 1400 kN again. From this point, it shows a quasi-constant behaviour until an axial force of ~2900 kN and a shortening of ~39% is reached.

Force-Shortening behaviour
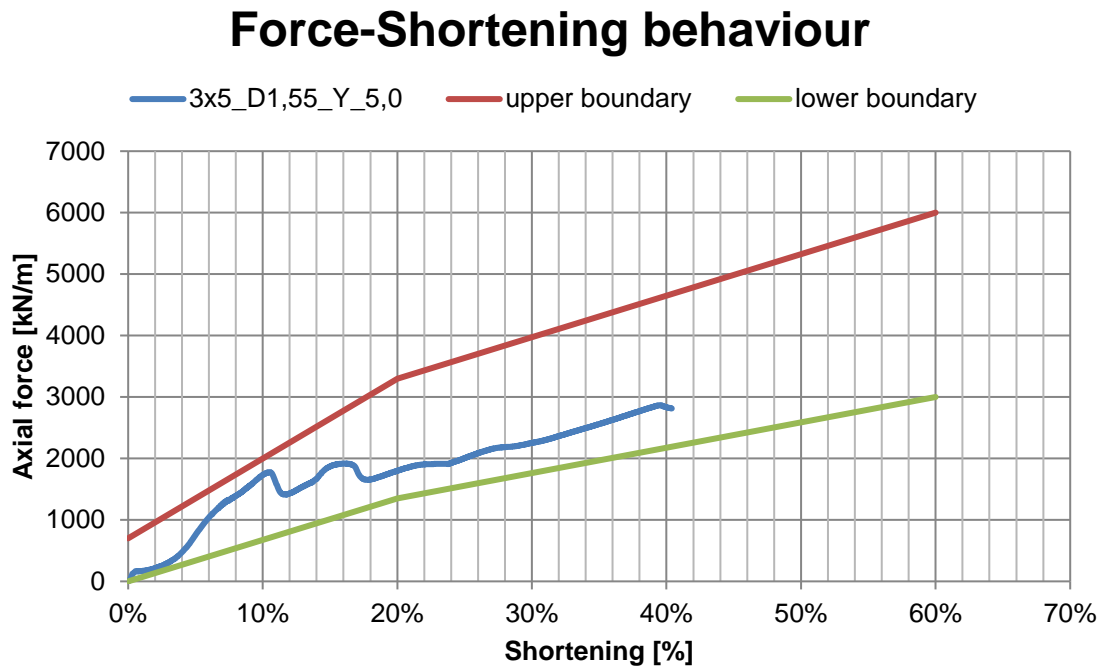
Figure 87: Force-Shortening behaviour "5_D1,55_Y_5,0" Type I

Force-Shortening behaviour
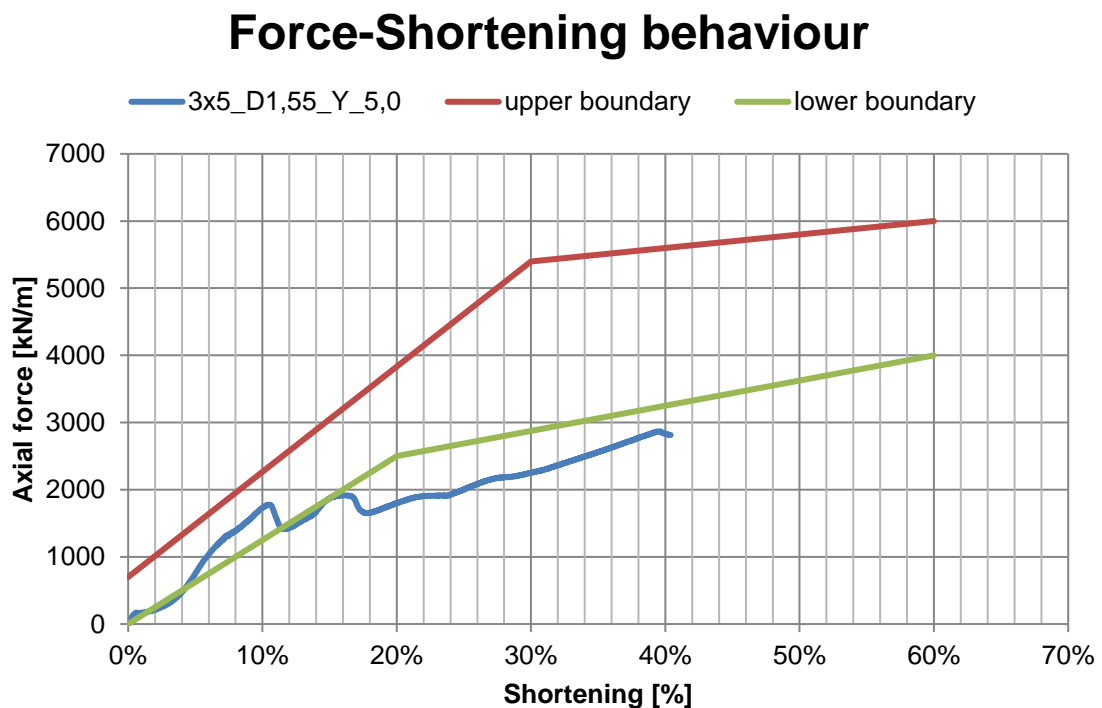
Figure 88: Force-Shortening behaviour "5_D1,55_Y_5,0" Type II

The used porous inlay effectively controls the initial behaviour. Type I gets fully fulfilled but to fulfil type II some changes at the system need to be done. The decrease of the force-shortening curve at ~34% shortening relates to the increase of the inner pressure which leads to bursting of the inner pipe.

Lab Test "4_D1,6_Y_5,0"

The filling material has been estimated with a density of 1.6 kg/dm³. To avoid a high initial stiffness, a 4 cm porous inlay with a compressive strength of 5 MPa is used. A compensation layer of gypsum needs to be installed to provide full contact. The boundaries refer to the tender documents of the Semmering Base Tunnel (see Figure 56).

Table 18: Specifications "4_D1,6_Y_5,0"

Filling material	Mass percentage		Inner pipe, steel quality, dimension	Outer pipe, steel quality, dimension	Inlay
D1,6	35.19%	CEM II/B-M (S-L) 32,5 N	S235+N 133x2.5x370	DD 11 140x2x50	4 cm porous inlay 5 MPa
	9.86%	Liapor 1-4 mm			
	38.48%	Sand 0-2 mm			
	0.47	W/C-ratio			

Figure 89: before/after "4_D1,6_Y_5,0"   Figure 90: Scheme "4_D1,6_Y_5,0"
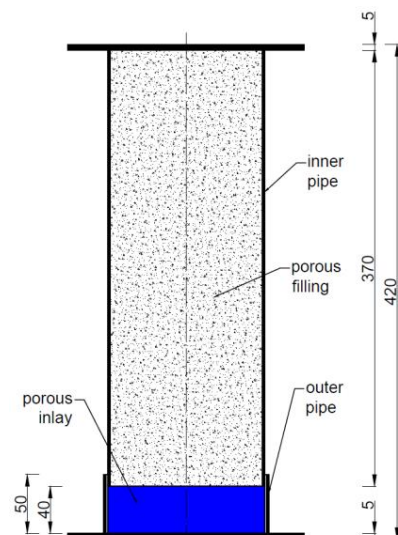
Type I: The force-shortening curve shows at the beginning a smooth increase and it stays in the specified range. The first peak appears at ~6% shortening and an axial force of ~1750 kN, therefore it intersects the upper boundary. Then it shows a quasi-constant behaviour until an axial force of ~8000 kN and a shortening of ~66% is reached.

Type II: The force-shortening curve shows at the beginning a smooth increase and it stays in the specified range. The first peak appears at ~6% shortening and an axial force of ~1750 kN, therefore it intersects the upper boundary. Then it shows a quasi-constant behaviour until an axial force of ~8000 kN and a shortening of ~66% is reached. It intersects the lower boundary at ~12% shortening and an axial force of ~1500 kN. At ~45% shortening and an axial force of ~3400 kN it lies in the specified range again.

Force-Shortening behaviour
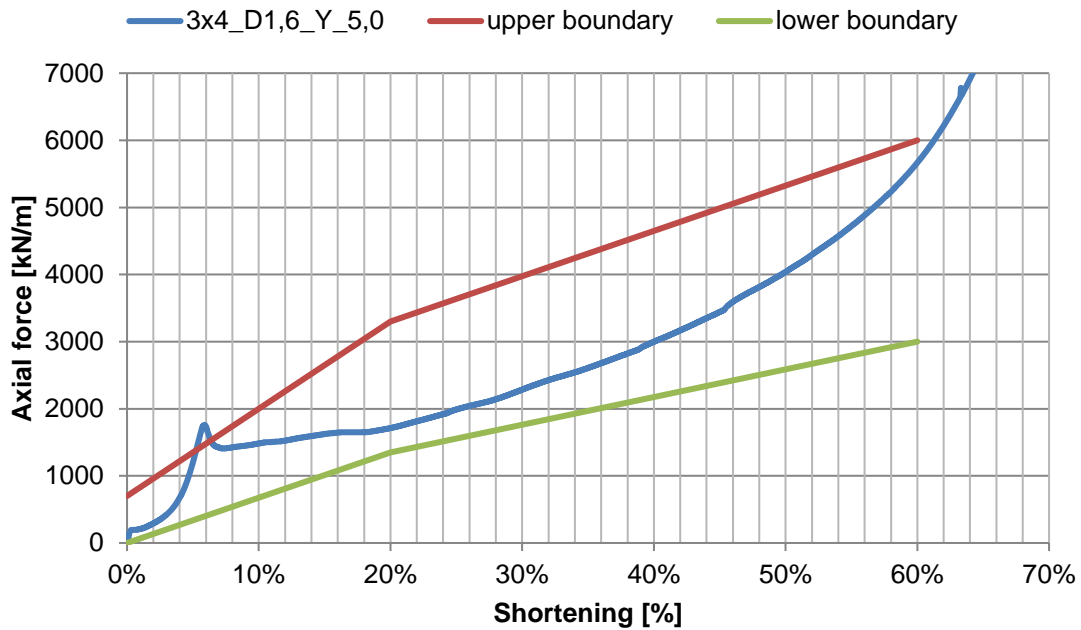
Figure 91: Force-Shortening behaviour "4_D1,6_Y_5,0" Type I

Force-Shortening behaviour
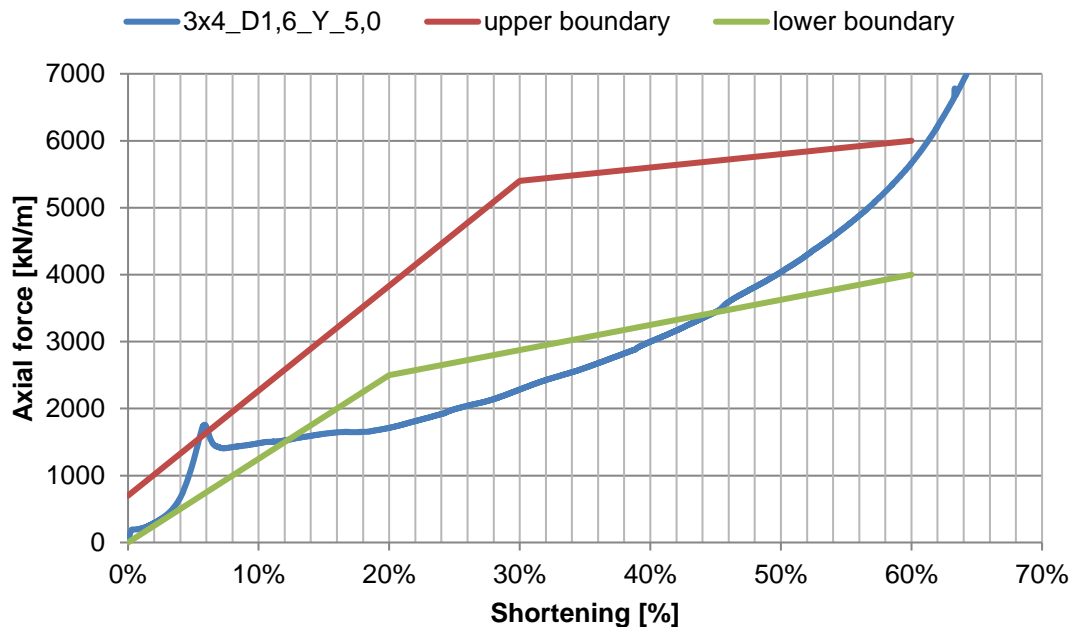
Figure 92: Force-Shortening behaviour "4_D1,6_Y_5,0" Type II

The used porous inlay effectively controls the initial behaviour. Type I gets almost fully fulfilled but to fulfil type II some changes at the system need to be done. The porous inlay is completely compressed at the first peak with ~6% shortening.

Lab Test "1_D1,55_Y_5,0"

The filling material has been estimated with a density of 1.55 kg/dm³. To avoid a high initial stiffness, a 4 cm porous inlay with a compressive strength of 5 MPa is used. A compensation layer of gypsum needs to be installed to provide full contact. The boundaries refer to the tender documents of the Semmering Base Tunnel (see Figure 56).

Table 19: Specifications "1_D1,55_Y_5,0"

Filling material	Mass percentage		Inner pipe, steel quality, dimension	Outer pipe, steel quality, dimension	Inlay
D1,55	34.03%	CEM II/B-M (S-L) 32,5 N	S235+N 133x2.5x370	DD 11 140x2x50	4 cm porous inlay 5 MPa
	12.19%	Liapor 1-4 mm			
	37.21%	Sand 0-2 mm			
	0.49	W/C-ratio			

Figure 93: before/after "1_D1,55_Y_5,0"
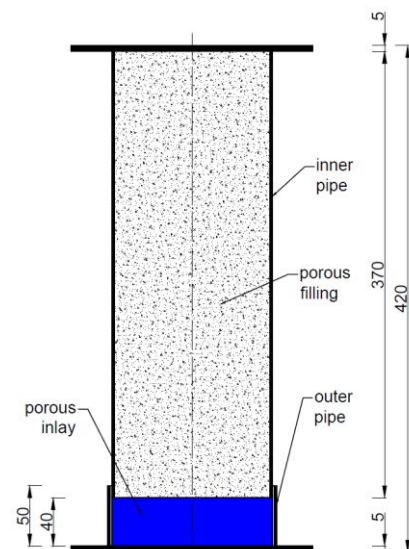
Figure 94: Scheme "1_D1,55_Y_5,0"

Type I: The force-shortening curve shows at the beginning a smooth increase and it stays in the specified range. The first peak appears at ~5.5% shortening and an axial force of ~1300 kN. Then it shows a quasi-constant behaviour until an axial force of ~6800 kN and a shortening of ~65% is reached.

Type II: The force-shortening curve shows at the beginning a smooth increase and it moves along the lower boundary but stays in the specified range. The first peak appears at ~5.5% shortening and an axial force of ~1300 kN. Then it shows a quasi-constant behaviour until an axial force of ~6800 kN and a shortening of ~65% is reached. It intersects the lower boundary at ~11% shortening and an axial force of ~1300 kN. At ~48% shortening and an axial force of ~3400 kN it lies in the specified range again.

Force-Shortening behaviour
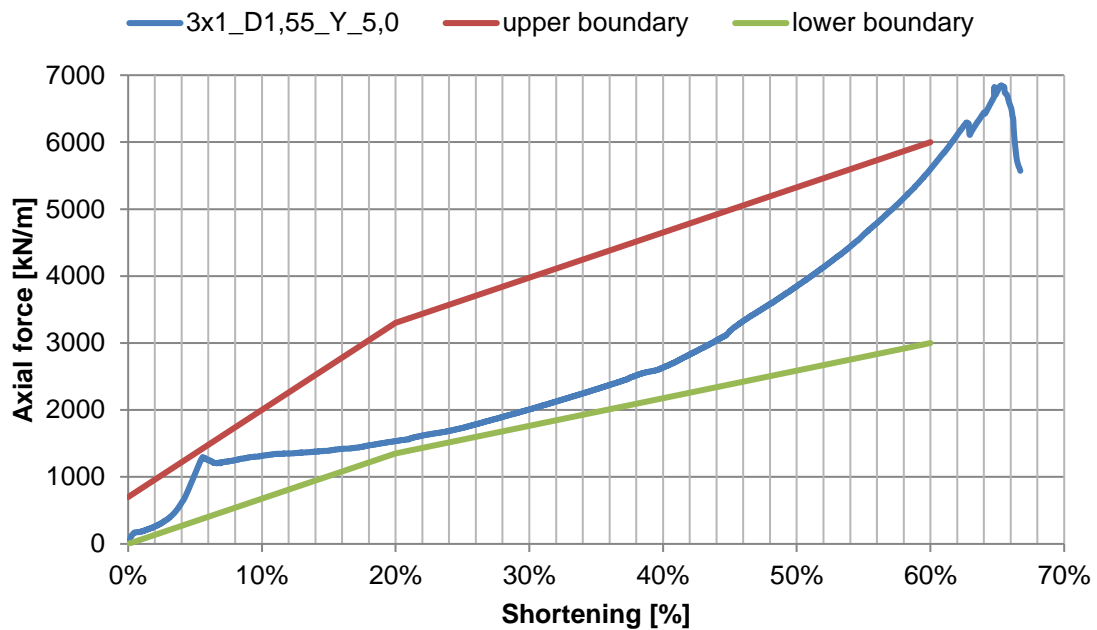
Figure 95: Force-Shortening behaviour "1_D1,55_Y_5,0" Type I

Force-Shortening behaviour
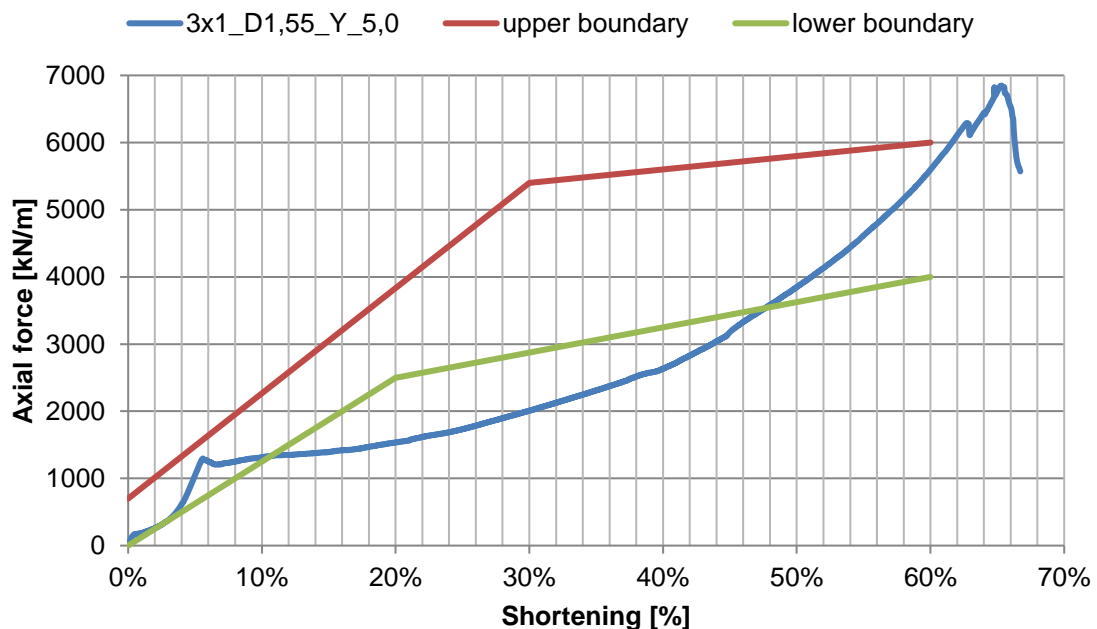
Figure 96: Force-Shortening behaviour "1_D1,55_Y_5,0" Type II

The used porous inlay effectively controls the initial behaviour. Type I gets fully fulfilled but to fulfil type II some changes at the system need to be done. The porous inlay is completely compressed at the first peak with ~5.5% shortening.

Lab Test "1_D1,55_4cm_Y"

The filling material has been estimated with a density of 1.55 kg/dm³. To avoid a high initial stiffness, a 4 cm porous inlay with a compressive strength of 5 MPa is used. A compensation layer of gypsum needs to be installed to provide full contact. The boundaries refer to the tender documents of the Semmering Base Tunnel (see Figure 56).

Table 20: Specifications "1_D1,55_4cm_Y"

Filling material	Mass percentage		Inner pipe, steel quality, dimension	Outer pipe, steel quality, dimension	Inlay
D1,55	34.03%	CEM II/B-M (S-L) 32,5 N	S235+N 133x2.5x360	DD 11 140x2x50	4 cm porous inlay 5 MPa
	12.19%	Liapor 1-4 mm			
	37.21%	Sand 0-2 mm			
	0.49	W/C-ratio			

Figure 97: before/after "1_D1,55_4cm_Y"   Figure 98: Scheme "1_D1,55_4cm_Y"

Type I: The force-shortening curve shows at the beginning a smooth increase and it stays in the specified range. The first peak appears at ~6% shortening and an axial force of ~1500 kN, therefore it intersects the upper boundary. Then it shows a quasi-constant behaviour until an axial force of ~8300 kN and a shortening of ~68% is reached.

Type II: The force-shortening curve shows at the beginning a smooth increase and it moves along the lower boundary but stays in the specified range. The first peak appears at ~6% shortening and an axial force of ~1500 kN. Then it shows a quasi-constant behaviour until an axial force of ~8300 kN and a shortening of ~68% is reached. It intersects the lower boundary at ~11% shortening and an axial force of ~1400 kN. At ~48% shortening and an axial force of ~3500 kN it lies in the specified range again.

Force-Shortening behaviour
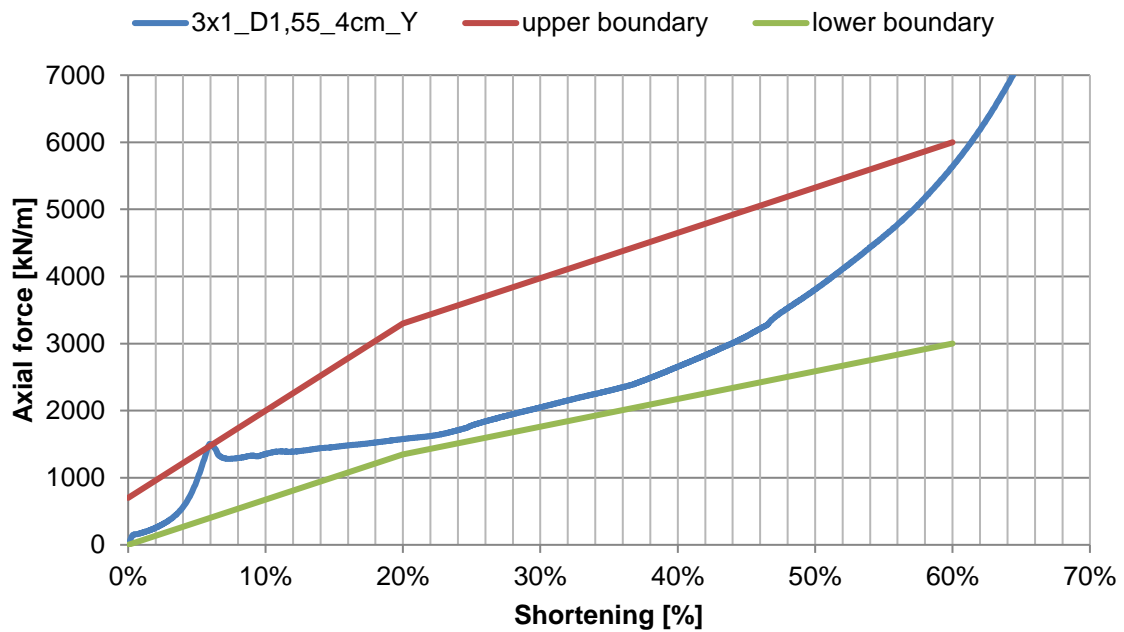
Figure 99: Force-Shortening behaviour "1_D1,55_4cm_Y" Type I

Force-Shortening behaviour
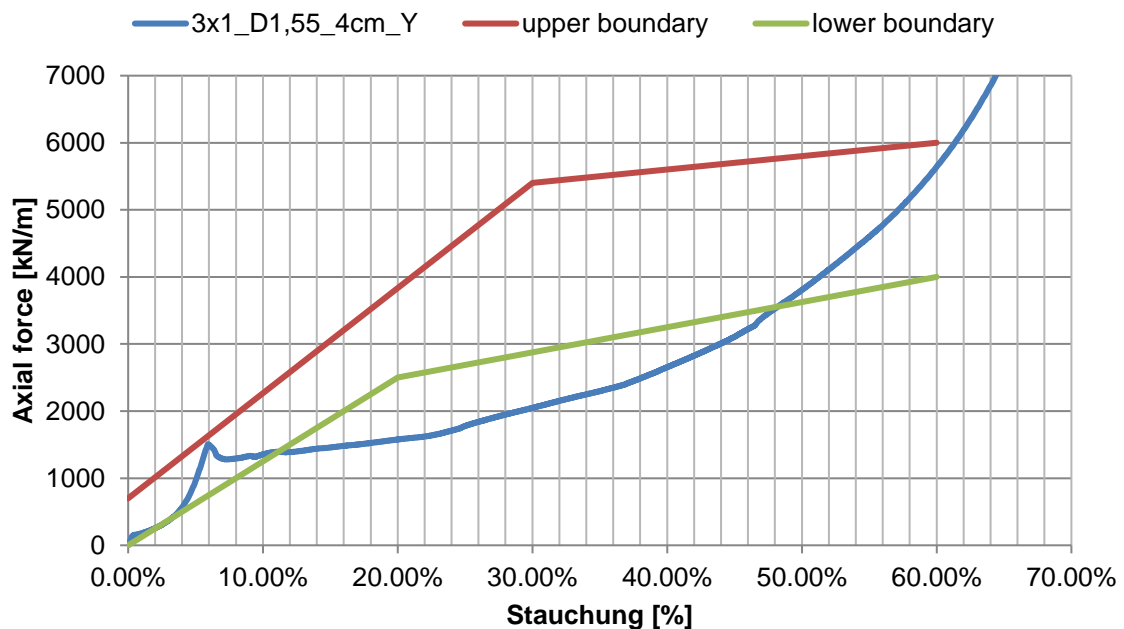
Figure 100: Force-Shortening behaviour "1_D1,55_4cm_Y" Type II

The used porous inlay effectively controls the initial behaviour. Type I gets fully fulfilled but to fulfil type II some changes at the system need to be done. The porous inlay is completely compressed at the first peak with ~6% shortening.

Lab Test "2_D1,55_4cm_Y"

The filling material has been estimated with a density of 1.55 kg/dm³. To avoid a high initial stiffness, a 4 cm porous inlay with a compressive strength of 5 MPa is used. A compensation layer of gypsum needs to be installed to provide full contact. The boundaries refer to the tender documents of the Semmering Base Tunnel (see Figure 56).

Table 21: Specifications "2_D1,55_4cm_Y"

Filling material	Mass percentage		Inner pipe, steel quality, dimension	Outer pipe, steel quality, dimension	Inlay
D1,55	34.03%	CEM II/B-M (S-L) 32,5 N	S235+N 133x2.5x360	DD 11 140x2x50	4 cm porous inlay 5 MPa
	12.19%	Liapor 1-4 mm			
	37.21%	Sand 0-2 mm			
	0.49	W/C-ratio			

Figure 101: before/after "2_D1,55_4cm_Y"   Figure 102: Scheme "2_D1,55_4cm_Y"
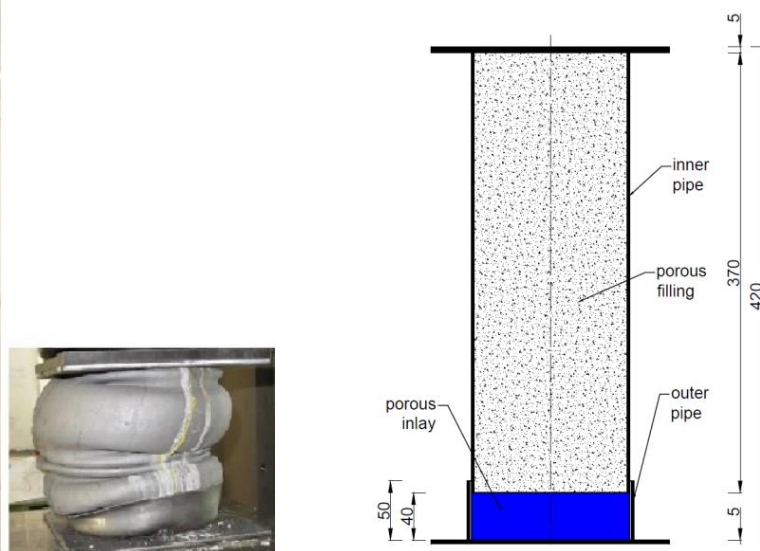
Type I: The force-shortening curve shows at the beginning a smooth increase and it stays in the specified range. The first peak appears at ~6% shortening and an axial force of ~1450 kN. Then it shows a quasi-constant behaviour until an axial force of ~7800 kN and a shortening of ~66% is reached.

Type II: The force-shortening curve shows at the beginning a smooth increase and it moves along the lower boundary but stays in the specified range. The first peak appears at ~6% shortening and an axial force of ~1450 kN. Then it shows a quasi-constant behaviour until an axial force of ~7800 kN and a shortening of ~66% is reached. It intersects the lower boundary at ~11% shortening and an axial force of ~1400 kN. At ~46% shortening and an axial force of ~3500 kN it lies in the specified range again.

Force-Shortening behaviour

Figure 103: Force-Shortening behaviour "2_D1,55_4cm_Y" Type I

Force-Shortening behaviour
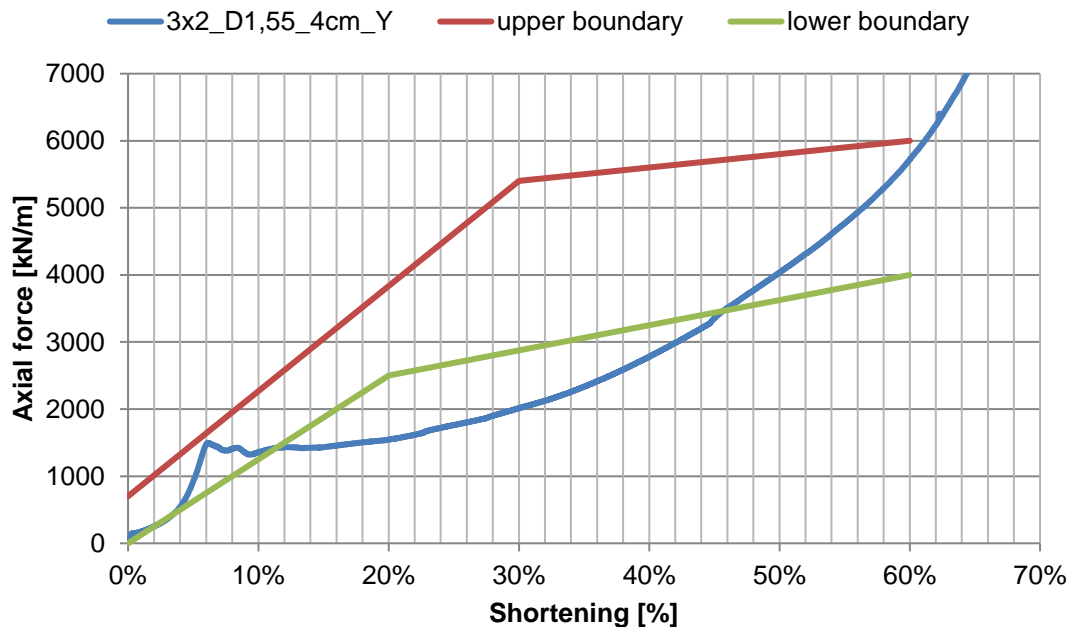
Figure 104: Force-Shortening behaviour "2_D1,55_4cm_Y" Type II

The used porous inlay effectively controls the initial behaviour. Type I gets fully fulfilled but to fulfil type II some changes at the system need to be done. The porous inlay is completely compressed at the first peak with ~6% shortening.

Lab Test "4_D1,55_2cm_Y"

The filling material has been estimated with a density of 1.55 kg/dm³. To avoid a high initial stiffness, a 2 cm porous inlay with a compressive strength of 5 MPa is used. A compensation layer of gypsum needs to be installed to provide full contact. The boundaries refer to the tender documents of the Semmering Base Tunnel (see Figure 56).

Table 22: Specifications "4_D1,55_2cm_Y"

Filling material	Mass percentage		Inner pipe, steel quality, dimension	Outer pipe, steel quality, dimension	Inlay
D1,55	34.03%	CEM II/B-M (S-L) 32,5 N	S235+N 133x2.5x380	DD 11 140x2x50	2 cm porous inlay 5 MPa
	12.19%	Liapor 1-4 mm			
	37.21%	Sand 0-2 mm			
	0.49	W/C-ratio			
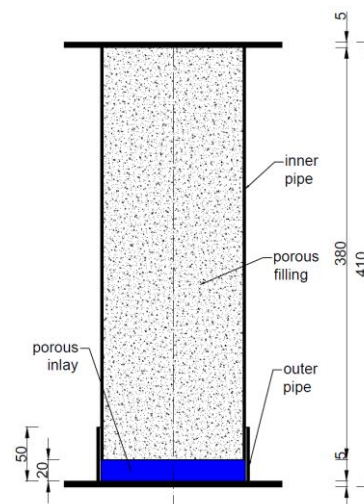
Figure 105: before/after "4_D1,55_2cm_Y"   Figure 106: Scheme "4_D1,55_2cm_Y"

Type I: The force-shortening curve shows at the beginning a smooth increase and it stays in the specified range. The first peak appears at ~4% shortening and an axial force of ~1500 kN, therefore it intersects the upper boundary. Then it shows a quasi-constant behaviour until an axial force of ~8000 kN and a shortening of ~66% is reached.

Type II: The force-shortening curve shows at the beginning a smooth increase and it moves along the lower boundary but stays in the specified range. The first peak appears at ~4% shortening and an axial force of ~1500 kN, therefore it intersects the upper boundary. Then it shows a quasi-constant behaviour until an axial force of ~8000 kN and a shortening of ~66% is reached. It intersects the lower boundary at ~11% shortening and an axial force of ~1400 kN. At ~46% shortening and an axial force of ~3500 kN it lies in the specified range again.

Force-Shortening behaviour

Figure 107: Force-Shortening behaviour "4_D1,55_2cm_Y" Type I

Force-Shortening behaviour
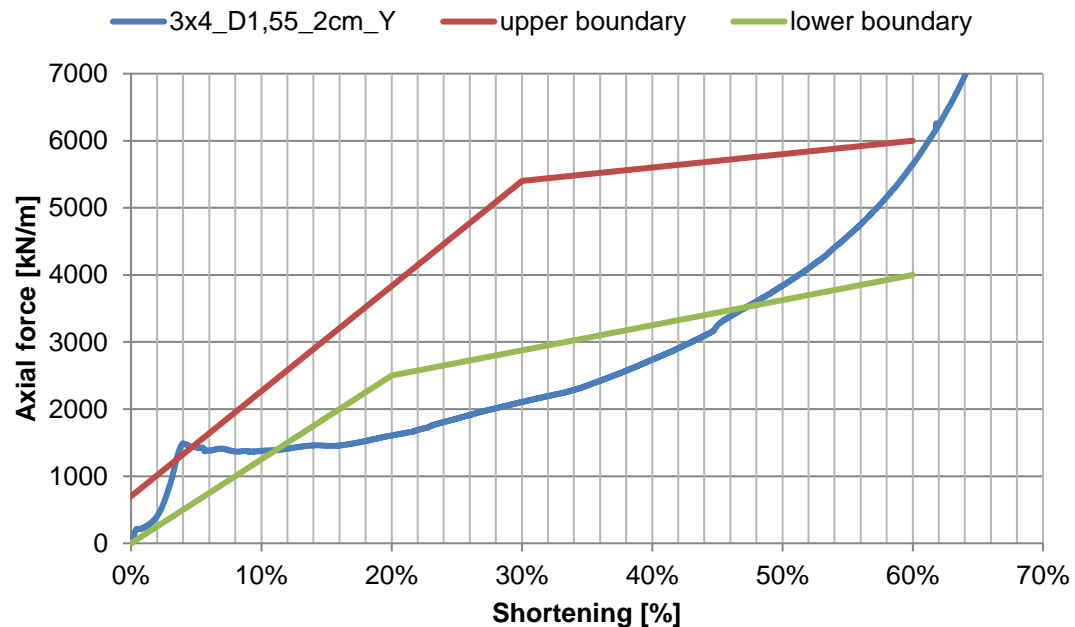
Figure 108: Force-Shortening behaviour "4_D1,55_2cm_Y" Type II

The used porous inlay effectively controls the initial behaviour. Type I gets almost fully fulfilled but to fulfil type II some changes at the system need to be done. The porous inlay is completely compressed at the first peak with ~4% shortening.

Lab Test "3_D1,55_6cm_Y"

The filling material has been estimated with a density of 1.55 kg/dm³. To avoid a high initial stiffness, a 6 cm porous inlay with a compressive strength of 5 MPa is used. A compensation layer of gypsum needs to be installed to provide full contact. The boundaries refer to the tender documents of the Semmering Base Tunnel (see Figure 56).

Table 23: Specifications "3_D1,55_6cm_Y"

Filling material	Mass percentage		Inner pipe, steel quality, dimension	Outer pipe, steel quality, dimension	Inlay
D1,55	34.03%	CEM II/B-M (S-L) 32,5 N	S235+N 133x2.5x340	DD 11 140x2x70	6 cm porous inlay 5 MPa
	12.19%	Liapor 1-4 mm			
	37.21%	Sand 0-2 mm			
	0.49	W/C-ratio			

Figure 109: before/after "3_D1,55_6cm_Y"   Figure 110: Scheme "3_D1,55_6cm_Y"
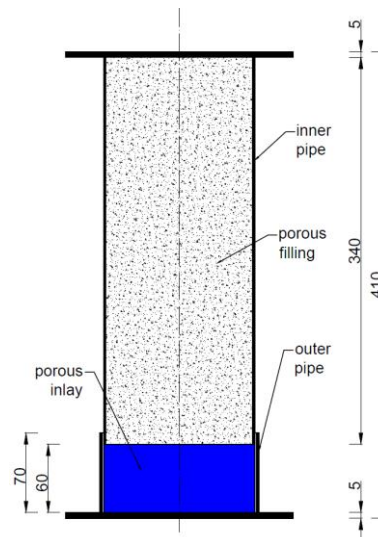
Type I: The force-shortening curve shows at the beginning a smooth increase and it stays in the specified range. The first peak appears at ~9% shortening and an axial force of ~1500 kN. Then it shows a quasi-constant behaviour until an axial force of ~8500 kN and a shortening of ~68% is reached.

Type II: The force-shortening curve shows at the beginning a smooth increase and it gets below the lower boundary from ~1-~8%. The first peak appears at ~9% shortening and an axial force of ~1500 kN. Then it shows a quasi-constant behaviour until an axial force of ~8500 kN and a shortening of ~68% is reached. It intersects the lower boundary at ~11.5% shortening and an axial force of ~1400 kN. At ~46% shortening and an axial force of ~3500 kN it lies in the specified range again.

Force-Shortening behaviour
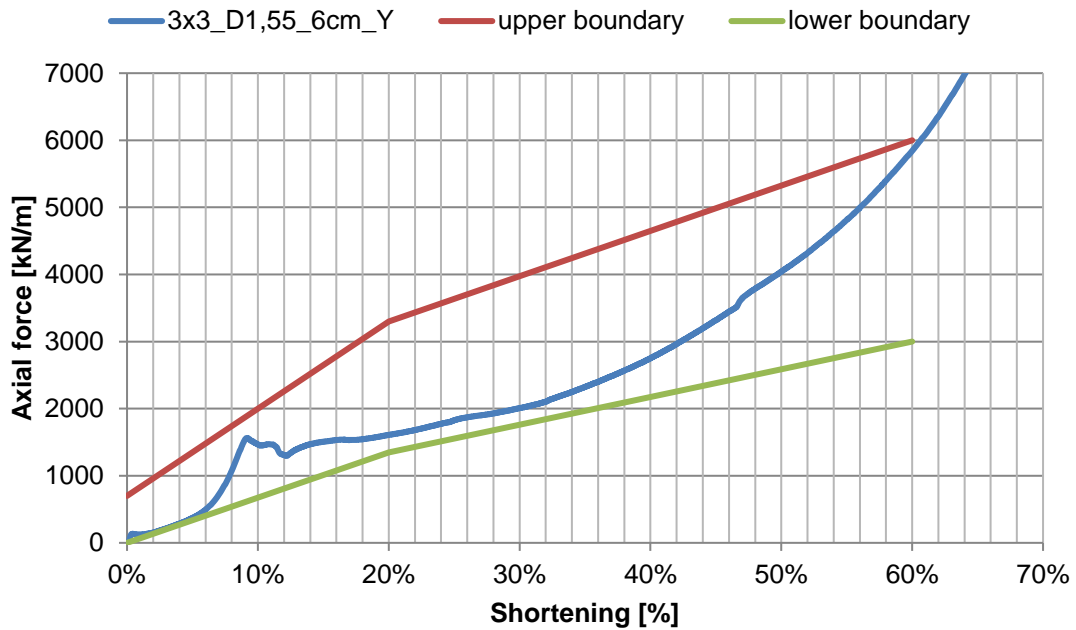
Figure 111: Force-Shortening behaviour "3_D1,55_6cm_Y" Type I

Force-Shortening behaviour
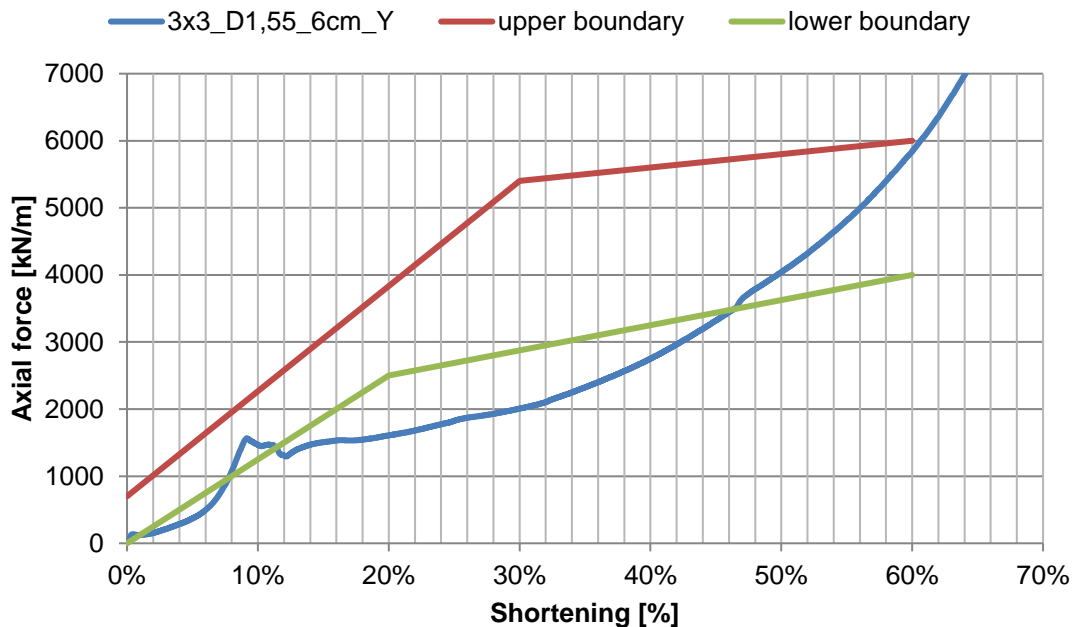
Figure 112: Force-Shortening behaviour "3_D1,55_6cm_Y" Type II

The used porous inlay effectively controls the initial behaviour. Type I gets fully fulfilled but to fulfil type II the initial increase of the force-shortening curve needs to be steeper. The porous inlay is completely compressed at the first peak with ~9% shortening.

Lab Test "D_1,55_7cm_Y_Bohrung"

The filling material has been estimated with a density of 1.55 kg/dm³. To avoid a high initial stiffness, a 7 cm porous inlay with a compressive strength of 5 MPa is used. A compensation layer of gypsum needs to be installed to provide full contact. Additionally, this lab test contains a central borehole with a diameter of 32 mm to obtain more volume where the destroyed material can expand into. The boundaries refer to the tender documents of the Semmering Base Tunnel (see Figure 56).

Table 24: Specifications "D1,55_7cm_Y_Bohrung"

Filling material	Mass percentage		Inner pipe, steel quality, dimension	Outer pipe, steel quality, dimension	Inlay
D1,55	34.03%	CEM II/B-M (S-L) 32,5 N	S235+N 133x2.5x330	DD 11 140x2x80	7 cm porous inlay 5 MPa, 32 mm borehole
	12.19%	Liapor 1-4 mm			
	37.21%	Sand 0-2 mm			
	0.49	W/C-ratio			

Figure 113: before/after "D1,55_7cm_Y_Bohrung" Figure 114: Scheme "D1,55_7cm_Y_Bohrung"

Type I: The force-shortening curve shows at the beginning a smooth increase and it moves along the lower boundary but stays in the specified range. The first peak appears at ~10% shortening and an axial force of ~1400 kN. Then it shows a quasi-constant behaviour until an axial force of ~8200 kN and a shortening of ~69% is reached. At a shortening of ~16% a jump appears and that's the reason why it leaves the specified range from ~25% - ~32% shortening.

Type II: The force-shortening curve shows at the beginning a smooth increase and it gets below the lower boundary from ~1% - ~9.5%. The first peak appears at ~10%

shortening and an axial force of ~1400 kN. Then it shows a quasi-constant behaviour until an axial force of ~8200 kN and a shortening of ~69% is reached. It intersects the lower boundary at ~11% shortening and an axial force of ~1400 kN. At ~48.5% shortening and an axial force of ~3600 kN it lies in the specified range again.

Force-Shortening behaviour
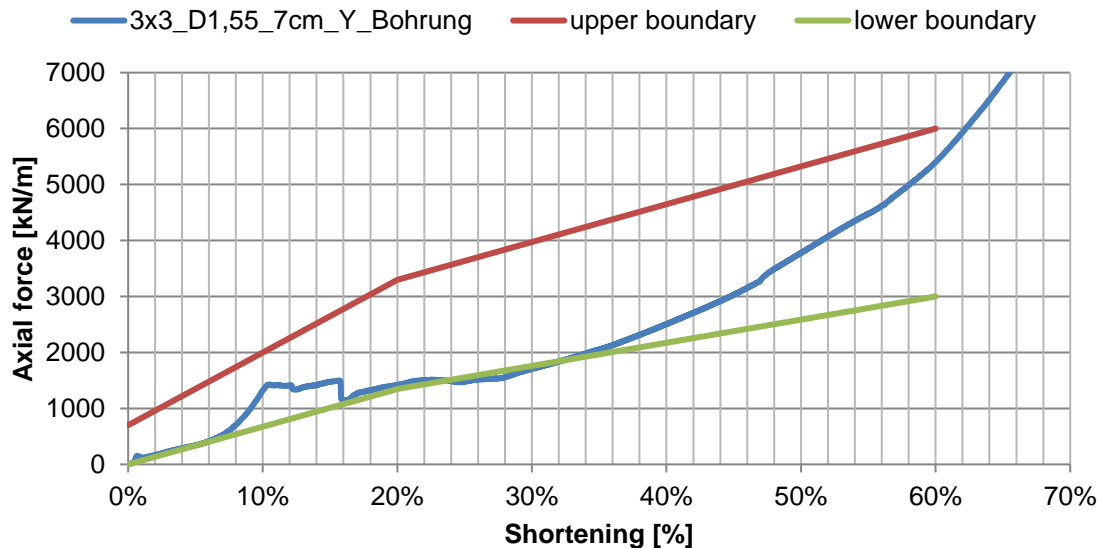
Figure 115: Force-Shortening behaviour "D1,55_7cm_Y_Bohrung" Type I

Force-Shortening behaviour
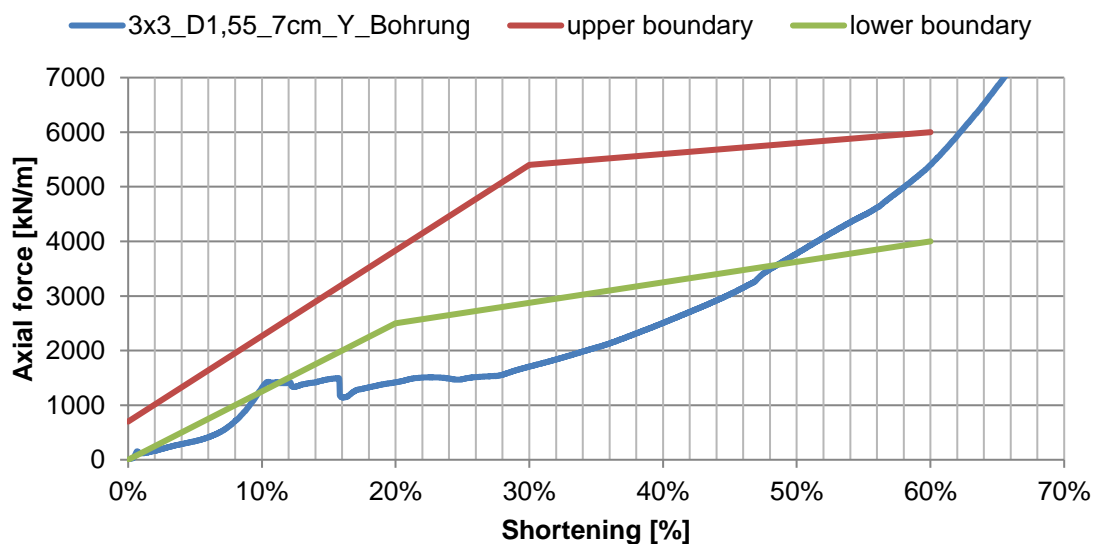
Figure 116: Force-Shortening behaviour "D1,55_7cm_Y_Bohrung" Type II

The used porous inlay effectively controls the initial behaviour but the borehole has a negative effect on the force-shortening behaviour. Type I and Type II cannot get fulfilled. The porous inlay is completely compressed at the first peak with ~10% shortening.

Lab Test "Botament_7cm_Y_Bohrung57"

The filling material has been estimated with a density of 1.55 kg/dm³. Therefore, a new binding material has been used. To avoid a high initial stiffness, a 7 cm porous inlay with a compressive strength of 5 MPa is used. A compensation layer of gypsum needs to be installed to provide full contact. Additionally, this lab test contains a central borehole with a diameter of 57 mm to obtain more volume where the destroyed material can expand into. The boundaries refer to the tender documents of the Semmering Base Tunnel (see Figure 56).

Table 25: Specifications "Botament_7cm_Y_Bohrung57"

Filling material	Mass percentage			Inner pipe, steel quality, dimension	Outer pipe, steel quality, dimension	Inlay
Botament 1,55	62.91% 17.35% 0.47	Botament Liapor 1-4 mm W/C-ratio		S235+N 133x2.5x330	DD 11 140x2x80	7 cm porous inlay 5 MPa, 57 mm borehole

Figure 117: before/after
"Botament_7cm_Y_Bohrung57"
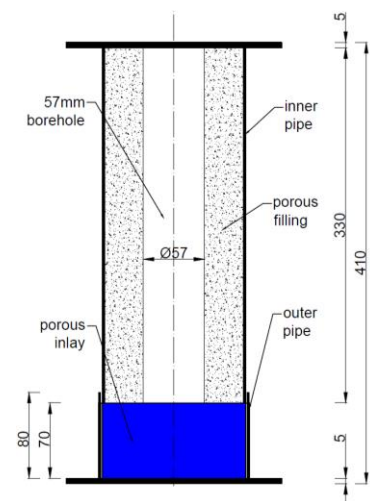
Figure 118: Scheme
"Botament_7cm_Y_Bohrung57"

Type I: The force-shortening curve shows at the beginning a smooth increase and it moves along the lower boundary but it leaves the specified range. The first peak appears at ~11% shortening and an axial force of ~1100 kN. Then it shows an oscillating behaviour until an axial force of ~1200 kN and a shortening of ~39% is reached. From this point it shows a quasi-constant behaviour until a shortening of ~69% and an axial force of 8000 kN is reached.

Type II: The force-shortening curve shows at the beginning a smooth increase and it

gets below the lower boundary from ~1% - ~57%. The first peak appears at ~11% shortening and an axial force of ~1100 kN. Then it shows an oscillating behaviour until an axial force of ~1200 kN and a shortening of ~39% is reached. From this point it shows a quasi-constant behaviour until a shortening of ~69% and an axial force of 8000 kN is reached.

Force-Shortening behaviour
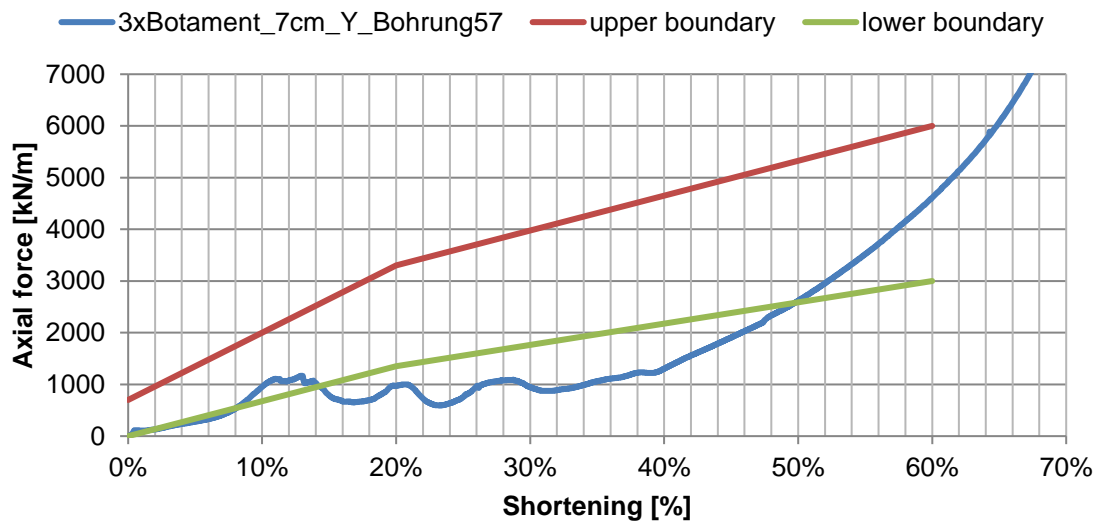
Figure 119: Force-Shortening behaviour "Botament_7cm_Y_Bohrung57" Type I

Force-Shortening behaviour
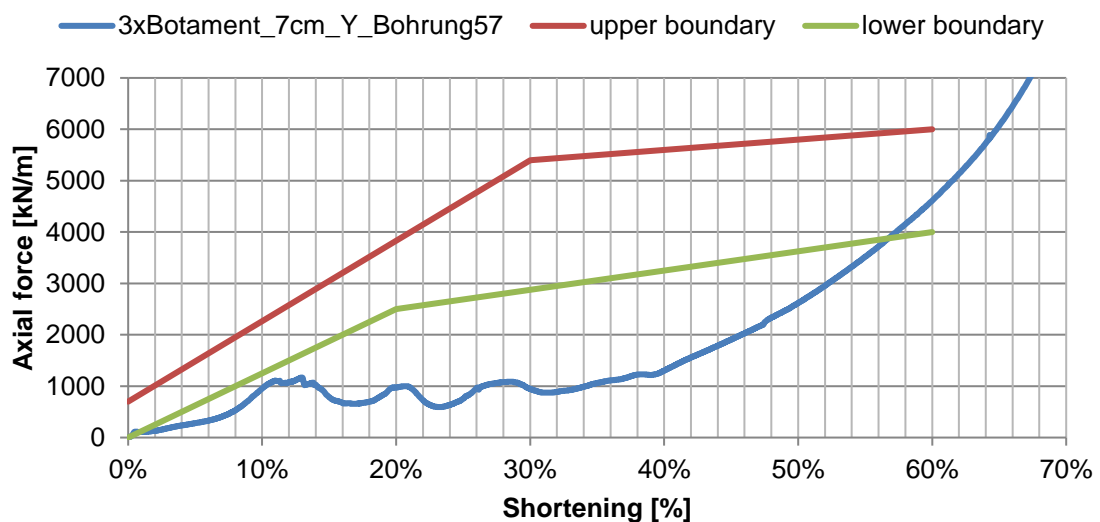
Figure 120: Force-Shortening behaviour "Botament_7cm_Y_Bohrung57" Type II

The used porous inlay effectively controls the initial behaviour but the borehole has a negative effect on the force-shortening behaviour. Type I and Type II cannot get fulfilled. The porous inlay is completely compressed at the first peak with ~11% shortening.

Lab Test "Botament1,37_7cm_Y"

The filling material has been estimated with a density of 1.37 kg/dm³. Therefore, a new binding material has been used. To avoid a high initial stiffness, a 7 cm porous inlay with a compressive strength of 5 MPa is used. A compensation layer of gypsum needs to be installed to provide full contact. The boundaries refer to the tender documents of the Semmering Base Tunnel (see Figure 56).

Table 26: Specifications "Botament1,37_7cm_Y"

Filling material	Mass percentage		Inner pipe, steel quality, dimension	Outer pipe, steel quality, dimension	Inlay
Botament 1,37	59.05%	Botament	S235+N 133x2.5x330	DD 11 140x2x80	7 cm porous inlay 5 MPa
	26.90%	Liapor 1-4 mm			
	0.51	W/C-ratio			
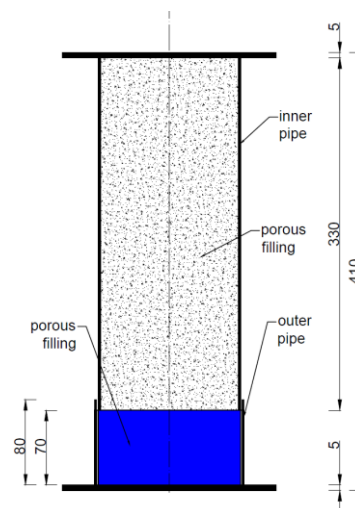
Figure 121: before/after "Botament1,37_7cm_Y"   Figure 122: Scheme "Botament1,37_7cm_Y"

Type I: The force-shortening curve shows at the beginning a smooth increase and it moves along the lower boundary but it stays in the specified range. The first peak appears at ~9% shortening and an axial force of ~1100 kN. Then it shows an oscillating behaviour until an axial force of ~1200 kN and a shortening of ~26%, where it intersects the lower boundary at ~14% shortening and an axial force of ~1000 kN. From this point, it shows a quasi-constant behaviour until a shortening of ~69% and an axial force of 7700 kN is reached.

Type II: The force-shortening curve shows at the beginning a smooth increase and it gets below the lower boundary from ~1% - ~52%. The first peak appears at ~9% shortening and an axial force of ~1100 kN. Then it shows an oscillating behaviour until an axial force of ~1200 kN and a shortening of ~26% is reached. From this point it shows a quasi-constant

behaviour until a shortening of ~69% and an axial force of 7700 kN is reached.

Force-Shortening behaviour
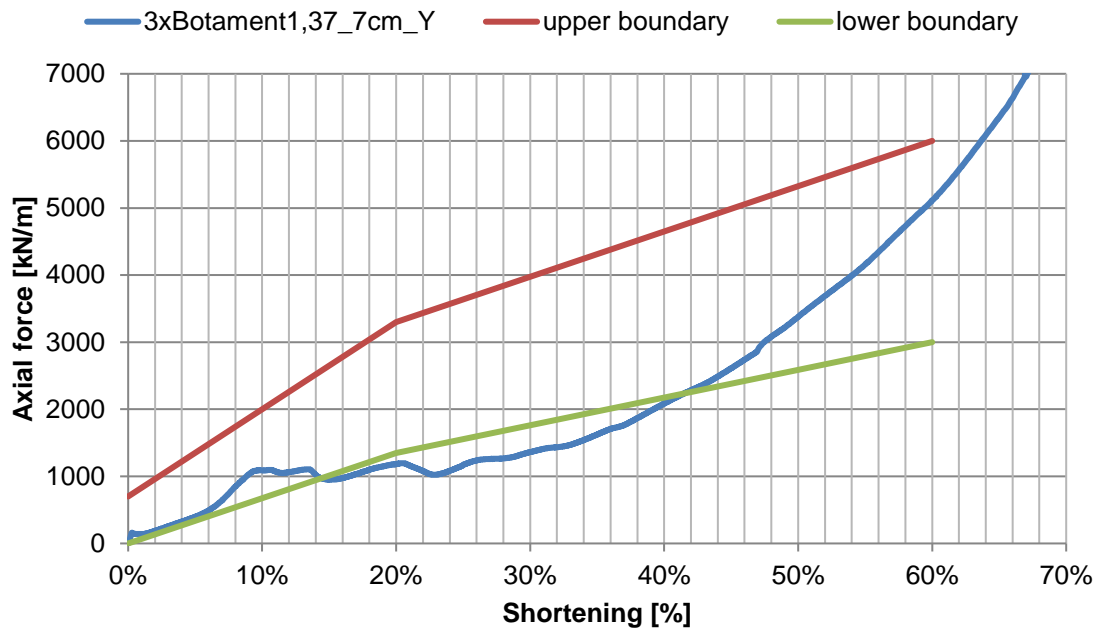
Figure 123: Force-Shortening behaviour "Botament1,37_7cm_Y" Type I

Force-Shortening behaviour
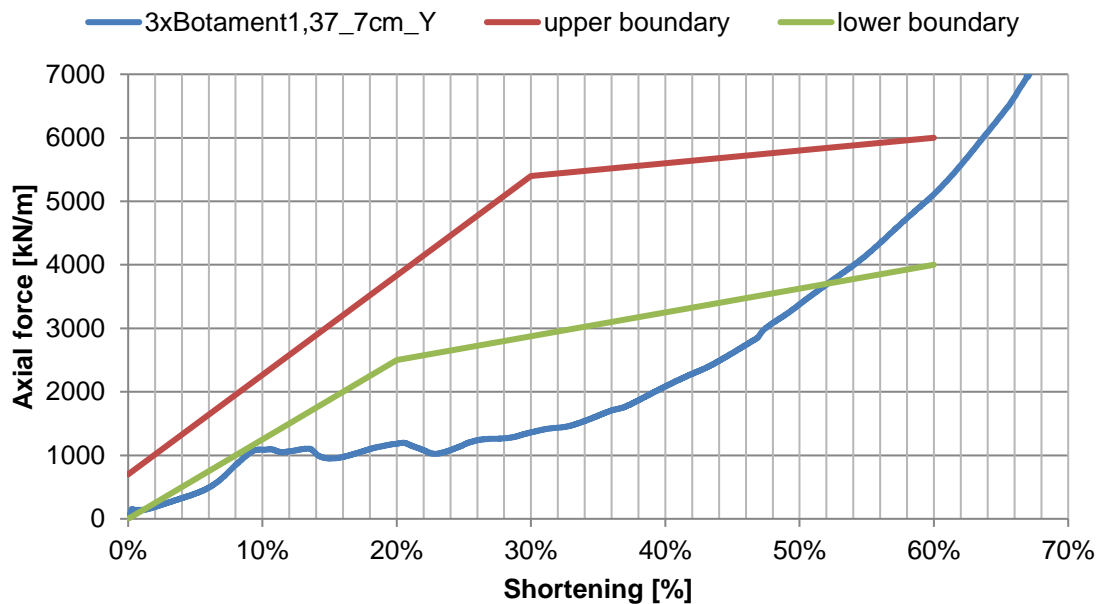
Figure 124: Force-Shortening behaviour "Botament1,37_7cm_Y" Type II

The used porous inlay effectively controls the initial behaviour. Type I and Type II cannot get fulfilled. The porous inlay is completely compressed at the first peak with ~9% shortening.

Lab Test "D1,37_7cm_Y"

The filling material has been estimated with a density of 1.37 kg/dm To avoid a high initial stiffness, a 7 cm porous inlay with a compressive strength of 5 MPa is used. A compensation layer of gypsum needs to be installed to provide full contact. The boundaries refer to the tender documents of the Semmering Base Tunnel (see Figure 56).

Table 27: Specifications "D1,37_7cm_Y"

Filling material	Mass percentage		Inner pipe, steel quality, dimension	Outer pipe, steel quality, dimension	Inlay
D1,37	29.85%	CEM II/B-M (S-L) 32,5 N	S235+N 133x2.5x330	DD 11 140x2x80	7 cm porous inlay 5 MPa
	20.58%	Liapor 1-4 mm			
	32.63%	Sand 0-2mm			
	0.57	W/C-ratio			

Figure 125: before/after "D1,37_7cm_Y"
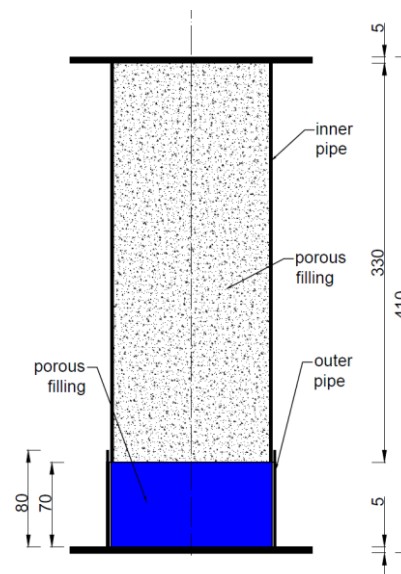
Figure 126: Scheme "D1,37_7cm_Y"

Type I: The force-shortening curve shows at the beginning a smooth increase and it moves along the lower boundary but it stays in the specified range. The first peak appears at ~9% shortening and an axial force of ~1100 kN. Then it shows a quasi-constant behaviour until a shortening of ~66% and an axial force of 6900 kN is reached. It leaves the specified range from ~16%-~37% shortening.

Type II: The force-shortening curve shows at the beginning a smooth increase and it gets below the lower boundary from ~1% - ~51%. The first peak appears at ~9% shortening and an axial force of ~1100 kN. Then it shows a quasi-constant behaviour until a shortening of ~66% and an axial force of 6900 kN is reached.

Force-Shortening behaviour
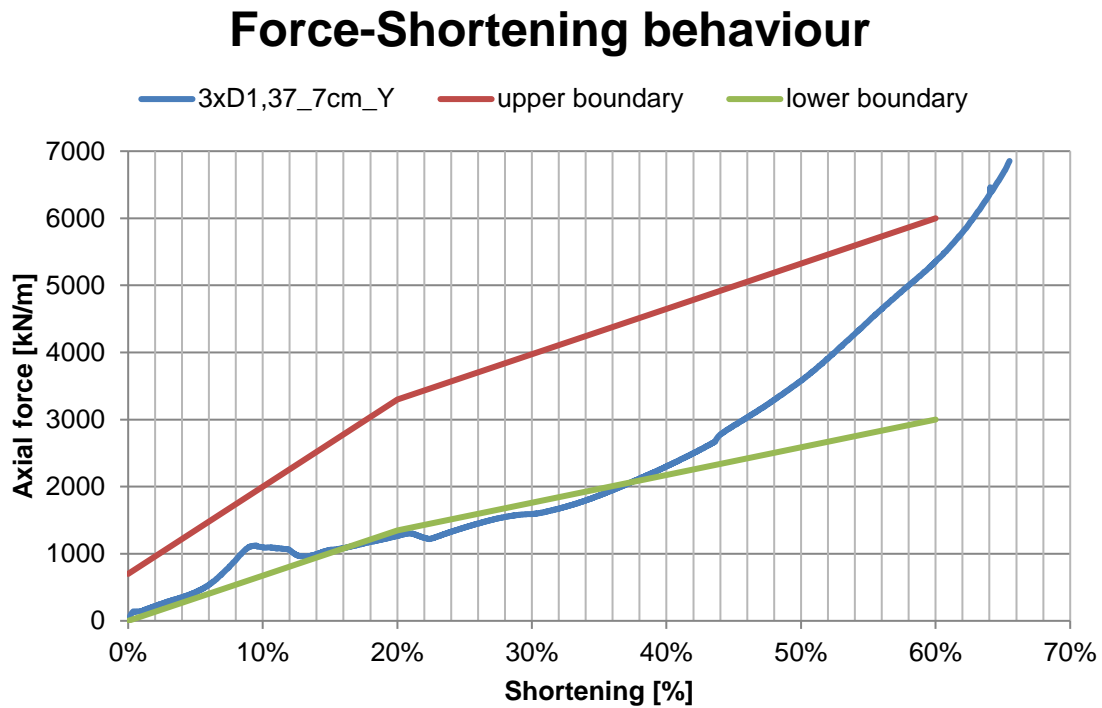
Figure 127: Force-Shortening behaviour "D1,37_7cm_Y" Type I

Force-Shortening behaviour
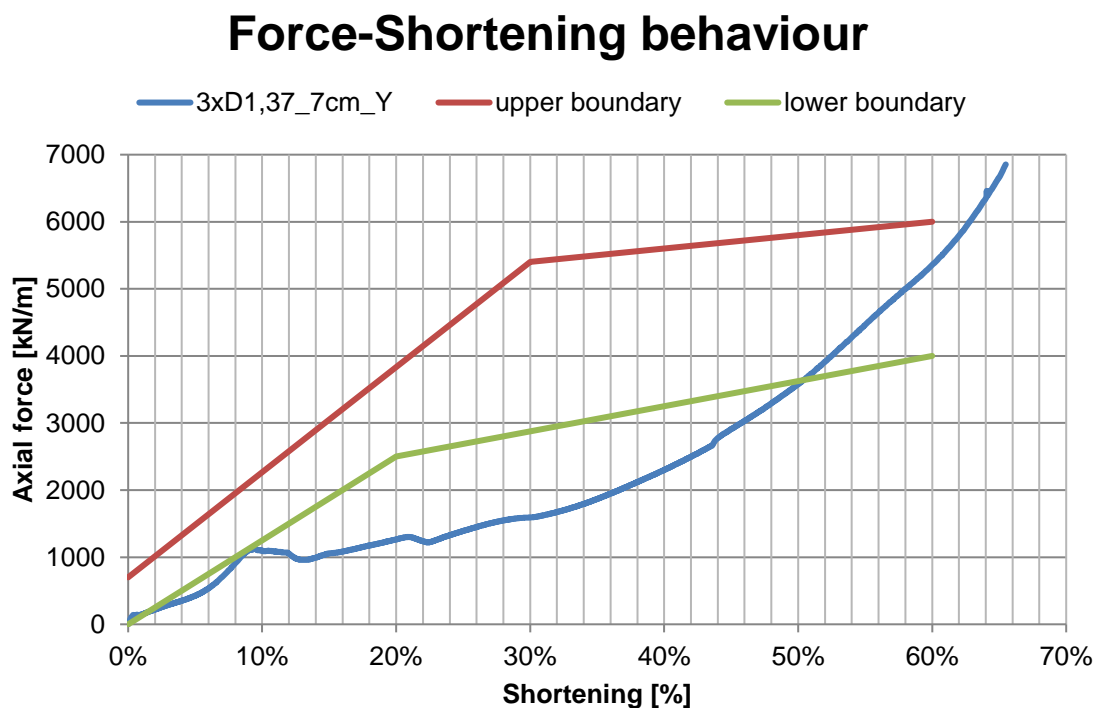
Figure 128: Force-Shortening behaviour "D1,37_7cm_Y" Type II

The used porous inlay effectively controls the initial behaviour. Type I and Type II cannot get fulfilled. The porous inlay is completely compressed at the first peak with ~9% shortening.

Lab Test "Liapor4_8_WZ0,75"

For this lab test a new filling material with a different size of the expanded clay (Liapor) has been used. The boundaries refer to the tender documents of the Semmering Base Tunnel (see Figure 56).

Table 28: Specifications "Liapor4_8_WZ0,75

Filling material	Mass percentage		Inner pipe, steel quality, dimension	Outer pipe, steel quality, dimension	Inlay
Liapor 4_8_WZ 0,75	35.19%	CEM II/B-M (S-L) 32,5 N	34CrMo4 133x2x370	DD 11 140x2x50	-
	9.86%	Liapor 1-4 mm			
	38.48%	Liapor 4-8 mm			
	0.75	W/C-ratio			

Figure 129: before/after "Liapor4_8_WZ0,75"
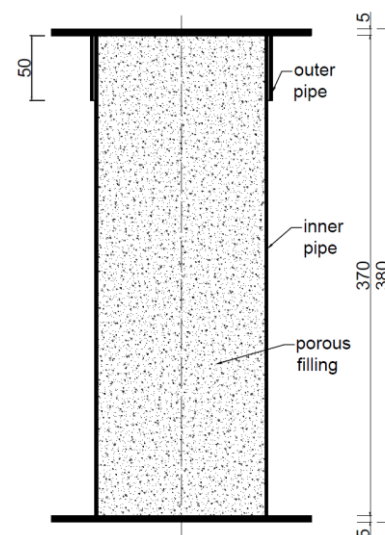
Figure 130: Scheme "Liapor4_8_WZ0,75"

Type I: The force-shortening curve shows at the beginning a steep increase and it intersects the upper boundary at a shortening of ~0.5% and an axial force of ~800 kN. The first peak appears at ~1.7% shortening and an axial force of ~1200 kN. Then it shows an oscillating behaviour until a shortening of ~54% and an axial force of 1900 kN is reached. It leaves the specified range at ~11% shortening.

Type II: The force-shortening curve shows at the beginning a steep increase and it intersects the upper boundary at a shortening of ~0.5% and an axial force of ~800 kN. The first peak appears at ~1.7% shortening and an axial force of ~1200 kN. Then it shows an oscillating behaviour until a shortening of ~54% and an axial force of 1900 kN is reached. It leaves the specified range at ~4% shortening.

Force-Shortening behaviour
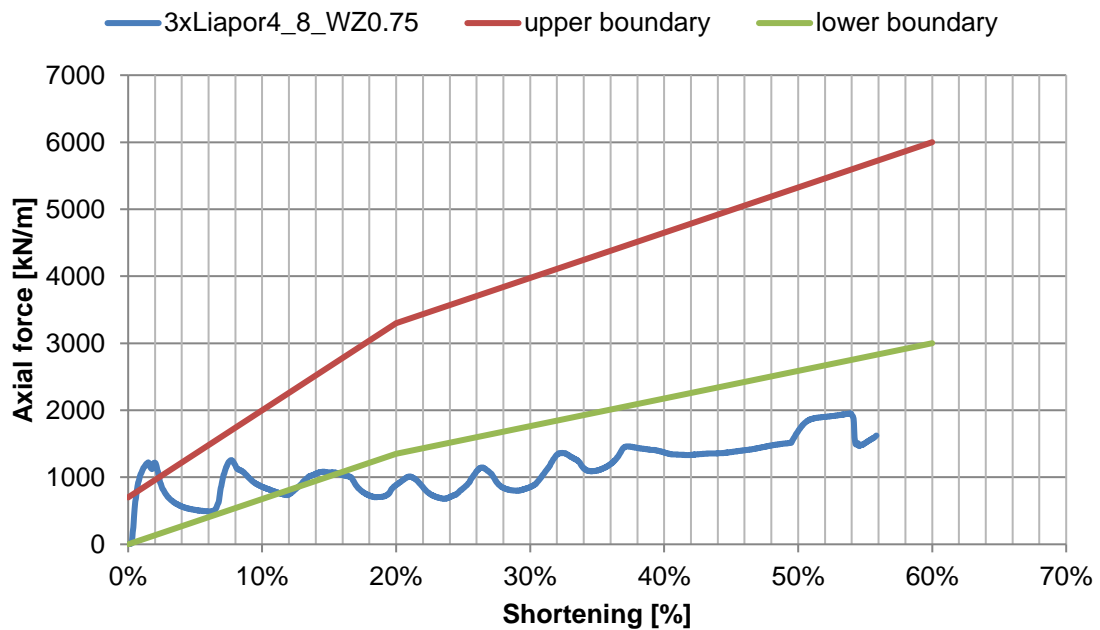
Figure 131: Force-Shortening behaviour "Liapor4_8_WZ0,75" Type I

Force-Shortening behaviour
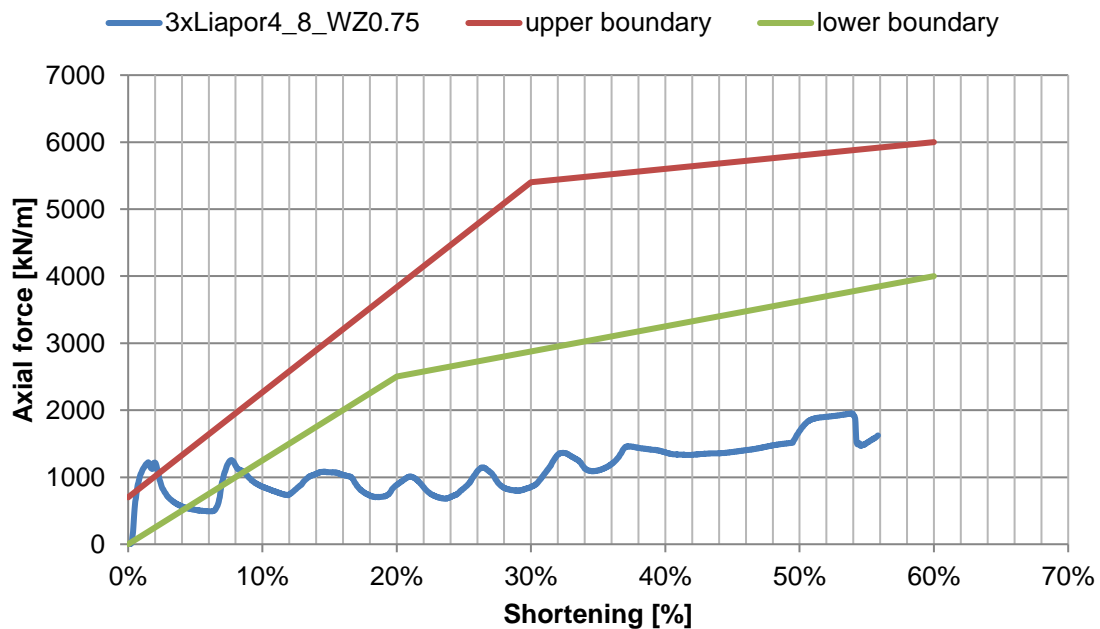
Figure 132: Force-Shortening behaviour "Liapor4_8_WZ0,75" Type II

The steep increase at the beginning relates to the direct contact of the inner pipe with its filling material and the endplate. The oscillating behaviour of the force-shortening curve relates to the high amount of expanded clay in the filling material.